

https://dspace.org/

Investigation into phenomena observed during the interaction of a focused high-energy laser beam with high voltage electric fields

West, Nicholas John

2010-04-14T07:26:55Z
http://hdl.handle.net/10539/7978

Downloaded from a DSpace repository. https://dspace.org/

INVESTIGATION INTO PHENOMENA OBSERVED DURING THE INTERACTION OF A FOCUSED HIGH-ENERGY LASER BEAM WITH HIGH VOLTAGE ELECTRIC FIELDS

Nicholas John West

A thesis submitted to the Faculty of Engineering and the Built Environment, University of the Witwatersrand, Johannesburg, in fulfilment of the requirements for the degree of Doctor of Philosophy.

Johannesburg, 2008

Declaration

I declare that this thesis is my own, unaided work, other than where specifically acknowledged. It is being submitted for the degree of Doctor of Philosophy in the University of the Witwatersrand, Johannesburg. It has not been submitted before for any degree or examination in any other university.

Signed this _____ day of _____ 2008

_____

Nicholas John West

Abstract

The work presented in this thesis extends and contributes knowledge to the field of laser-induced breakdown of a spark gap in air. Previous work has shown that laser-triggering of a spark gap is very effective in the case of a coaxially triggered spark gap (where the beam is directed along the axis of the gap). Although a coaxially triggered gap presents a very intuitive approach, it is not practical. Therefore, the main focus of this work is to investigate how effective laser-triggering is in the case of an orthogonally arranged gap (beam at right angles to the gap axis). The effects of the laser beam intensity, the gap length used and the position of the plasma in the gap were found to play important roles in the breakdown process of an orthogonally triggered gap. It was found that directing and focusing the laser beam at right angles to the gap axis reduces the breakdown voltage of the gap dramatically. An almost 70% reduction of the breakdown voltage of a 50 mm gap was recorded. Also, the spatial and temporal relation between the laser-induced plasma and the resulting arc was investigated. Although the laser-triggered arc was expected to attach to the conductive laser-induced plasma, experiments showed that this is not the case. Whether attachment occurs depends on the relative timing of the initiation of the plasma and the high voltage arc and on the overall breakdown probability of the spark gap. This represents a unique and valuable contribution to engineers working in the field of triggered spark gaps and other high voltage triggering applications.

To family and friends

"And so dear listeners we sat and waited.
Sometimes we stood and waited,
Which is the same as sitting down only higher
Ha-hum"

The Goon Show, 6th series, No. 8, Broadcast 8 November 1955

Acknowledgements

The author would like to acknowledge the National Laser Centre (NLC) for use of their equipment (lasers and optics) for the completion of this project and the staff of the G Laboratories for their assistance in manufacturing the impulse generator and the spark gaps used in the project. The author would also like to thank Eskom for support received through the TESP programme; the NRF for support of the High Voltage research programme; and the DTI for support received through the THRIP programme. The author will also like to thank CBi-Electric for their on-going support of the Chair of Lightning with in the School of Electrical and Information Engineering of the University of the Witwatersrand, Johannesburg.

Contents

Declaration i

Abstract ii

Acknowledgements iv

Contents v

List of Figures viii

List of Tables xi

List of Symbols xii

1 Introduction 1

1.0.1 Chapter 2 – Lasers and laser-induced plasmas 3
1.0.2 Chapter 3 – Breakdown experiments using an Nd:YAG laser 3
1.0.3 Chapter 4 – Gated camera experiments 3
1.0.4 Chapter 5 – Conclusion 3
1.0.5 Appendix – Useful Information 4

2 Lasers and laser-induced plasmas 5

2.1 Introduction 5
2.2 Lasers and laser parameters 6
2.2.1 Population inversion 6
2.2.2 Important laser parameters 10
2.3 Laser-induced plasmas 18
2.4 Conclusion 23

3 Breakdown experiments using an Nd:YAG laser 25

3.1 Introduction 25
3.2 Experimental setup 26
3.3 Variation of breakdown voltage with Q-switch 28
3.4 Variation of breakdown voltage with changing plasma position . . . 33

3.5 Maxwell simulations . . . 35
3.5.1 Electric field verification . . . 38
3.5.2 Application of laser beam with 1 kV across the gap . . . 39
3.5.3 Application of laser beam with 50 kV across the gap . . . 40
3.6 Effect of the lens focal length on the breakdown voltage . . . 42
3.7 Conclusion . . . 43

4 Gated camera experiments **44**
4.1 Introduction . . . 44
4.2 Experimental setup . . . 45
4.3 Spark gaps and conducting floating objects . . . 47
4.4 Spatial orientation of the laser-induced plasma . . . 49
4.5 Description of feature . . . 51
4.5.1 Symmetry of feature . . . 52
4.5.2 Size of feature . . . 55
4.6 Using the Spellman Generator and Cooke Corporation Camera . . . 56
4.7 Time line-experiments . . . 60
4.7.1 Plasma life times . . . 60
4.7.2 Arc appearance . . . 61
4.8 Explanation of arc shape . . . 64
4.9 Conclusion . . . 67

5 Conclusion **68**

A Electrical breakdown in gases **69**
A.1 Introduction . . . 69
A.2 Ionisation methods . . . 69
A.2.1 Ionisation by collision . . . 70
A.2.2 Photoionisation . . . 71
A.2.3 Ionisation by metastable atoms . . . 71
A.2.4 Thermal ionisation . . . 72
A.3 The Townsend Mechanism . . . 72
A.4 The Streamer mechanism . . . 74
A.5 Electronegative gases . . . 76
A.5.1 Mechanisms and applications . . . 76
A.5.2 The attachment coefficient . . . 77
A.6 Time lags in electrical breakdown . . . 79
A.7 Conclusion . . . 79

B Head-on and Side images of observed 'feature' **81**
B.1 Head-on view of 'feature' . . . 81
B.2 Side view of 'feature' . . . 99

References **116**

List of Figures

2.1 Spontaneous emission 6
2.2 Typical laser layout 10
2.3 Measurement of the FWHM of a laser pulse 13
2.4 Typical Gaussian intensity profile 15
2.5 The Rayleigh range of a Gaussian laser beam 15
2.6 Set-up of beam and scanner 17
3.1 Optics set-up for breakdown experiments with YAG laser 26
3.2 Variation of laser energy and pulse width with Q-switch delay 27
3.3 Variation of breakdown voltage width with Q-switch delay 29
3.4 Variation of laser energy and peak intensity with Q-switch delay . . 30
3.5 Variation of peak intensity and breakdown voltage with Q-switch delay 31
3.6 Gradients of peak intensity and breakdown voltage plots 32
3.7 Gap set-up for plasma position variation experiments 34
3.8 Variation of breakdown voltage with plasma position 34
3.9 Maxwell model for E-field vs. plasma position simulations 36
3.10 Dimensions used for the simulation of the spark gap electrodes . . . 36
3.11 Model used for the laser-induced plasma 37
3.12 Dimensions used for the laser-induced plasma – all dimensions in mm 37
3.13 Electric field magnitude control simulation 38
3.14 Electric field magnitude vector control simulation 39
3.15 Electric field vector plot (1kV across 30 mm) 40
3.16 Electric field vector plot (50kV across 30 mm) 41
4.1 Camera, delay generator, laser block and timing diagrams 45
4.2 Camera angles and optical setup 46
4.3 High voltage generator used in the experiments 46
4.4 Experimental setup for 1.2/50 μs impulse experiments 48
4.5 Laser and impulse breakdown voltage plot 49
4.6 Drawing of the arc 'feature' observed with the naked eye 51
4.7 Head-on view of the laser-induced plasma and resulting arc 52
4.8 'Head-on' view of arc encircling the laser-induced plasma 53
4.9 Two separate side views of arc and laser-induced plasma 53
4.10 Drawing of spacial relationship between plasma and arc 54

4.11 Calibration image used to measure dimensions of observed 'feature' . 54
4.12 Parameters L, D and ϕ of the observed feature 55
4.13 Cooke Corporation Camera image of breakdown (30 kV, 30 mm) . . 57
4.14 Arc images for 30, 40 and 50 kV across 30 mm 58
4.15 Arc image for 40 and 50 kV (E= 1 kV/mm) 59
4.16 'Head-on' and 'side' view of the laser-induced plasma 60
4.17 Plasma life time vs. laser Q-switch delay 61
4.18 Breakdown time delay seen on an oscilloscope 63
4.19 Time-line of events for a 30 mm gap and laser at 190 μs Q-switch . . 64
4.20 Drawing explaining the formation of observed arc shape 66
A.1 The Townsend mechanism 73
A.2 Field distortion caused by electron avalanche 75
B.1 Calibration image used to measure dimensions of observed 'feature' . 82
B.2 Feature 1 L=14 mm $\phi = 8.13°$ 83
B.3 Feature 2 L=12 mm $\phi = 4.46°$ 83
B.4 Feature 3 L=12 mm $\phi = 0°$ 84
B.5 Feature 4 L=13 mm $\phi = 0°$ 84
B.6 Feature 5 L=11 mm $\phi = 10.3°$ 85
B.7 Feature 6 L=14 mm $\phi = 4.09°$ 85
B.8 Feature 7 L=14 mm $\phi = 4.9°$ 86
B.9 Feature 8 L=13 mm $\phi = 0°$ 86
B.10 Feature 9 L=14 mm $\phi = 4.09°$ 87
B.11 Feature 10 L=12 mm $\phi = 2.39°$ 87
B.12 Feature 11 L=14 mm $\phi = 8.13°$ 88
B.13 Feature 12 L=12 mm $\phi = 4.76°$ 88
B.14 Feature 13 L=12 mm $\phi = 0°$ 89
B.15 Feature 14 L=13 mm $\phi = 4.4°$ 89
B.16 Feature 15 L=14 mm $\phi = 12.09°$ 90
B.17 Feature 16 L=13 mm $\phi = 12.99°$ 90
B.18 Feature 17 L=10 mm $\phi = 16.7°$ 91
B.19 Feature 18 L=10 mm $\phi = 16.7°$ 92
B.20 Feature 19 L=13 mm $\phi = 4.4°$ 92
B.21 Feature 20 L=10 mm $\phi = 14.3°$ 93
B.22 Feature 21 L=15 mm $\phi = 3.81°$ 93
B.23 Feature 22 L=12 mm $\phi = 3.39°$ 94
B.24 Feature 23 L=11 mm $\phi = 10.3°$ 94
B.25 Feature 24 L=12 mm $\phi = 9.46°$ 95
B.26 Feature 25 L=13 mm $\phi = 8.75°$ 95
B.27 Feature 26 L=13 mm $\phi = 0°$ 96
B.28 Feature 27 L=10 mm $\phi = 5.71°$ 96

B.29 Feature 28 L=10 mm $\phi = 0°$ 97
B.30 Feature 29 L=12 mm $\phi = 9.46°$ 97
B.31 Feature 30 L=14 mm $\phi = 19.65°$ 98
B.32 Feature 31 L=11 mm $\phi = 10.3°$ 100
B.33 Feature 32 L=10 mm $\phi = 5.71°$ 100
B.34 Feature 33 L=10 mm $\phi = 5.71°$ 101
B.35 Feature 34 L=9 mm $\phi = 6.34°$ 101
B.36 Feature 35 L=13 mm $\phi = 2.2°$ 102
B.37 Feature 36 L=11 mm $\phi = 2.6°$ 102
B.38 Feature 37 L=11 mm $\phi = 12.8°$ 103
B.39 Feature 38 L=11 mm $\phi = 19.98°$ 104
B.40 Feature 39 L=11 mm $\phi = 2.6°$ 104
B.41 Feature 40 L=11 mm $\phi = 5.19°$ 105
B.42 Feature 41 L=13 mm $\phi = 8.5°$ 105
B.43 Feature 42 L=12 mm $\phi = 9.46°$ 106
B.44 Feature 43 L=11 mm $\phi = 2.6°$ 107
B.45 Feature 44 L=10 mm $\phi = 0°$ 107
B.46 Feature 45 L=12 mm $\phi = 0°$ 108
B.47 Feature 46 L=10 mm $\phi = 5.71°$ 108
B.48 Feature 47 L=9 mm $\phi = 12.3°$ 109
B.49 Feature 48 L=11 mm $\phi = 2.6°$ 110
B.50 Feature 49 L=12 mm $\phi = 4.76°$ 110
B.51 Feature 50 L=12 mm $\phi = 2.39°$ 111
B.52 Feature 51 L=10 mm $\phi = 11.3°$ 111
B.53 Feature 52 L=12 mm $\phi = 9.46°$ 112
B.54 Feature 53 L=11 mm $\phi = 10.3°$ 112
B.55 Feature 54 L=13 mm $\phi = 4.4°$ 113
B.56 Feature 55 L=11 mm $\phi = 5.19°$ 113
B.57 Feature 56 L=10 mm $\phi = 5.71°$ 114
B.58 Feature 57 L=12 mm $\phi = 4.76°$ 114
B.59 Feature 58 L=11 mm $\phi = 0°$ 115
B.60 Feature 59 L=12 mm $\phi = 19.4°$ 115

List of Tables

2.1 Common active media and associated wavelengths 9
2.2 The electromagnetic spectrum 11
2.3 Some common elements and their associated ionisation potentials . . 19
3.1 Minimum breakdown voltages achieved for three different focal lengths 29
3.2 Breakdown ranges achieved with a focused laser beam 30
3.3 The four gradients of the intensity and voltage graphs 32
3.4 Correlation coefficients for the three different lenses used 33
3.5 Comparison of focal lengths, beam radius and peak intensity 42
4.1 Tabulated results of impulse experiments for the 8 different geometries 50
4.2 DC voltage laser-triggered breakdown results for various gap lengths 50
4.3 Positions of the feature relative to the laser-induced plasma 55
4.4 Average dimensions of feature 56
4.5 Electric fields for 3 different gap geometries 57
4.6 Laser-induced breakdown time delays for 3 different Q-switch settings 62
4.7 Laser-induced breakdown time delays at optimum Q-switch 63
4.8 Shock and thermal wave velocities and expansion 65

List of Symbols

The principal symbols used in this thesis are summarized below, each providing a reference to the equation in which it is first used:

A_{21}	Einstein's transition probability coefficient	Eq. (2.1)
g_1	degeneracies of the lower states	Eq. (2.2)
g_2	degeneracies of the upper states	Eq. (2.2)
B_{12}	Einstein's B probability coefficient	Eq. (2.4)
E_p	Photon energy [J]	Eq. (2.7)
h	Plank's constant (6.63×10^{-34} [Js])	Eq. (2.7)
ν	photon frequency [Hz]	Eq. (2.7)
ϕ_0	Peak fluence [J/cm^2]	Eq. (2.8)
ω_x	Beam waists in the x direction [m]	Eq. (2.8)
ω_y	Beam waists in the y direction [m]	Eq. (2.8)
P_0	Peak power [W]	Eq. (2.9)
E_T	Total pulse energy [J]	Eq. (2.9)
τ	FWHM pulse width [s]	Eq. (2.9)
$\overline{P}$	Average power [W]	Eq. (2.10)
N_p	Number of pulses	Eq. (2.10)
t	Time [s]	Eq. (2.10)
f_r	Laser repetition rate [Hz]	Eq. (2.11)
I_0	Peak intensity [W/cm^2]	Eq. (2.13)
ω_f	Beam radius at focal point [m]	Eq. (2.13)
f	Focal length of lens [m]	Eq. (2.13)
M^2	Beam quality factor	Eq. (2.13)
λ	Laser wavelength [m]	Eq. (2.13)

ω	Beam radius (waist) [m]	Eq. (2.14)
z_R	Rayleigh range	Eq. (2.16)
ω_0	Minimum beam waist	Eq. (2.16)
E_i	Ionisation potential of atom [eV]	Eq. (2.20)
W_i	Ionisation rate per atom	Eq. (2.22)
σ	Photon absorption cross-section area of atom	Eq. (2.22)
F	Photon flux density (Photons/cm^{2}s)	Eq. (2.22)
ε	Energy of free electrons	Eq. (2.23)
e	Electron charge	Eq. (2.23)
m_e	Electron mass	Eq. (2.23)
ν_{eff}	Effective electron collision frequency	Eq. (2.23)
n_e	Electron density	Eq. (2.23)
I	Laser beam intensity	Eq. (2.23)
ω_c	frequency of radiation (cyclic)	Eq. (2.23)
E_i	First ionisation potential	Eq. (2.23)
M	Mass of background gas neutral particle	Eq. (2.23)

Chapter 1

Introduction

Ever since the formation of a laser-induced plasma in air was first observed by Maker, Terhume and Savage in the 1960s [1, 2], research has been ongoing in order to understand the physical mechanisms that govern the formation of laser-induced plasmas. At the same time, this phenomenon has been used in many different applications. When the phenomenon of laser-induced breakdown of air was first observed, the possibility of developing a fast, accurate and efficient trigger mechanism for high voltage systems [3, 4]. Research was also performed in simply trying to experimentally determine the laser parameters such as the beam intensity required to achieve breakdown in air and various gases such as H_2, He and N_2 [5]. The generation of a laser-induced spark in air also found applications in fuel ignition systems [6, 7]. Another very interesting application of laser-induced breakdown is that of laser-triggering of lightning. Researchers have realised that a focused laser beam may be able under certain conditions to help initiate an upward leader from an earthed object and thus trigger lighting [8, 9].

Most of the research relating to laser-induced plasmas revolves around understanding the physical mechanisms that govern the formation of the plasma and the application of laser-induced breakdown fields such as laser-induced plasma spectroscopy and laser-triggered ignition and firing systems. The laser-induced plasma generated is by definition a highly conductive body. When electrical breakdown is initiated in a laser-triggered spark gap, the assumption is that the arc will tend to attach itself to the laser-induced plasma. Not much research has been performed in order to determine the spatial and temporal relationship between the laser-induced plasma and and the laser-triggered arc. The question remains whether the arc will behave as expected (attach itself to the laser-induced plasma) or exhibit some other behaviour.

When dealing with high voltage triggering experiments, one can use one of two main strategies: These are the 'coaxial' and 'orthogonal' triggering configurations. In the coaxial approach, the beam is directed along the axis of the spark gap in a direction, say, from anode to cathode. In the orthogonal situation, the laser beam is allowed to travel perpendicular to the gap axis. These two strategies each have their advantages and disadvantages. Research has been performed in order to explore the differences between various triggering geometries [10]. However, most of the research is limited to low-power systems and short gap lengths. Typically gaps in the order of 5 mm are used. In very short gaps, there is not much difference in performance between the two above mentioned triggering geometries. Does the same apply to longer gaps? Since the coaxial approach is more intuitive (the laser beam is allowed to irradiate the entire gap) it has been the preferred laser-triggered spark gap configuration in many experimental set-ups. An orthogonal configuration in many ways provides a more practical solution to laser-triggering applications, even though it is not as intuitive as the coaxial approach. One of the aims of this research is to investigate how efficient an orthogonal triggering approach is in the case of longer gaps (gap lengths larger than 20 mm).

The work presented in this thesis covers a series of experiments dealing with laser-induced breakdown of gaps having lengths between 20 and 50 mm. In particular, the experiments are focused on the interaction of the laser-induced plasma with the resulting high voltage arc. The thesis presented here can be roughly divided into two main sections:

1. Experiments involving an evaluation of the orthogonal gap arrangement in terms of its breakdown performance and experiments intended to explore the spatial and temporal relationship between laser-induced plasma and resulting arc. In this thesis, a brief background to lasers and laser-induced breakdown is presented in order to familiarise the reader with the underlying physical mechanisms. These will be used at a later stage to provide explanations for the very interesting phenomena observed.

2. Following this background section, the various experiments are presented together with the results obtained.

Thesis plan

1.0.1 Chapter 2 – Lasers and laser-induced plasmas

In this chapter the background to lasers and laser-triggered plasmas is presented. The basic physics behind laser operation is presented together with definitions of some important laser parameters such as pulse energy, fluence, pulse width, power, intensity and beam shape. Laser-induced plasmas are discussed. The basic theories of laser-induced plasma formation and development are described. Also high electrical breakdown considerations of short gaps are presented.

1.0.2 Chapter 3 – Breakdown experiments using an Nd:YAG laser

Here, the experiments conducted at the National Laser Centre of the CSIR are presented. The laser used was a high-powered Nd:YAG laser and the experiments were restricted to the orthogonal spark gap arrangement. The aim of the experiments presented here was to link laser parameters (pulse width, energy and intensity) with electrical breakdown parameters such as gap length, applied voltage and position of the trigger stimulus in the gap. In this chapter, interesting laser-induced plasma and resulting arc phenomena will be presented. In all experiments, an orthogonal gap arrangement was used.

1.0.3 Chapter 4 – Gated camera experiments

In this chapter, experiments involving the spatial and temporal relationship between the laser-induced plasma and the laser-induced arc are presented. The laser used was the same Nd:YAG laser described in Chapter 3. A Cooke Corporation FlashCam gated camera was used to capture images the observed anomalous behaviour of the laser-triggered arc and to explain the nature of the spatial and temporal plasma and arc relationship.

1.0.4 Chapter 5 – Conclusion

Concluding remarks are presented in this Chapter.

1.0.5 Appendix – Useful Information

Two Appendices are presented: One relating to background on the electrical breakdown of gases and one containing figured captured by the CSIR gated camera.

Chapter 2

Lasers and laser-induced plasmas

2.1 Introduction

Lasers have proven to be one of the most versatile devices that have ever been developed. A laser is able to produce light that is **monochromatic** (in other words, the photons all have the same wavelength), **directional** and **coherent**. Because of these characteristics, lasers have found many uses from the medical world (laser surgery) to physics and engineering. In the mid-1960s, P.D. Maker, R. W. Terhume and C. M. Savage, for the first time, observed the formation of a laser-induced plasma. During experiments it was noticed that when the laser beam emitted from a ruby laser was focused, a spark was generated in air at the focal point of the lens [1]. Loosely, a plasma can be defined as a gas of charged and neutral particles which exhibit collective behaviour [11]. The fact that a focused laser beam is able, under certain conditions, to generate a plasma in unbiased air is of great importance. Electrical breakdown in a laser-triggered spark gap can be attributed mainly to the fact that the appearance of a laser-induced plasma in the gap causes a sudden and sharp modification in the resultant electric field which consists of the externally applied field and the superimposed field from space charges. This behaviour can be used to explain the very low laser-induced breakdown voltages obtained. The fact that a large distortion of the electric field takes place during breakdown can also help explain some observed anomalous behaviour of the laser-generated arc and plasma. Since the laser-induced plasma is nothing more than a collection of charged particles, it is highly conductive. During laser-induced electrical breakdown, the resulting arc is expected to attach to the laser-induced plasma. However, during experiments described in the following chapters, it was noted than in some cases

the arc did not exhibit this expected behaviour. In order to understand and explain these phenomena, in this chapter, some laser-related background is presented in order to familiarise the reader with the terminology and the underlying physical mechanisms of laser-induced breakdown. For this reason, a brief introduction to the operation of lasers is presented followed by a section describing some of the key laser parameters such as laser energy, intensity and wavelength. A description of the formation of a laser-induced plasma is also presented.

2.2 Lasers and laser parameters

2.2.1 Population inversion

The word laser is nothing more than an acronym: Light Amplification by the Stimulated Emission of Radiation. To understand the principle of laser operation, one has to explore the concept of a population inversion.

Under normal conditions, in a collection of atoms, the electrons tend to stay in the ground state of these atoms. However, when external stimulation is present e.g. in the form of atomic collision or exposure to radiation, electrons located in the higher orbits can be pushed up to higher energy levels. When these electrons return to their original state, energy is released. This can be seen in *Figure 2.1* [12].

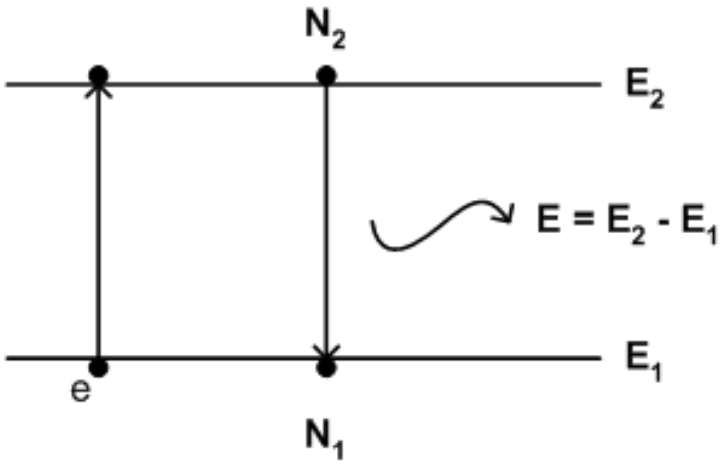


Figure 2.1: Spontaneous emission

In *Figure 2.1* E_1 and E_2 represent two energy states where $E_1 < E_2$. Also let N_1

represent the number of atoms per unit volume with energy E_1 and N_2 represent the number of atoms per unit volume with energy E_2. In this figure e represents an electron moving from energy state E_1 to state E_2. If this transition occurs spontaneously without any external influence, then it is called spontaneous emission. The energy released during the decay of the electron from state E_1 to state E_2 is given by $E = h\nu_{12} = E_1 - E_2$

Since this a spontaneous event, a probability can be associated with its occurrence. This probability is described by means of Einstein's A coefficient. Therefore it can be said that

$$\frac{dN_2}{dt} = -A_{21}N_2 \tag{2.1}$$

where

A_{21} = Einstein's transition probability coefficient

From *Equation 2.1* it is evident that the number of emissions that take place in time dt is proportional to N_2 and dt.

It is known that in thermal equilibrium according to Boltzmann statistics, we have the following relationship:

$$\frac{N_2}{N_1} = \frac{g_1}{g_2}e^{-\frac{E_2-E_1}{kT}} \tag{2.2}$$

where

g_1 = degeneracies of the lower states

g_2 = degeneracies of the upper states

Equation 2.2 also implies that the higher the energy level, the smaller the number of atoms that occupy that level. Based on *Equations 2.1* and *2.2* and assuming that $E_2 - E_1 << kT$, one can solve for the equilibrium value of N_2. This will be the simple exponential:

$$N_2(t) = N_2(0)e^{-\frac{t}{\tau_{21}}} \tag{2.3}$$

The other very significant process is that of absorption. The rate of energy absorption depends on two parameters: The number of available atoms in the lower energy states and on the density of the radiation. Let ρ be the density of radiation of frequency ν_{12}. Therefore, the number of absorptions per unity volume is

$$N_1 B_{12} \rho(\nu_{12}) \tag{2.4}$$

where

B_{12} = Einstein's B probability coefficient

There is also a phenomenon called stimulated emission. As the name implies, an electron is induced to transcend from a higher to a lower energy state. This is done by providing energy of the same wavelength as the energy that would have been released during spontaneous emission between these energy states. Once again, the stimulated emission rate depends on the number of atoms in the upper energy state and on the radiation present. In the same way as before:

$$N_2 B_{21} \rho(\nu_{21}) \tag{2.5}$$

It follows that at thermal equilibrium, the rates of upward and downward transition are equal. In other words:

$$N_1 B_{12} \rho(\nu_{12}) = A_{21} N_2 + N_2 B_{21} \rho(\nu_{21}) \tag{2.6}$$

In order for 'light amplification' to occur (in other words, a lasing action) a light beam is needed to traverse a line of atoms that are all in their excited state. However, this is not a real-life situation since one would expect the majority of atoms to be in their ground state according to the Boltzmann distribution (*Equation 2.2*). If $E_1 < E_2$ then it is expected that $N_1 > N_2$. This means than a prerequisite to having laser operation is $N_2 > N_1$ in other words an inverted Boltzmann distribution. This is known as a population inversion.

So far, the physical process of laser light generation has been sketched, and the concept of stimulated emission explored. In a working laser, one can identify the following components:

- An active medium
- A source of excitation
- A means to direct the laser beam in one direction efficiently

An active medium is nothing more than the source of atoms that will be involved in the population inversion process. The medium can be solid, liquid or gaseous. A wide range of media are used in the construction of lasers, depending on the desired laser wavelength. For example, if a mixture of 12.5% CO_2, 25% N_2 and balance He is used, then a wavelength of 10.6 μm is obtained (Infra Red – IR) Another common gas mixture used in Eximer lasers is Kr, F_2 and He or Ne. This mixture produces a beam that has a wavelength of 248 nm (ulraviolet – UV). In the case of an Nd:YAG[1] laser, a solid crystal is used as the active medium where as in dye lasers, the medium is pumped through the laser in the form of a liquid dye. *Table 2.1* shows some common active media used in lasers and their resulting wavelengths [13].

Table 2.1: Some common active media used in lasers and their associated wavelengths

Active medium	**Medium type**	**Wavelength [nm]**
ArF	Gas	193
KrF	Gas	248
N_2	Gas	337
HeNe	Gas	632
Nd:YAG	Solid-state	1064, 532, 355, 266
Ti - Sapphire	Solid-state	660 - 1180

The source of excitation as the name implies is responsible for exciting the active medium to bring about a population inversion. The two most common laser excitation mechanisms are optical (flash lamps) and electrical (eg. capacitor discharge). In a YAG laser, the excitation is performed via high-intensity Xenon flash-lamps whereas in most gas lasers (CO_2 laser), an electrical discharge is used to create the necessary population inversion.

The vast majority of lases also have a back reflector and an output coupler in addition to the two above-mentioned components. The back reflector and output coupler are nothing more than two mirrors with 99% reflection and 60% reflection respectively. This effectively increases the length of the active medium. At the same time, it places boundaries upon the electromagnetic field (laser beam) that develops between the two reflecting surfaces. The result is that photons generated to be accumulated

[1]Nd:YAG stands for "Neodynium doped Yttrium-Aluminim-Garnet" – it refers to the type of crystal used as the active medium in this type of laser

between these two mirrors with some of the photons escpaping through the output coupler. This allows for efficient oprtation of the laser. A simple drawing showing the operation of a laser can be seen in *Figure 2.2*

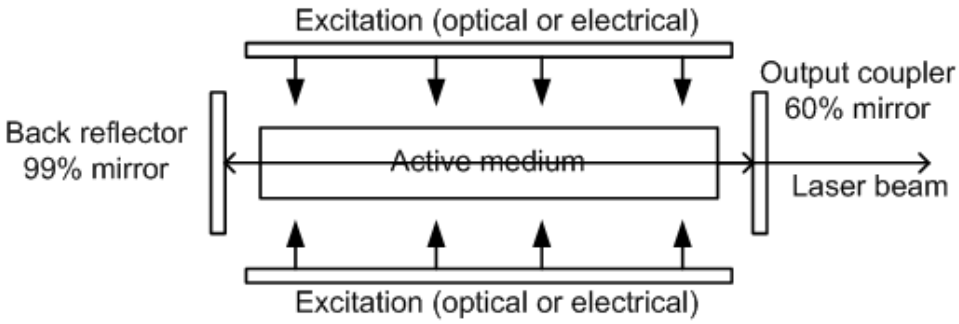


Figure 2.2: Drawing of a typical laser showing the active medium, excitation and reflectors

This set-up of two reflecting mirrors spaced a distance d apart is known as a laser resonator or a Farby-Perot cavity. Since we are dealing with a laser resonator and laser light (which is an TEM wave), the results is the development of transverse electromagnetic or TEM modes. These TEM modes are designated as TEM_{pq}. The lowest order is TEM_{00} which is also referred to as a Gaussian beam.

According to the mode of operation, laser are split into to major categories: Pulsed and continuous wave (CW). In other words, a laser is able to deliver the laser beam in short pulses are continuous over time. In the experiments presented in this thesis, the lasers used are pulsed lasers. This choice was made since a pulsed laser is able to deliver much higher peak power. Specifically an Nd:YAG laser was chosen. For this laser, with a pulse energy of 800 mJ and a pulse width of about 10 ns, a power of 80 MW per pulse may be obtained. High peak power is very important in order to achieve the required laser-induced breakdown in air.

2.2.2 Important laser parameters

When dealing with lasers there a number of very important parameters that must be taken into account. These are: laser energy, intensity, wavelength of the output beam, size and shape of the laser pulse (for pulsed lases) and the laser beam shape. These are parameters that govern the formation of a laser-induced plasma. For

example, the higher the laser beam energy and intensity, the easier a plasma can be generated. The life time of the plasma can also depend on the beam intensity.

Laser energy, fluence and wavelength

When dealing with lasers, it is very important to know the what wavelength the laser is emitting at. As mentioned before, the wavelength of the beam is dependent on the active medium used. It is known that the energy per photon is given by:

$$E_p = h\nu \tag{2.7}$$

where
E_p = Photon energy [J]
h = Plank's constant (6.63×10^{-34} [Js])
ν = photon frequency [Hz]

The wavelength of the laser light is important for laser-triggering applications. From *Equation 2.7* it can be seen that the higher the frequency ν (the shorter the wavelength), the higher the energy per photon. This means that breakdown can occur more easily when dealing with lasers that can generate shorter wavelengths. *Table 2.2* shows the energies related for various frequency ranges of the EM spectrum [14].

Table 2.2: The electromagnetic spectrum

Region	**Wavelength**	**Frequency [Hz]**	**Energy [eV]**
Radio	> 0.1 m	$< 3\times10^{9}$	10μeV
Microwave	0.1 m - 100 μm	3×10^{9} - 3×10^{12}	10μeV - 10 meV
Infrared	100 μm - 700 nm	3×10^{12} - 3×10^{14}	10 meV - 2 eV
Visible	700 nm - 400 nm	4.3×10^{14} - 7.5×10^{14}	2 eV - 3 eV
Ultraviolet	400 nm - 1 nm	7.5×10^{14} - 3×10^{17}	3 eV - 10 keV
X-Rays	1 nm - 10 pm	3×10^{17} - 3×10^{19}	10 keV - 100 keV
γ-Rays	$<$ 10 pm	$> 3\times10^{19}$	$>$ 100 keV

From *Table 2.2* it can be seen that the smaller the laser beam wavelength (the higher the frequency), the higher the photon energy. The laser used in the experiments to be described, is an Nd:YAG laser emitting in the Near Infra Red (NIR) at 1 064 nm. This translates to an energy of about 1.12 eV/photon. The choice of laser (and

of course wavelength) was concious. An Nd:YAG laser operating at its fundamental wavelength (1 064 nm) is capable of very high peak power and offers a Gaussian beam unlike most Excimer lasers that operate in the ultraviolet range.

A laser beam produced by a pulsed laser contains a certain amount of energy per pulse and it is measured in Joules (J). The energy density of the beam is known as the fluence and it is measured in J/cm^2. The general expression for the fluence of a laser beam is given by

$$\phi(x,y) = \phi_0 e^{-2[\frac{x^2}{\omega_x^2} - \frac{y^2}{\omega_y^2}]} \tag{2.8}$$

where

ϕ_0 = Peak fluence [J/cm^2]

ω_x = Beam waists in the x direction [m]

ω_y = Beam waists in the y direction [m]

Laser Power and beam intensity

When dealing with pulsed lasers, one has to take into account the pulse width. In most cases, FWHM measurement is used. The way the FWHM (Full Width Half Maximum) of a pulse is defined can be seen in *Figure 2.3*

As can be seen from *Figure 2.3*, the FWHM is just about 1.2.

The laser beam intensity is the power density of the laser beam measured in W/cm^2. It is evident that the intensity of a laser beam (being a measure of power) is dependent on the pulse energy of the beam, the pulse width τ of the laser pulse and the size (area) of the laser beam. The peak power of a laser beam per pulse is

$$P_0 = \frac{E_T}{\tau}. \tag{2.9}$$

where

P_0 = Peak power [W]

E_T = Total pulse energy [J]

τ = FWHM pulse width [s]

This means that the higher the total pulse energy and the shorter the pulse width, the higher the peak power of the laser beam (per pulse). The total average power of

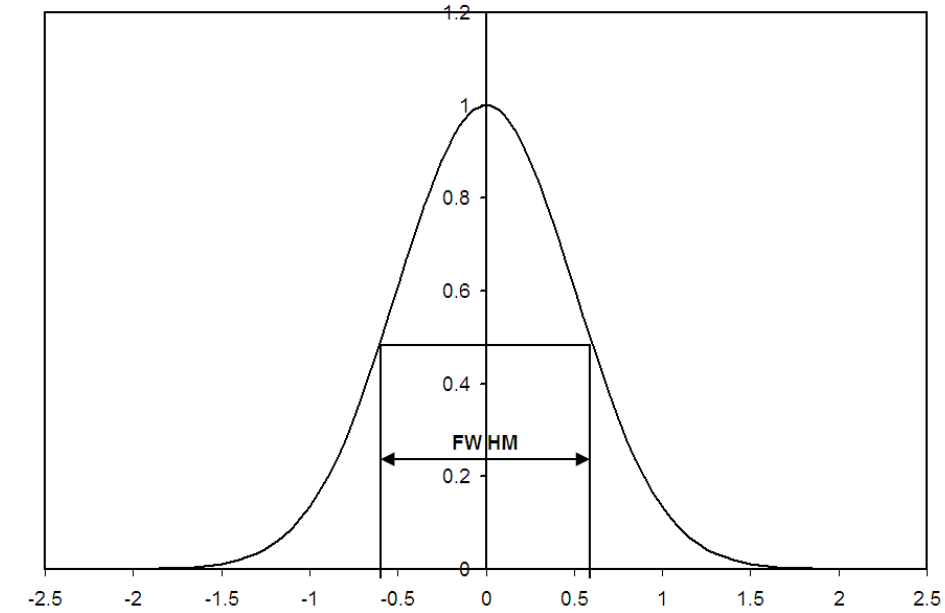


Figure 2.3: Measurement of the FWHM of a laser pulse

the laser beam is defined as the energy of the laser beam multiplied by the number of pulses:

$$\overline{P} = \frac{N_p \times E_T}{t} \tag{2.10}$$

where

$\overline{P}$ = Average power [W]

N_p = Number of pulses

t = Time [s]

This equation can be simplified to the product of the repetition rate of the laser and the laser pulse energy:

$$\overline{P} = f_r \times E_T \tag{2.11}$$

where

f_r = Laser repetition rate [Hz]

As mentioned above, the intensity of the beam is not only dependant on time, but also on area. It is a power density. For any laser beam, the peak intensity is given by:

$$I_0 = \frac{2E_T}{\pi\omega_f\tau} \tag{2.12}$$

Where ω_f is given by:

$$\omega_f = \frac{M^2\lambda f}{\pi\omega_0} \tag{2.13}$$

where

I_0 = Peak intensity [W/cm^2]
ω_f = Beam radius at focal point [m]
f = Focal length of lens [m]
M^2 = Beam quality factor
λ = Laser wavelength [m]

The beam quality factor M^2, as the name implies, is used as a measure of quality of a laser beam by comparing it to a Gaussian beam. The beam quality factor for a Gaussian beam is 1. This means that all other intensity profiles have an M^2 value greater that 1. When performing laser experiments, it is very important to know what the M^2 value of the beam is. Without this value, one is not able to calculate the size of the beam at the focal point as can be seen from *Equation 2.13*. Not knowing the value of the beam quality factor means that the peak intensity cannot be calculated accurately.

Beam shape and beam parameters

As mentioned above, the fact that a laser resonator allows for the development of various TEM modes, it follows that the shape of the resulting laser beam depends on the way the laser cavity is set up. Each beam shape has its own advantages and disadvantages. Gaussian beams are the most commonly used form of laser beam. In many cases, Gaussian beams are preferred because of their high peak power, low divergence and ease of focusing.

Since the laser used throughout the experiments was an Nd:YAG laser producing a Gaussian beam, it is important to familiarise the reader with some of the relationships that govern Gaussian beams.

The intensity of a Gaussian beam (as expected) is given by the following relationship:

$$I = I_0 e^{-2(\frac{r}{\omega})^2} \tag{2.14}$$

where

ω = Beam radius (waist) [m]

By definition, 86.5% of the beam's energy is located within the waist of the beam. This can be seen in *Figure 2.4*.

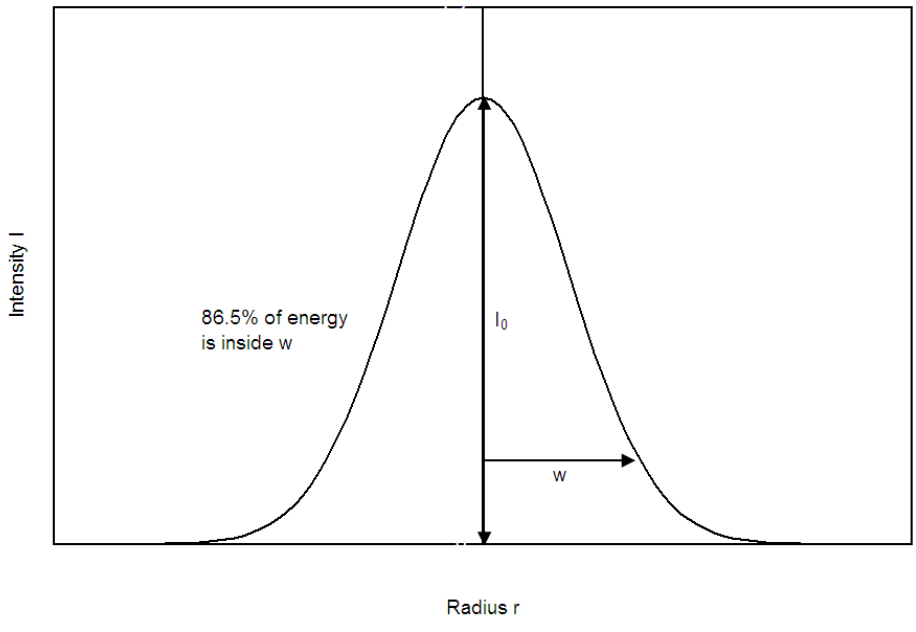


Figure 2.4: Typical Gaussian intensity profile

In the case of a Gaussian beam, there are two main parameters: The minimum waist ω_0 and the Rayleigh range [15]. These parameters can be seen in *Figure 2.5*

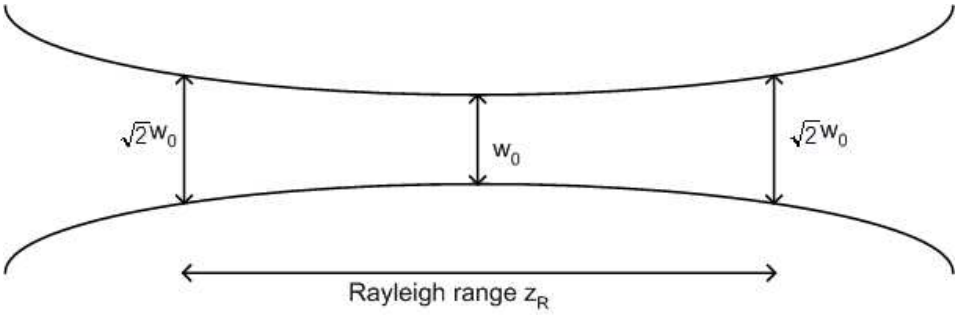


Figure 2.5: The Rayleigh range of a Gaussian laser beam

For any Gaussian beam the following relationship holds:

$$\omega(z) = \omega_0 \sqrt{\left(1 + \frac{z^2}{z_R^2}\right)} \tag{2.15}$$

and

$$z_R = \frac{\pi \omega_0}{\lambda} \tag{2.16}$$

where

z_R = Rayleigh range

ω_0 = Minimum beam waist

In the case of non-Gaussian beams, as mentioned above, the M^2 propagation constant is used. This value is a positive integer and describes the relationship of the real beam to an ideal Gaussian beam (M^2 for a Gaussian beam is unity). Thus, in the case of a real (non-Gaussian) beam, the Rayleigh range will be:

$$z_R = \frac{\pi \omega_0^2}{M^2 \lambda} \tag{2.17}$$

It can be shown that for any laser beam, the waist of the beam can be given by the following relationship:

$$\omega^2(z) = \omega_0^2 \left[1 + \left(\frac{z - z_0}{z_R}\right)^2\right] \tag{2.18}$$

where z_R, as before, is defined as the Rayleigh range and is given by *Equations 2.16* and *2.17*

Using this equation (*2.18*), one can experimentally work out parameters such as ω_0, z_0 and M^2 value of the laser beam. This is done by modifying this equation and putting it into the form $\omega^2(z) = az^2 + bz + c$. This exercise yields the following relationship:

$$\omega^2(z) = \left(\frac{M^4 \lambda^2}{\pi \omega_0^2}\right) z^2 - \left(\frac{2M^4 \lambda^2 z_0}{\pi \omega_0^2}\right) z + \left(\omega_0^2 + \frac{M^4 \lambda^2 z_0^2}{\pi \omega_0^2}\right) \tag{2.19}$$

By using a beam scanner, one is able to accurately find the energy distribution profile of the beam. One of the most common scanners used is a pin-hole scanner. A pin-hole scanner is a metal plate with a small pin-hole drilled into it. The hole has a nominal radius of 0.5 mm. The plate is then fitted in front of an energy meter and placed on an x,y,z translation stage, thus enabling the user to scan the entire area of the beam and along the length of the beam (*Figure 2.6*).

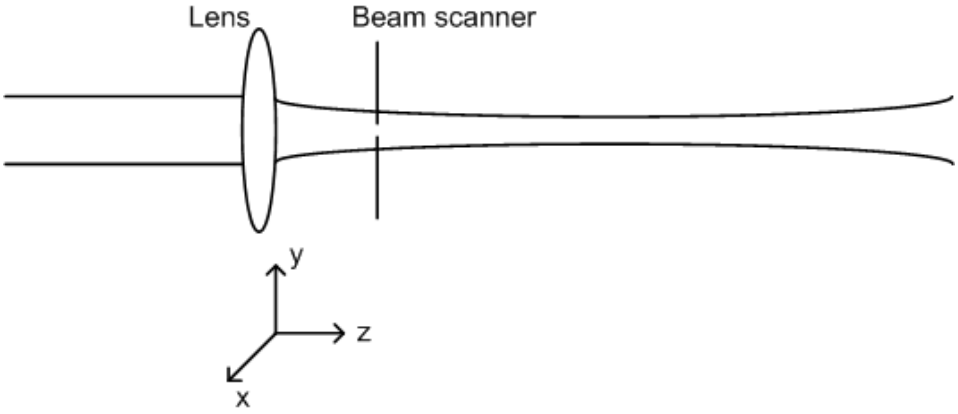


Figure 2.6: Set-up of beam and scanner

Once the beam radii have been experimentally ascertained, the beam parameters ω_0, z_0 and M^2 can be calculated using the following relationships:

$$z_0 = \frac{b}{2a}$$
$$\omega_0 = \sqrt{c - \frac{b}{2}}$$
$$M^2 = \frac{\pi}{\lambda}\sqrt{a\left(c - \frac{b}{2}\right)}$$

Where a, b and c are the coefficients of the quadratic $\omega^2(z) = az^2 + bz + c$

From all the above, it is evident that the key laser parameters that influence the formation of a laser-induced plasma are the wavelength, intensity and M^2 value of the beam. Although the wavelength of the beam is an important factor, it can be shown that the beam quality and intensity of the beam have a far more significant effect on the breakdown process.

2.3 Laser-induced plasmas

In the early 1960s it was noted that when a focused high powered laser beam interacted with air, a spark was generated at the focal point [1]. It was also noted that the plasma plume moved in a direction opposite to that of the laser beam. In other words it moved towards the focusing lens. In order to generate a spark in air, intensities in the order of 10-100 MW/cm^2 are required. These translate to electric fields of about 10^7 V/m (100 MV/m) [5]. The generation of a laser-induced plasma is also accompanied by high pressure shock waves. These waves can have velocities up to 1500 m/s [18].

The generation of a laser-induced plasma at the focal point of the lens can be thought of as the result of ionisation of air molecules. As with any transient phenomenon, one can identify four main stages:

1. Initiation
2. Formative growth
3. Plasma development
4. Extinction

The **initiation** stage is the time taken for a free electron to become available to start a breakdown process that will eventually lead to the formation of the laser-induced plasma. In essence, this stage can be defined as the time between the arrival of the laser pulse to the release of the free electrons and thus lead to the growth of the electron and ion concentrations. It has been found that for relatively short wavelengths such as those produced by Nd:YAG lasers (1 064 nm) this time lag is negligible. However when dealing with the longer wavelengths of a CO_2 laser (10.6 μm), it has been found that the time lag is not negligible.

The **formative growth** stage of the laser-induced plasma formation (as the name implies) refers to the time taken for the plasma to form and grow. During this stage an increase in the number of free electrons and ions is observed through cascade ionisation helped in some cases by the inverse Bremsstrahlung absorption process [5, 16]. Breakdown occurs when the concentration of free electrons reaches a critical level. It was found that the duration of the initiation and formative growth stages combined was in the region of a couple of ns.

Following the formative growth is the main **plasma development** phase of the process. This stage starts with the initial formation of a plasma and involves its development into a hot and highly conductive and ionised 'gas' which expands at a great rate.

In the final **extinction** stage, the plasma dies away as a result of diffusion, recombination and attachment of electrons and ions that were generated in the plasma. This continues until s state of electrical and thermal equilibrium is with the surrounding gas is achieved.

Knowing what the overall plasma life time is, is very important. Since the plasma formation is dependent on the intensity of the laser beam used, it follows that the plasma life time is also dependent on the intensity. This is useful information to know when trying and draw up the basic time line of events for a laser-triggered spark gap. In order to do this, one needs to understand how a laser-induced plasma is generated. Of the four phases mentioned above, the first three (initiation, formative growth and development stage) are the most relevant to the research presented in this thesis and are discussed below.

Multiphoton ionisation and the plasma initiation stage

As mentioned, when a laser beam is focused in air, a plasma is generated at the focal point of the lens. This means that the laser is able to successfully ionise air. However, if one considers the photon energy of a laser beam (a Nd:YAG laser with $\lambda = 1\ 064$ nm has a photon energy of 1.12 eV) it will be noted that it is much less than the ionisation potential of say, Nitrogen which is about 14.534 eV as can be seen from *Table 2.3*[2],

Table 2.3: Some common elements and their associated ionisation potentials

Element	**Ionisation potential [eV]**
H	13.598
O	13.618
N	14.534
He	24.587

[2]Taken from the 'Periodic Table of Elements' produced by Sargent-Welch

Taking the above fact into consideration, theoretically, the laser beam should not be able to ionise Nitrogen (or any of the gases shown in the). In order to achieve ionisation, the gas must absorb about 13 photons of wavelength 1 064 nm (1.12 eV/photon). This process is known as multiphoton ionisation [5, 17].

In any atom, there exist discrete energy states. A photon can be absorbed by the atom only if resonance is achieved between this photon with energy $h\nu$ and an allowed state. Multiphoton ionisation can be explained by the absorption of photons by so called 'virtual' states for a time $\Delta t \sim \frac{1}{\nu}$. This time Δt is governed by the uncertainty principle. For a photon of energy $2h\nu$, the absorption into a virtual state will happen in time $\Delta t \sim \frac{1}{2\nu}$. The number of photon absorptions per atom is given by:

$$k = \left\langle \frac{E_i}{h\nu} \right\rangle \tag{2.20}$$

where

E_i = Ionisation potential of atom [eV]

The angle brackets in *Equation 2.20* signify that k is the next larger integer. For example, for a Helium atom with an ionisation potential of 24.587 eV and for a YAG laser emitting at 1 064 nm, the number of photons absorbed per atom will be $k = \left\langle \frac{E_i}{h\nu} \right\rangle = \left\langle \frac{24.587}{1.1659} \right\rangle = 22$ photons.

During the multiphoton ionisation process, the following events take place:

1. Transition of atoms from the ground state to the 1st virtual state
2. Atoms naturally decay from the 1st virtual state to the ground state
3. Transition of atoms from the 1st virtual state to the 2nd virtual state and so on

If the atom has r=0,1,2...k energy states where r=0 is the ground state and r=k is the ionised state (r=1,2,3...k-1 being the virtual states) one can write down an equation for the rate of atoms in an rth virtual state:

$$\frac{df_r}{dt} = B_{r-1} f_{r-1} - f_r \lambda_r - B_r f_r$$

Where f_r denotes the fraction of atoms in the rth state, B_r is the number of transitions per unit time from state r to state r+1 and λ_r is the decay rate from

the rth state back to ground state (r=0). This expression can be simplified by considering that $\lambda_r >> B_r$, thus:

$$\frac{df_r}{dt} = B_{r-1}f_{r-1} - f_r\lambda_r$$

And for the kth state (ionisation) the expression becomes (since there are no transitions to a higher state than k):

$$\frac{df_k}{dt} = B_{k-1}f_{k-1} \tag{2.21}$$

By mathematically manipulating *Equation 2.21*, one can deduce the ionisation rate per atom which is given by

$$W_i = \frac{\sigma^k}{\nu^k(k-1)!}F^k \tag{2.22}$$

where

W_i = Ionisation rate per atom

σ = Photon absorption cross-section area of atom

F = Photon flux density (Photons/cm^{2}s)

Equation 2.22 shows that the key to starting a laser-induced plasma is the photon flux F. Since the photon flux is measured in photons/cm^2 is almost akin to the laser beam fluence (J/cm^2). When the time pulse is incorporated into the picture, it can be seen that once again, the laser beam intensity (W/cm^2) emerges as one of the most important laser beam parameters that influence laser-induced breakdown.

Formative growth and inverse Bremsstrahlung absorption

It is important to note that the multiphoton ionisation process plays an important role only in this first initiation stage of the plasma. The formative plasma growth on the other hand, relies heavily on a cascade ionisation process very similar to the classical Townsend breakdown mechanism for gap breakdown (see *Appendix A*). In fact, this electron cascade is assisted by the inverse Bremsstrahlung mechanism. Free electrons are able to absorb photons and gain energy (through inverse Bremsstrahlung absorption), assisting in the increase of the number of free electrons. It was found in fact that at very high intensities the effect of multiphoton ionisation decreases compared to that of cascade ionisation. It can also be shown that the

inverse Bremsstrahlung mechanisms is most effective when the product of the gas pressure P and the laser pulse width τ is greater than 10^{-7} ($P\tau > 10^{-7}$).

A criterion for cascade growth in gas can be expressed by the following relationship[16]:

$$\frac{d\varepsilon}{dt} = \frac{4\pi^2 e^2 I \nu_{eff}}{n_e c \omega_c^2} - \frac{2 m_e \nu_{eff} E_i}{M} \tag{2.23}$$

where

ε = Energy of free electrons
e = Electron charge
m_e = Electron mass
ν_{eff} = Effective electron collision frequency
n_e = Electron density
I = Laser beam intensity
ω_c = frequency of radiation (cyclic)
E_i = First ionisation potential
M = Mass of background gas neutral particle

The above equation simply states that the rate of change of free electron energy has to remain positive. In other words, the free electrons must keep on gaining energy in order to sustain a cascade ionisation growth.

Plasma development stage and shock waves

In the plasma development stage, as the name implies, the plasma rapidly grows in size as a highly conductive and hot expanding gas. In this stage powerful shock waves are generated that can radiate at high velocities symmetrically around the plasma core. However, the shock wave is more pronounced in the direction opposite to the direction of travel of the laser beam (shock wave moves towards the focusing lens) [18]. In fact, two separate waves have been observed relating to the formation of the laser-induced plasma. These are the above mentioned shock wave and a slower moving thermal wave.

Experimental studies [18, 19] have shown that the shock wave can reach velocities up to 1500 m/s with an average of about 460 m/s. As mentioned, this shock wave expands very symmetrically in all directions, but it is slightly more pronounced in the direction towards the focusing lens. On the other hand, the thermal wave generated during the plasma formation, is much slower. Velocities of about 40 m/s have been recorded (almost 10 times slower). Unlike the shock wave, the thermal wave is very

asymmetrical. It expands very fast in the x-direction (along the laser beam) towards the focusing lens (at approximately 40 m/s) in the direction of the lase beam (after the focal point) the velocity is much slower (about 4 m/s). In the y-direction, the expansion of the thermal shock wave is fairly symmetrical. It is important to note that during the formation of a laser-induced plasma, very high temperatures are developed. These can be between 10^4 to 10^5 K [18]. These temperatures are high enough to cause further ionisation of air (thermal ionisation)

Knowing the nature of any shock waves generated, helps to fully understand the process of laser-triggering of a spark gap and the effect the laser-induced plasma has (if any) on the resulting arc. It is known that air movement can affect the shape of a high voltage arc. It is therefore a distinct possibility that these shock waves can somehow influence the shape of the laser-induced plasma. A gated camera can be used in order to probe the interaction between the laser-induced plasma and the laser-triggered arc. In other words, the relationship between the plasma and the arc can be investigated by experimentally finding the spatial and temporal relationship between the two.

2.4 Conclusion

In this chapter, some laser fundamentals have been presented. This information will help the reader understand the phenomena and results presented and explained in the chapters to come.

In general, a focused high-power laser beam is able to generate a plasma in air. The generation of the laser-induced plasma depends on various laser parameters such as laser energy and pulse width, intensity, focusing lens and laser wavelength. Of these, the most critical parameter is the laser beam intensity. The higher the intensity, the easier a laser-induced plasma can be generated. A first approximation for the minimum intensity required for breakdown in air is 10-100 GW/cm^2.

The development of a laser-induced plasma can be described in four main steps: The initiation, formative growth, plasma development and extinction stages. Multiphoton ionisation is dominant in the first (initiation) stage where as the plasma growth stage is dominated by a cascade ionisation mechanisms assisted by the Inverse Bremsstrahlung process. During the plasma development stage, strong shock waves and thermal waves are generated. The shock waves have been found to be as fast as

1500 m/s (with an average of 460 m/s) whereas the slower moving thermal waves have a velocity of about 40 m/s.

In the following chapter, breakdown experiments using a pulsed YAG laser are presented. The aim of these experiments is to find experimentally what the minimum laser-induced breakdown voltage is for a Rogowski profile spark gap of varying gap lengths. These results can be applied to many high voltage triggering applications. They also provide useful insight into the plasma-arc interaction. A comparison of these voltages is made with U_{50} tests performed on the gap with an impulse generator producing a standard 1.2/50 μs lightning waveform.

Chapter 3

Breakdown experiments using an Nd:YAG laser

3.1 Introduction

In the previous chapter a basic overview of laser-related topics was presented. The effect of the important laser parameters such as wavelength, energy and intensity on the generation of a laser-induced plasma was described. The theory presented, is now put into practice in the following chapters. In particular, in this section, experiments using a YAG laser are described. The aim was to experimentally determine the breakdown voltage for a Rogowski profile electrode arrangement. In the experiments, an orthogonal gap arrangement was used as opposed to the more traditional coaxial geometry. The aim of the experiments is to explore the breakdown behaviour of this laser-triggered gap by evaluating its breakdown voltage range (ΔV_R). This range is defined as the difference between the breakdown voltage of the gap (V_B) minus the laser-triggered voltage obtained (V_L). In other words: $\Delta V_R = V_B - V_L$. The laser-triggered voltage can also be expressed as a percentage of breakdown voltage: $\%V_L = \frac{V_L}{V_B} \times 100$. In the experiments, breakdown voltage of the gap was measured for varying Q-switch delay which translates to a varying laser beam intensity. The position of the laser-induced plasma was also varies vertically along the axis of the gap. By knowing how the orthogonally laser-triggered Rogowski profile gap behaves under varying intensity and plasma position, one is able to gain the insight needed in order to explain the results obtained during the gated camera work to be presented in the next chapter.

3.2 Experimental setup

The experimental setup used can be seen in *Figure 3.1*

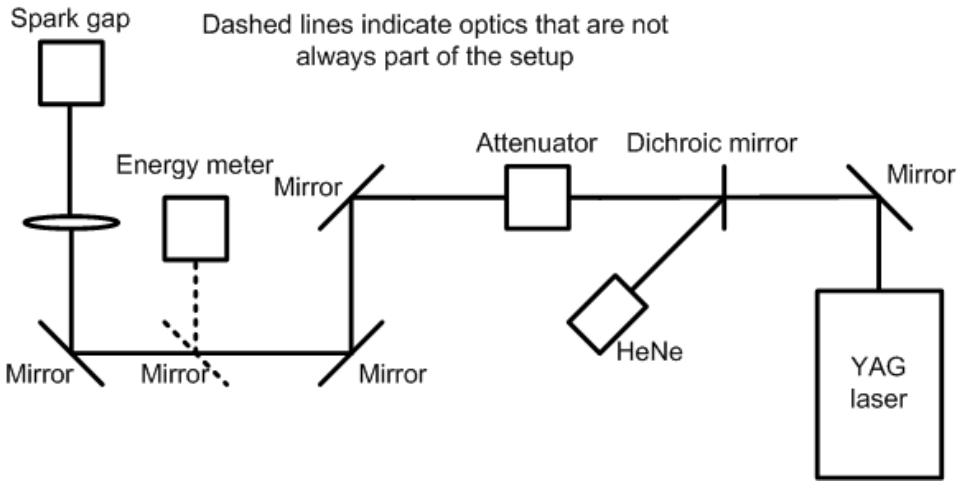


Figure 3.1: Optics set-up for breakdown experiments with YAG laser

In this figure, the main laser is a Q-switched, flash-lamped pumped Nd:YAG laser (Continuum, Powerlite) operating at the fundamental frequency of 1 064 nm. The linearly polarised output beam could be varied in both energy and pulse width through adjustment of the Q-switch delay. The repetition rate of the laser was set at a fixed 10 Hz throughout the experiments. A visible Helium Neon laser was aligned collinear to the Nd:YAG laser for ease of optical alignment. The laser beam passed through two Brewster windows which could be rotated, thus allowing energy attenuation external to the laser cavity. A pop-up mirror allowed for the laser beam to be directed to laser diagnostics: laser pulse duration was measured with a fast Si photodiode (ThorLabs, model DET210) and an energy meter (Gentec, model ED200) was used to determined the total pulse energy.

With the pop-up mirror in the down position, the laser beam was delivered to a final focussing lens (uncoated quartz, plano-convex) for plasma generation. The spot size at the focus could be changed by altering the focal length of the lens. The electrodes of the spark gap had a Rogowski profile and were arranged in such a way so as to allow the laser beam to intersect the gap axis at right angles. Rogowski profiles were used in order to create as uniform a field as possible in the spark gap. The vertical position of the focal point in the gap was varied by adjusting the height of the spark gap off the laser table, at a fixed gap length of 30 mm. The DC voltage applied

to the spark gap was monitored by means of a Fluke 80K-40 high voltage probe. The Rogowski profiles were constructed from Aluminium with a Tungsten-Carbide coating. All experiments presented were performed in air at atmospheric pressure and at an average temperature of 18°C[1]. Experiments were performed at an altitude of 1400 m above sea level (at the NLC, in Pretoria, South Africa).

Before conducting the main breakdown experiments, a series of experiments was performed in order to calibrate the measuring equipment and the YAG laser. The variation of pulse width and energy with varying Q-switch delay together with the linearity of the energy meter was tested. In *Figure 3.2*, one can see the variation of laser energy and pulse width (FWHM) with varying Q-switch delay.

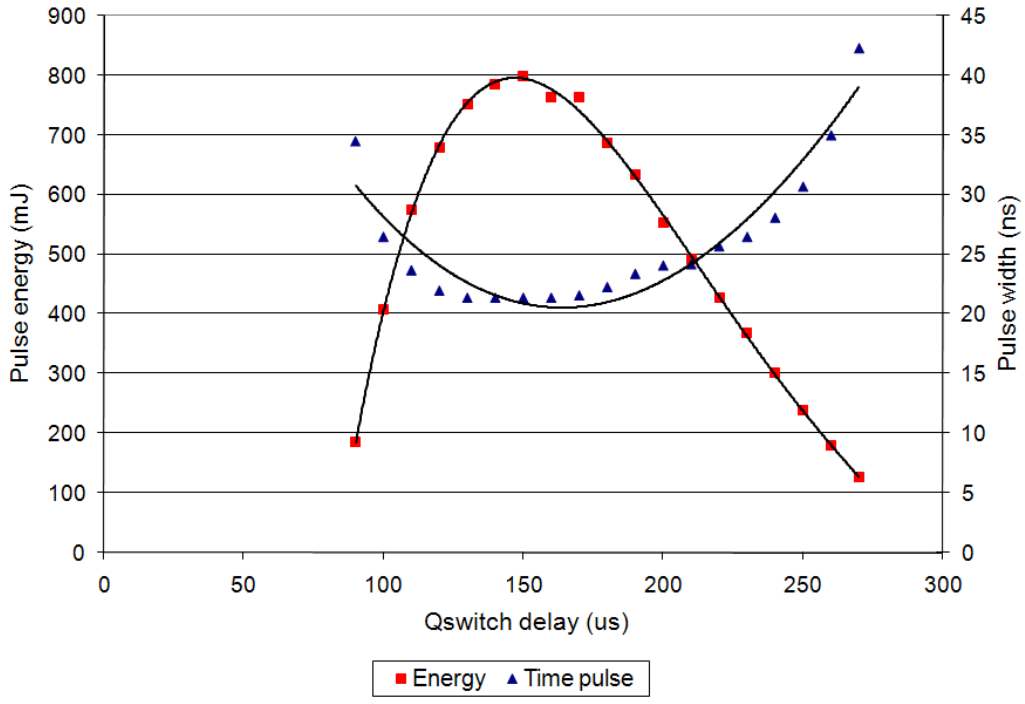


Figure 3.2: Variation of laser energy and pulse width with Q-switch delay

From this figure, one can easily see that the optimum Q-switch value was found to be around 150 μs. At this Q-switch value, the laser energy and time pulse are 800 mJ and 20 ns respectively.

Two main experiments were considered: The first involved measuring the breakdown voltage achieved for different values of Q-switch delay (with the laser induced plasma

[1]For these experiments, the average atmospheric conditions were: 18°C, 37% Humidity, 870 mbar Pressure

directed at 90 degrees to the gap axis and focused at the centre of the gap). This experiment was conducted for lenses with 3 different focal lengths. The second set of experiments involved varying the position of the laser-induced plasma along the gap axis and measuring the breakdown voltage achieved. This was also done for 3 different lenses (150, 200 and 250 mm).

3.3 Variation of breakdown voltage with Q-switch

As mentioned, in these experiments, the aim was to evaluate the breakdown voltage for a 30 mm Rogowski profile spark gap for various values of Q-switch delay ranging from about 90 μs to about 270 μs. The resulting values were plotted and compared to the pulse width – Q-switch and energy – Q-switch curves obtained.

The laser operated at a 10 Hz repetition rate. Each experiment was conducted as follows: The spark gap was charged to a certain voltage. The laser was then fired for a period of 30 seconds. This is equivalent to 30 s $\times$ 10 Hz = 300 laser shots. The experiment was stopped when laser-induced breakdown of the gap was observed. If after 30 s no breakdown was observed, the voltage was raised until breakdown occurred. In the case of breakdown, the voltage was then lowered until the minimum breakdown voltage conditions were reached. As the main aim of this thesis is the interaction between the laser-induced plasma and the laser-triggered spark, the time delay between application of the laser beam and breakdown of the gap is very important. This question is further addressed in *Chapter 4*.

This experiment was then repeated for 3 different lens focal lengths. These were 150, 200 and 250 mm.

The resulting graph of breakdown voltage vs. Q-switch delay for the laser can be seem below in *Figure 3.3*

This graph shows what is expected: That is that the breakdown voltage at low and very high Q-switch values is very high. This is due to the low laser beam intensities at very low and very high Q-switch values.

From this graph, it can be seen that for optimum Q-switch delay, the breakdown voltage achieved was in the region of 17 kV. In fact, for the three different lenses used, the breakdown voltages achieved can be seen in *Table 3.1*

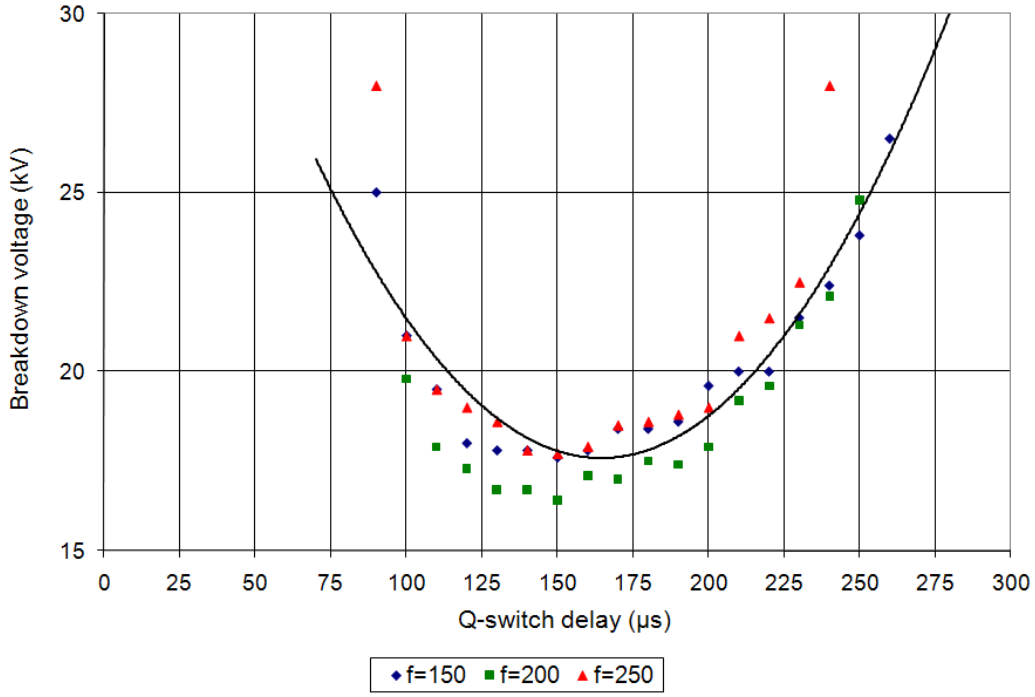


Figure 3.3: Variation of breakdown voltage width with Q-switch delay

Table 3.1: Minimum breakdown voltages achieved for three different focal lengths

Focal length [mm]	**Breakdown voltage [kV]**
150	17 ± 1 kV
200	16 ± 1 kV
250	17 ± 1 kV

Taking into account that the breakdown strength of air is about 2.7 kV/mm [2], the spark gap in question (30 mm gap) has a breakdown voltage of about 81 kV. The breakdown voltage range achieved is therefore $\Delta V_R = V_B - V_L$ or ΔV_R=81-17=64 kV or as a percentage of breakdown voltage: $\%V_L = \frac{V_L}{V_B} \times 100$ therefore $\%V_L$=$\frac{17}{81}\times$ 100=20% of the self-breakdown voltage of the gap (81 kV[3]). *Table 3.2* shows these results in summary:

It is known that the peak power of a laser beam is given by the relationship $P_{pulse} = \frac{E_T}{\tau}$ and that the peak intensity of the laser beam is the peak power per cm^2 (τ is the FWHM time pulse of the laser beam).

[2] see *Appendix A*

[3] This value is calculated taking into account the brteakdown strength of air – using the value of 2.7 kV/mm: 2.7 kV/mm × 30 mm = 81 kV

Table 3.2: Breakdown ranges achieved with a focused laser beam

Focal length [mm]	**Breakdown voltage range [kV]**	**% Breakdown voltage**
150	64	20
200	65	19.7
250	64	20

Experimentally, the beam diameter of the beam was measured with a slit scanner and found to be approximately 8 mm. This means that the beam radius is 4 mm (or 0.4 cm). This translates to a beam area of $A = \pi \times 0.4^2 = 0.52$ cm^2. Therefore, the peak intensity of the laser beam can easily be calculated and plotted for each value of Q-switch. (*Figure 3.4*)

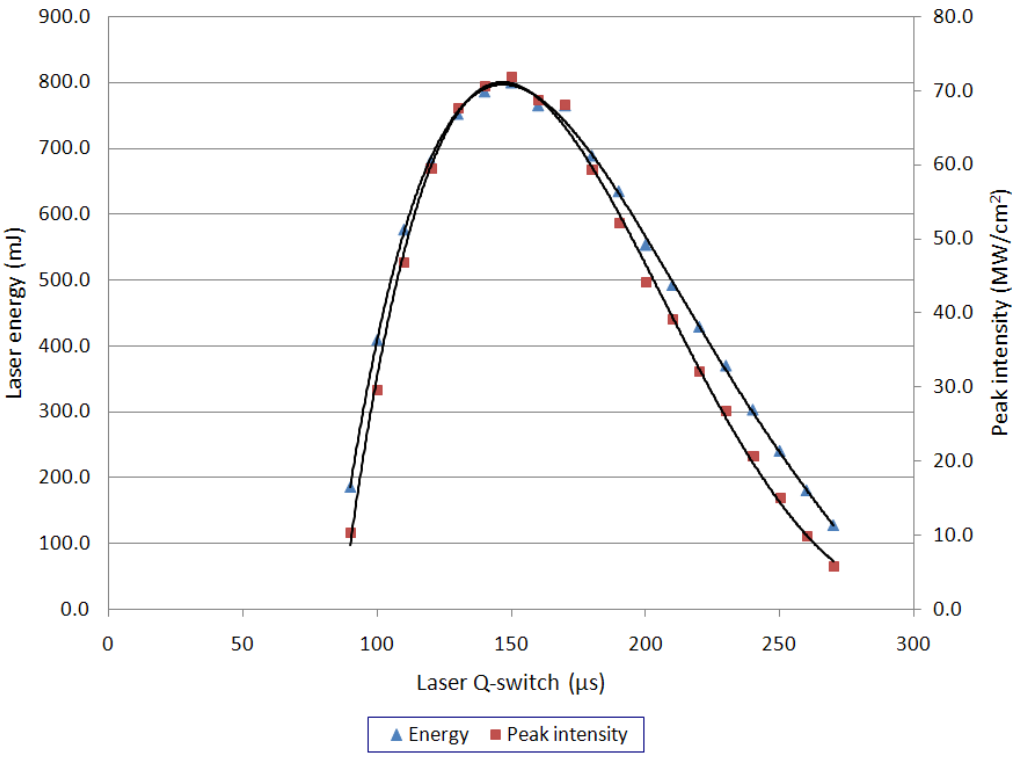


Figure 3.4: Variation of laser energy and peak intensity with Q-switch delay

The peak intensity and the breakdown voltage can be plotted say for the 150 mm lens used vs. the Q-switch delay. This can be seen in *Figure 3.5*

From *Figure 3.5* it is quite evident that the breakdown voltage is dependant on the

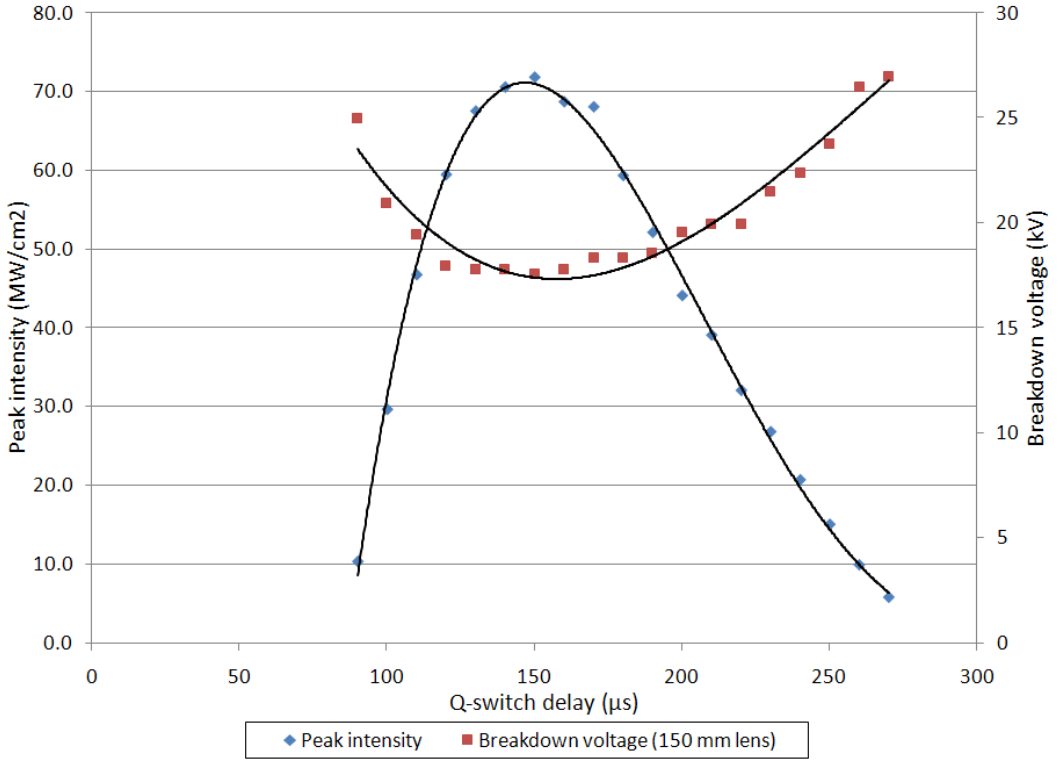


Figure 3.5: Variation of peak intensity and breakdown voltage with Q-switch delay

the laser beam intensity. As the intensity increases with increasing Q-switch delay (until the optimal value of 150 μs) so does the breakdown voltage decrease to some minimum value. The inverse happens for Q-switch values that are greater than the optimum delay.

By examining the graph of *Figure 3.3* one makes the following important observations:

- For Q-switch values $70 \leq$ Q-switch < 150 μs the breakdown voltage decreases as the intensity increases. The gradient of the decrease in breakdown voltage is similar to that of the increase in intensity
- For Q-switch values $150 \leq$ Q-switch ≤ 270 μs the breakdown voltage increases as the intensity decreases. The gradient of the increase in breakdown voltage is similar to that of the decrease in intensity

This can be shown by taking a simple linear approximation of the intensity and breakdown voltage graphs for the two above mentioned sections ($70 \leq$ Q-switch < 150

and 150 $\leq$ Q-switch $\leq$ 270 μs). One then can compare the four resulting gradients. This can be seen in *Figure 3.6*

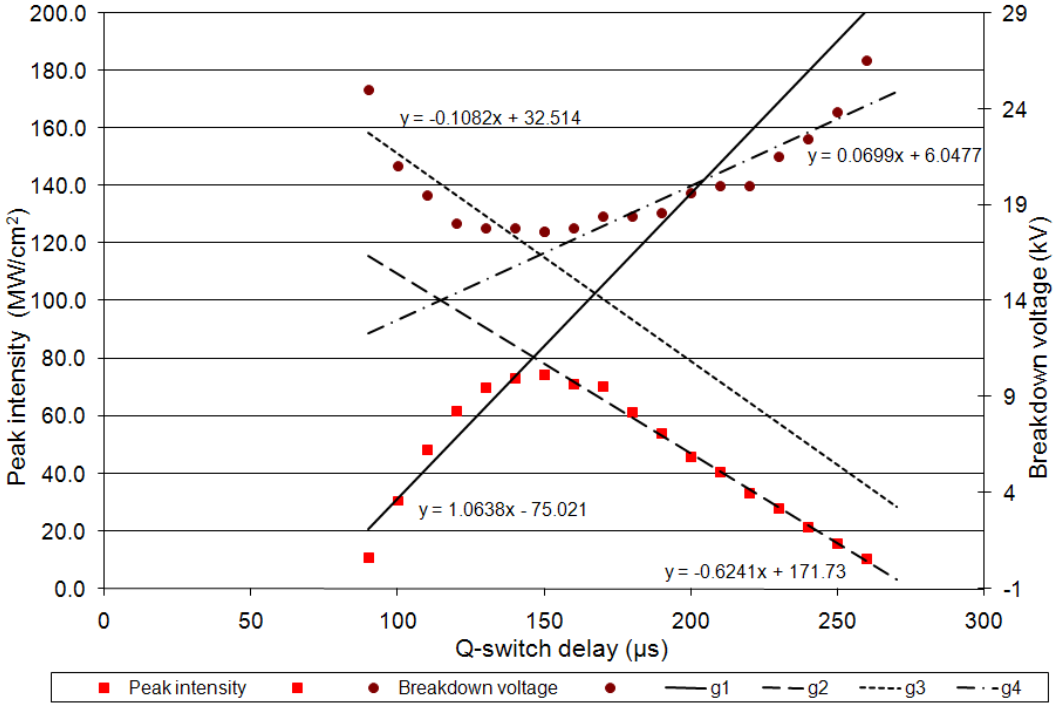


Figure 3.6: Gradients of peak intensity and breakdown voltage plots

From *Figure 3.6* it can be seen that the gradients g1, g2, g3, and g4 are as follows:

Table 3.3: The four gradients of the intensity and voltage graphs

Gradient name	**Value**
g1	1.0638
g2	-0.6241
g3	-0.1082
g4	0.0699

From the *Table 3.3* it is evident that the two pairs g1 and g3 and g2 and g4 are similar but not identical.

One can also use the correlation function to evaluate the correlation coefficient ρ_{xy} for the two sets of data (Q-switch, I(Q-switch)) and (Q-switch, V(Q-switch)) as can be seen in *Equation 3.1* for two variables x and y.

$$\rho_{xy} = \frac{\sum(x-\overline{x})(y-\overline{y})}{\sqrt{\sum(x-\overline{x})^2 \sum(y-\overline{y})^2}} \tag{3.1}$$

The correlation coefficients for the three different focal lengths used (150, 200 and 250 mm) can be seen in *Table 3.4*

Table 3.4: Correlation coefficients for the three different lenses used

Focal length f [mm]	**Correlation coefficient**
150	-0.940
200	-0.922
250	-0.885

From *Table 3.4* it can be seen that the correlation between the change in peak intensity and the breakdown voltage is relatively high. The average correlation of the three cases is -0.915 or (91.5%) similar. This shows that the breakdown voltage is indeed strongly dependent on the intensity of the laser beam.

3.4 Variation of breakdown voltage with changing plasma position

The next set of experiments involved changing the position of the laser-induced plasma in the spark gap and finding the breakdown voltage for each position of the plasma. This was achieved by raising or lowering the spark gap (by means of a suitable lab-jack) so as to place the focal point of the lens at a different point along the gap axis. The plasma was moved with millimetre resolution. Once again, an orthogonal spark gap and laser geometry was used. The voltage breakdown was measured according to the above-mentioned procedure (in section 5.3). The gap geometry can be seen in *Figure 3.7*

The experiments yielded the following results for all three different focal lengths. These can be seen in *Figure 3.8*.

From this graph (*3.8*) one can see an interesting trend: When the plasma is focused at y=-15 mm with respect to the gap axis mid-point (plasma on the surface of the cathode) the resulting breakdown voltage is relatively high (around 30 kV). As the plasma approaches the gap axis mid-point (y=0 mm) the laser-induced breakdown

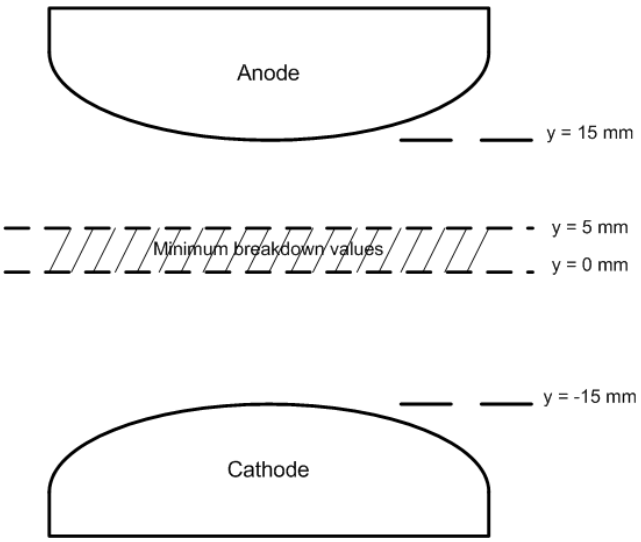


Figure 3.7: Gap set-up for plasma position variation experiments

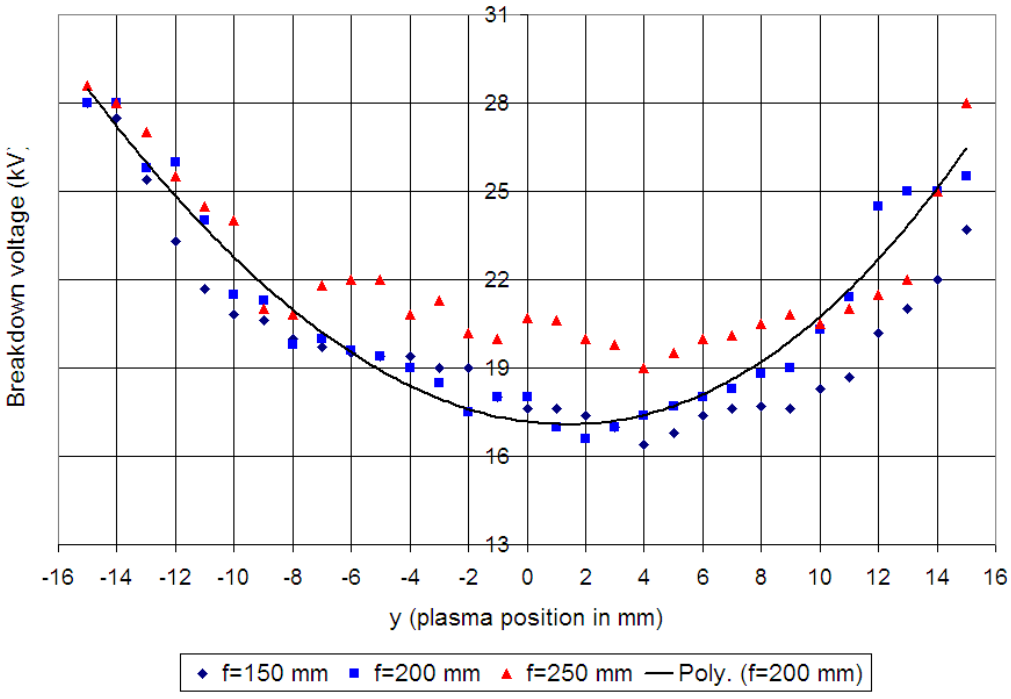


Figure 3.8: Variation of breakdown voltage with plasma position

voltage decreases to a minimum (approximately 17 kV). For values $0 < y < 15$ mm, the voltage increases again until it again reaches a maximum at the surface of the anode (26 kV). This behaviour can be explained by taking into account the streamer and Townsend criteria for breakdown in short gaps.

When the laser-induced plasma is positioned close to the anode, the free electrons that are made available are re-absorbed by the anode before an electron avalanche can develop. Thus, the gap breaks down with difficulty, resulting in a high breakdown voltage. On the other hand, when the plasma is located close to the cathode, the free electrons are readily accelerated by the electric field in the gap. However, the avalanche has to cross the entire gap in order for electric breakdown to occur. This once again leads to high breakdown voltages. It follows that somewhere in the middle of the gap, a balance exists where the conditions are correct for sustained electron avalanche to occur and lead to gap breakdown. This is mirrored in the graph, since it can be seen that roughly at y=0 mm the voltage is at a minimum of 17 kV.

Another way of looking at the problem is to consider the following scenario: The effect that laser-induced plasma has on the spark gap is that of a field-distortion. The electric field of the laser-induced plasma itself is very high. The transient presence of such a field in the spark gap, will have the effect of distorting the existing field to such an extent, that breakdown of the gap is the net result.

3.5 Maxwell simulations

A set of simple Maxwell simulations [4] were conducted. The model used in Maxwell can be seen below in *Figure 3.9*.

The electrode dimensions were chosen to be as close to the dimensions of the actual electrodes used. These can be seen in *Figure 3.10*. In the simulations the electrode material that was chosen was Aluminium. The gap length was set at 30 mm.

When air is ionised (by a high energy laser pulse or otherwise) a high density of charge carriers is produced. These charge carriers are made up of free electrons and positive ions. Thus, the laser-induced plasma is electrically neutral. This means that the plasma cannot be simulated as a purely positive or negative charge. The main difference between the two types of charge carriers (apart from their charge) is their mass. Electrons are much lighter than the positive ions. Thus, during the formation of a laser-induced plasma, regions of positive and negative space charge are set up. In the simulations, the laser-induced plasma was simulated as two coaxial cylinders each bearing a certain charge. This can be seen in *Figure 3.11*

[4] Ansoft Maxwell SV, www.ansoft.com/Maxwellsv/

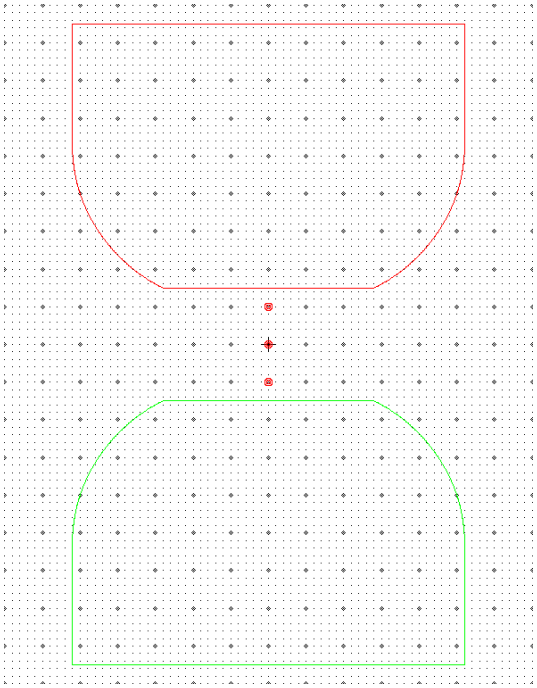


Figure 3.9: Maxwell model for E-field vs. plasma position simulations

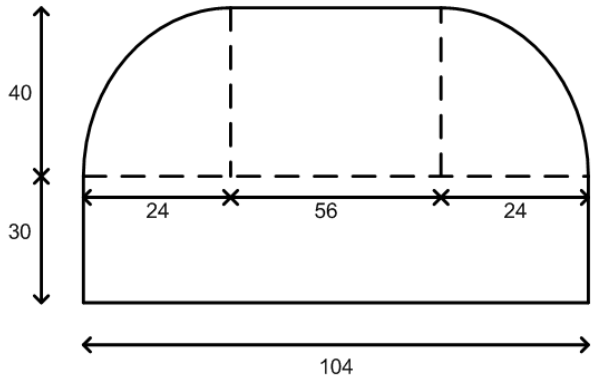


Figure 3.10: Dimensions used for the simulation of the spark gap electrodes. All dimensions in mm

The dimensions for the plasma simulation can be seen in *Figure 3.12*

From experiments, it was found that a typical laser-induced plasma has an electron density of about 7×10^{17} cm^{-3} [20]. It is known that the charge of an electron is -1.67×10^{-19} C. Experimentally, the laser-induced plasma was found to be roughly cylindrical with the following dimensions:

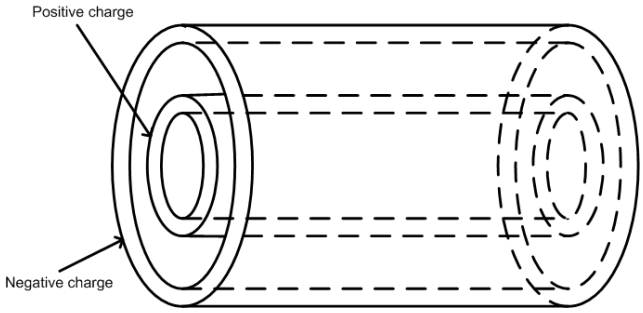


Figure 3.11: Model used for the laser-induced plasma

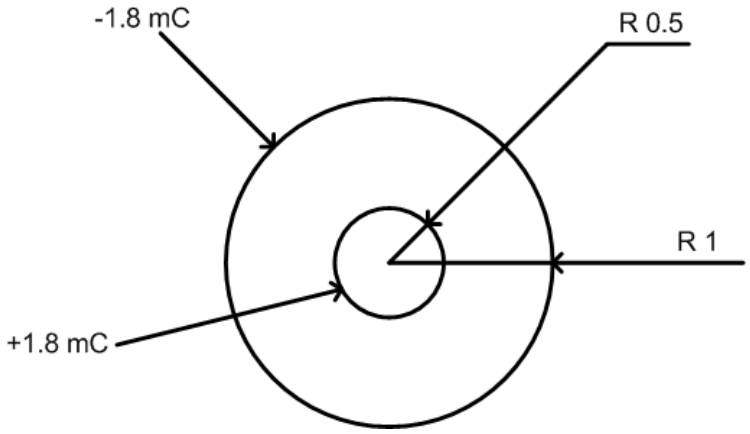


Figure 3.12: Dimensions used for the laser-induced plasma – all dimensions in mm

- Plasma diameter: 2 mm
- Plasma length: 5 mm

The volume of the plasma can then be calculated as $Vol = \pi r^2 h$ or $Vol = \pi \left(\frac{(0.2)}{2}\right)^2 \times (0.5) = 15.7 \times 10^{-3}$ cm^3. This means that the total electron charge of the plasma is Q_{plasma}=-1.8 mC. Therefore, in the simulations, the outer sheath was given a charge of -1.8 mC and the inner sheath, a charge of +1.8 mC thus ensuring the neutrality of the plasma. The magnitude and the vector of the electric field in the gap was plotted.

To verify the model, a number of simulations were done. Three simulations were done:

- Verification of electric field in the gap

- Inability of a laser-induced plasma to cause breakdown when a voltage of 1 kV is applied across the 30 mm gap
- Ability of a laser-induced plasma to cause breakdown when a voltage of 50 kV is applied across the 30 mm hap

3.5.1 Electric field verification

In the simulations a field of 20 kV was applied across the gap and the field magnitude and vector were plotted. For a gap length of 30 mm, the electric field was expected to be $E = \frac{V}{d} = \frac{20\times10^3}{30\times10^{-3}} = 667$ kV/m

The simulations showed exactly that. This can be seen in *Figure 3.13* and *3.14*

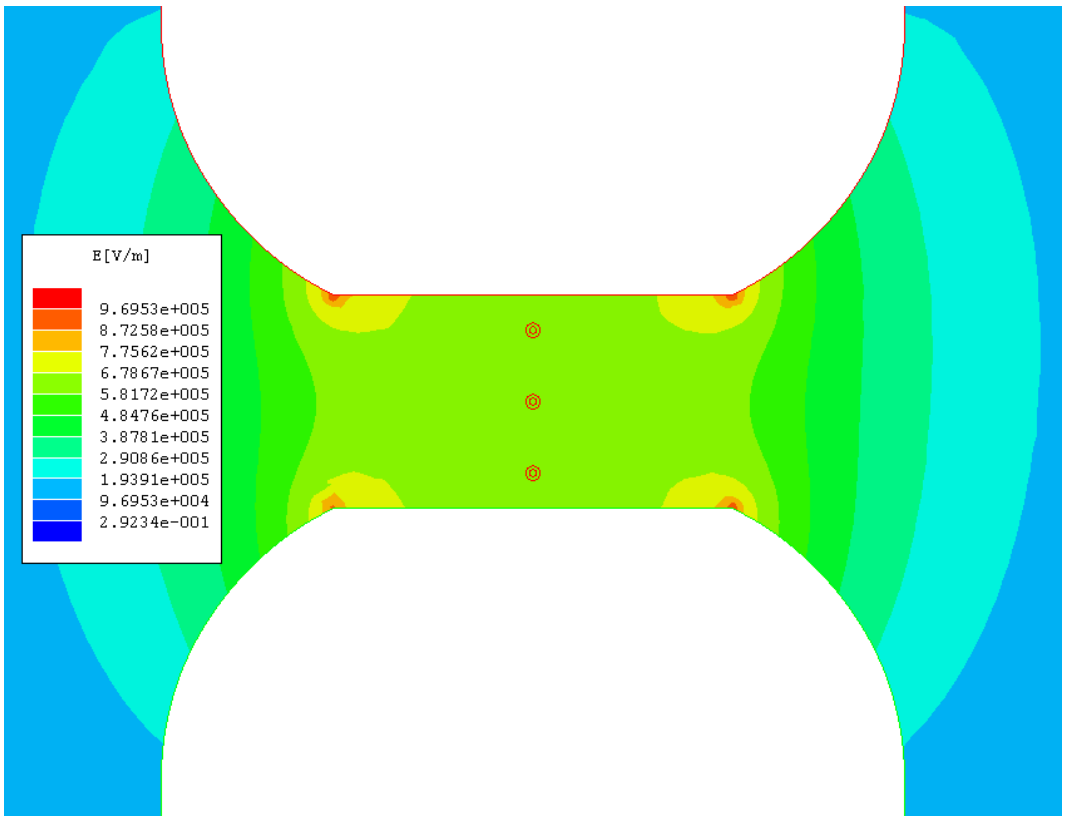


Figure 3.13: Plot of Electric field magnitude for a gap of 30 mm with a voltage of 20 kV applied across it

From these two figures (*3.13*) and *3.14* it can be seen that the calculated electric field in the gap is between 5.8 $\times$ 10^5 V/m and 6.7 $\times$ 10^5 V/m which correlates with

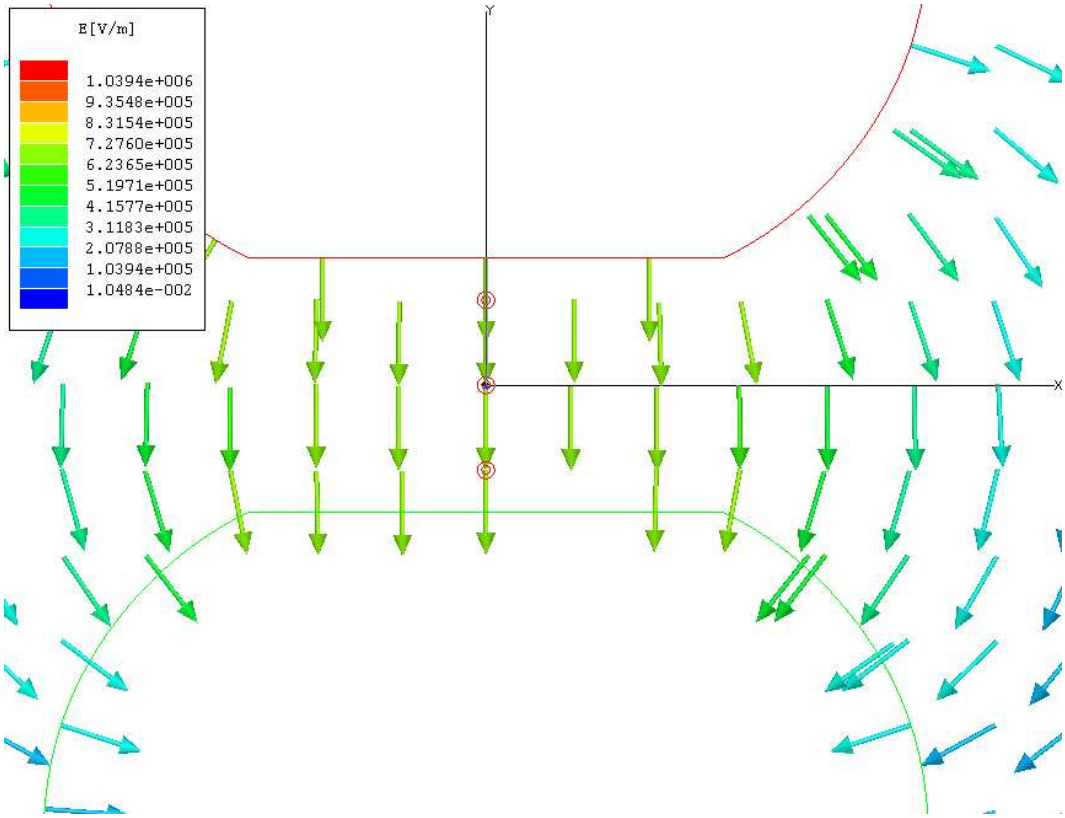


Figure 3.14: Plot of Electric field vector for a gap of 30 mm with a voltage of 20 kV applied across it

the theoretically predicted value of 667 kV/m.

3.5.2 Application of laser beam with 1 kV across the gap

If 1 kV is applied across 30 mm, the electric field is not high enough to allow laser-induced breakdown of the gap. The background electric field should be $E = \frac{V}{d} = \frac{1\times10^3}{30\times10^{-3}} = 33$ kV/m. Air breaks down at a value of 27 kV/cm or 2.7 MV/m. The simulation results can be seen in *Figure 3.15*. In this figure, the Electric field vector was plotted.

Once again, it can be seen from the simulation that the electric field magnitude in the gap is between 5.6×10^3 V/m and 1.4×10^5 V/m (mid value of 72 kV/m) which is much lower than the required 2.7 MV/m. This shows that the laser should not be able to break down a gap across which an electric field of 33 kV/m is applied.

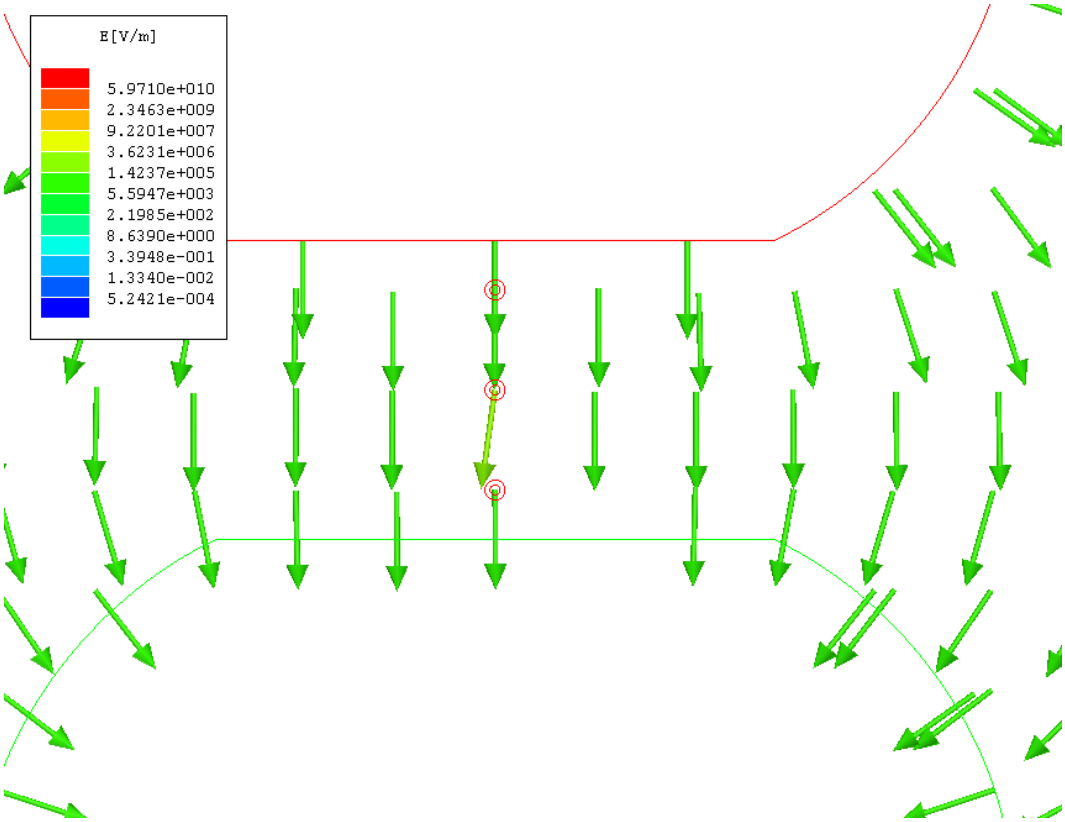


Figure 3.15: Electric field vector for attempted laser-induced breakdown of a 30 mm gap with 1 kV applied across it

3.5.3 Application of laser beam with 50 kV across the gap

Experimentally, it was verified that application of a laser beam in a 30 mm gap across which 50 kV is applied should lead to electrical breakdown. The background field in this case is $E = \frac{V}{d} = \frac{50\times10^3}{30\times10^{-3}} = 1.67$ MV/m. The electrical field vector was once again plotted. This plot can be seen in *Figure 3.16*

Once again, it can be seen that the magnitude of the electric field is between 5.5 $\times$ 10^3 V/m and 1.0 $\times$ 10^7 V/m (mid value of 5.2 MV/m). This value is much greater than the required 2.7 MV/m required to breakdown air. This shows that a laser-induced plasma is able to breakdown a 30 mm gap with an electric field of 1.67 MV/m.

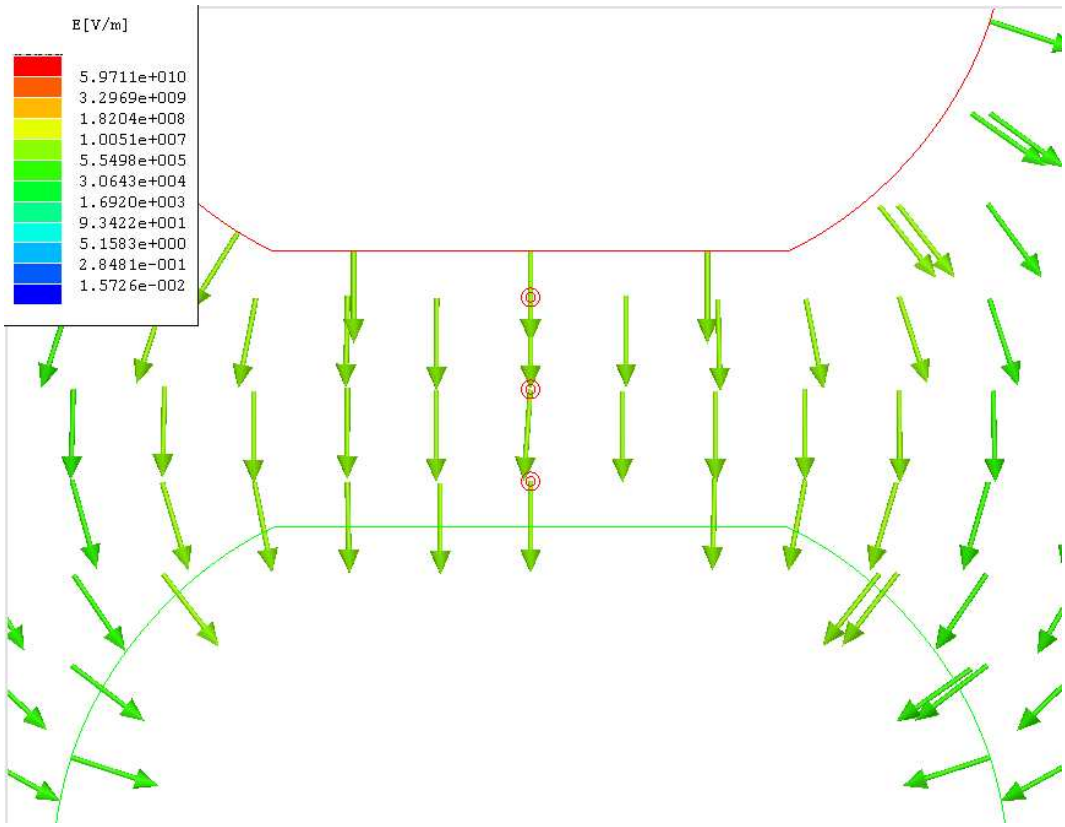


Figure 3.16: Electric field vector for attempted laser-induced breakdown of a 30 mm gap with 50 kV applied across it

3.6 Effect of the lens focal length on the breakdown voltage

As mentioned, the breakdown experiments were performed for three lenses of different focal lengths (150, 200, 250 mm). It is important to note what effect the focal length of the lens used has on the laser beam intensity and hence on the breakdown voltage achieved.

It is known that for a laser beam, the spot size at the focal point (which will in turn determine the beam intensity at this point) is given by *Equation 2.12 and 2.13* described in Chapter 3:

$$I_0 = \frac{2E_T}{\pi\omega_f\tau}$$

Where ω_f is given by:

$$\omega_f = \frac{M^2\lambda f}{\pi\omega_0}$$

By normalising the equations above for a focal length of 150 mm (assuming that the beam radius and intensity are 1) and by simple algebraic manipulation, one can draw up *Table 3.5* [21]

Table 3.5: Comparison of focal lengths, beam radius and peak intensity

Focal length f [mm]	**Beam radius ω_f**	**Peak intensity I_0**
150	1.00	1.00
200	1.33	0.56
250	1.67	0.36

From *Table 3.5* one can see that an increase in focal length from 150 to 250 mm increased the beam radius by a factor of 1.67 and reduced the peak intensity by a factor of 0.36. From *Figure 3.3* it can be seen that there is no significant change in breakdown voltage with varying lens focal length. This shows that although the focal length of the lens used does indeed affect the intensity and the beam radius, it does not affect it enough to produce a significant change in breakdown voltage. A much greater change in focal length is required to have an effect on the breakdown voltage achieved.

3.7 Conclusion

In this chapter, laser-induced breakdown experiments were performed using a high-powered Nd:YAG laser operating at 1 064 nm with a pulse energy of 800 mJ. The aim of the experiments performed was to determine if the breakdown voltage of the gap is a dependent on parameters such as the intensity of the laser beam, the focal length of the lens used and the position of the laser-induced plasma in the gap. Experiments showed that the measured breakdown voltage is definitely a function of the laser beam intensity. In fact, it was shown that the laser beam intensity is one of the most important parameters that govern the generation of a laser-induced plasma. It was also shown that the plot of the breakdown voltage vs. the Q-switch delay for the YAG laser used, showed marked similarities to that of the energy (and peak power) vs. Q-switch delay. It follows that the higher the laser beam intensity, the easier it is to achieve electrical breakdown in the gap. A breakdown range of about 64 kV was achieved. This result is significant since the minimum breakdown voltage was found to be 17 kV for a 30 mm Rogowski profile gap.

Experimentation showed that the key parameter that governs the effectiveness of the breakdown process is the laser beam intensity. The gap length and the position of the plasma within the gap also play an important role. Electrical breakdown can be thought of as a result of a severe modification of the background field. This field modification is a direct result of the appearance of the laser-induced plasma. The focal length of the lens used did not affect the breakdown results dramatically. From the above it can be seen that an orthogonal laser-triggering geometry is a very efficient and effective way of triggering a spark gap over a very wide range of voltages. An orthogonally triggered spark gap is also more versatile and easier to construct than the more intuitive coaxial arrangement. This is a very useful consideration that one can take into account when designing remote-triggered wide-range laser-triggered spark gaps.

Thus, the behaviour of a simple 30 mm Rogowski profile gap under varying laser beam intensity and plasma position has been investigated. In the following chapter, experiments involving the spatial and temporal relationship between the laser-induced plasma and laser-induced arc are presented. Two gated cameras are used in the experiments in order to obtain images of laser-induced breakdown. The nature of this relationship is explored and possible explanations are presented.

Chapter 4

Gated camera experiments

4.1 Introduction

In the previous chapter, experiments involving the parameters that govern the laser-induced breakdown voltage were presented. These parameters include the position of the plasma in the gap, the intensity of the laser beam and the focal length used. It was shown that the laser beam intensity is one of the most important parameters that influence the ability of a laser beam to breakdown a spark gap. Thus, through the experiments performed, the behaviour of a laser-triggered spark gap was described. This is important for the next set of experiments. The aim of these experiments is to probe and explain phenomena observed during the interaction of a laser-induced plasma and the laser-triggered arc. These experiments are presented in this chapter. A nanosecond gated camera was used in order to observe the development of the laser-induced plasma and also the interaction of this laser induced plasma with the resulting high voltage arc that bridges the gap. The aim of the experiments was to try and draw analogies between the presence of a floating object and the laser-induced plasma in the spark gap and to explore the spatial and temporal relationship between the laser-induced plasma and the resulting laser-triggered arc. It is known that the presence of a conducting object in a spark gap reduces the breakdown voltage of the gap. The same applies for a laser-induced plasma. To what extent are these two cases the same or differ?

4.2 Experimental setup

For the experiments described in this chapter, the same orthogonal, Rogowski profile spark gap described in the previous chapter was used. The gap spacing was set to 30 mm. The difference being that now, a gated camera (Xybion, model ISG-250) was used to observe the temporal and spacial development of the laser-induced plasma. The camera and optics were arranged in such a way as to allow a 'head-on' and a 'side' view of the plasma and the high voltage arc. This was achieved by using the pop-up mirror labelled in *Figure 4.2* as Mpu1. This will allow the beam enter the spark gap at an angle of 90 ° to the initial direction of travel. The gate of the camera was fully adjustable. However, for the purposes of the experiments, a 50 ns gate time was chosen. This gate was delayed relative to the laser pulse by means of a Stanford Delay Generator (model DG-535). The block diagram, timing diagrams and optical setup for this experiment can be seen in *Figures 4.1* and *4.2*

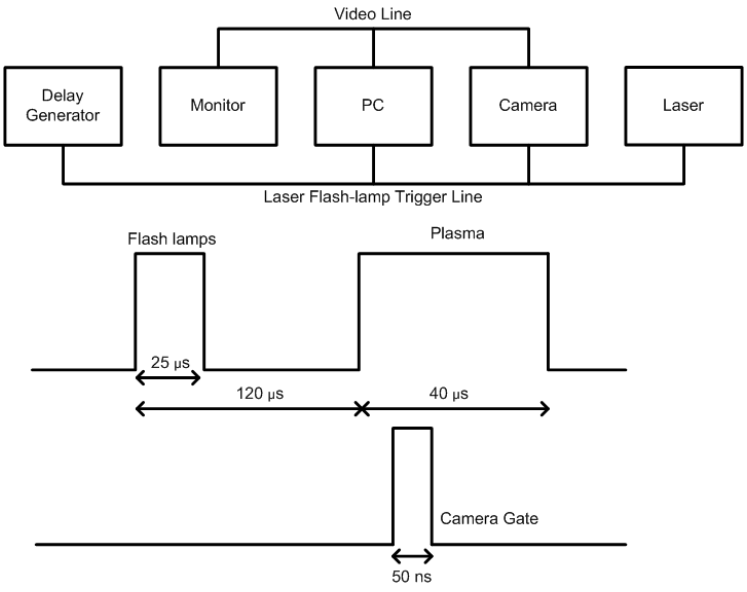


Figure 4.1: Camera, delay generator, laser block and timing diagrams

In order to ensure that the camera did not saturate, the following procedure was performed: the brightest image of the plasma formation was determined and the camera gain reduced until the saturation was minimised. All further images were recorded at this gain setting. The images obtained by this process were stored and post-processed in order to obtain key-features. The angle α between the gap centre line and the camera is very important. The smaller the angle the better. The ideal position for the camera would be 'head-on', in other words, directly in line with the

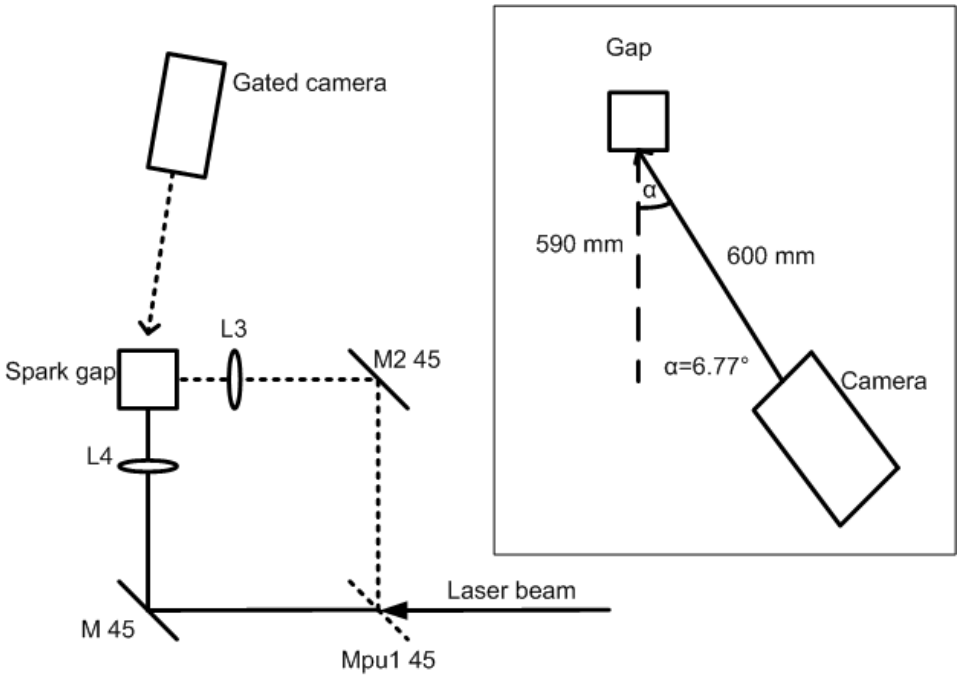


Figure 4.2: Camera angles and optical setup

laser beam and the spark gap. However, this could damage to the camera. An angle α=6.77 degrees was chosen. This allows the camera to be as close as possible to the laser beam direction of travel and far enough to protect the camera.

In terms of the electrical side of the experiments, the half-wave circuit shown in *Figure 4.3*.

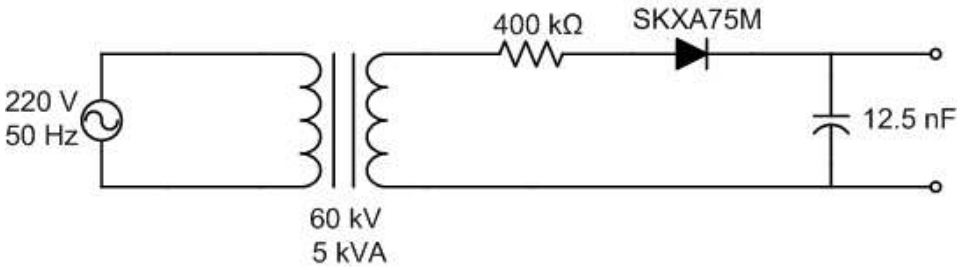


Figure 4.3: High voltage generator used in the experiments

For comparison, the Spellman DC generator was also used in conjunction with a gated camera with μs resolution (Cook Corporation FlashCam Pro). With this camera, the gate time could be varied from 1 μs to 999 μs in 1 μs increments. The gate was shifted in time by means of a Stanford delay generator. The camera

was triggered whenever the laser Q-switch was fired. For this reason, the laser was operated in 'single shot' mode.

4.3 Spark gaps and conducting floating objects

When one or more conduction floating objects are suspended in a spark gap, its breakdown strength is reduced [22, 23]. Most of the work has been done for the case of leader breakdown in long gaps. The reduction in breakdown voltage due to a conductive floating object is also evident in short gaps where the streamer process is prevalent.

A floating conductive object is suspended in a spark gap can be thought of as a 'bridge' between the two electrodes. The more objects exist in the gap, the lower the resultant breakdown voltage of the gap. During breakdown, the arc uses the floating body as a stepping stone in the process. In other words, the discharge channel passes through the conductive object.

In the case of laser-induced breakdown one could say that the breakdown process is not dissimilar to the above mentioned situation. The laser induced plasma is itself a conductive object in the gap. It is made up of free electrons of a certain density and positive ions. The main difference is that the laser-induced plasma has its own electric field (therefore cannot be thought of as 'floating'). One main question arises: What does the discharge channel do? Does it pass directly through the laser-induced plasma (since the plasma is conductive) or does it follow some other path?

A set of experiments was conducted on the Rogowski profile spark gap used in the laser-triggered experiments. The gap was subjected to lightning impulses (1.2/50 μs[1]). This particular waveform was chosen since it is widely understood and provides a good reference for comparison. A DC voltage could also be used in these experiments. The standard lighting impulse waveform was chosen since its duration ($\pm$50 μs) is comparable to the life time of the laser-induced plasma (see *Section 4.7*) Four gap lengths were used (20, 30, 40 and 50 mm) and two geometries (with a floating object and without). The floating object used was chosen so that it had roughly the same dimensions as the laser-induced plasma. In other words cylindrical with dimensions (3 mm diameter and 5 mm length). This body was suspended in the gap by means of a thin length of fishing line. The atmospheric conditions

[1]This waveform as described in SANS IEC 60061-1:1989 "High-voltage test techniques, Part 1: General definitions and test requirements"

(temperature, humidity and pressure) were monitored so that the correction factor and hence the breakdown voltage at standard conditions could be obtained.

The experimental setup can be seen below in *Figure 4.4*

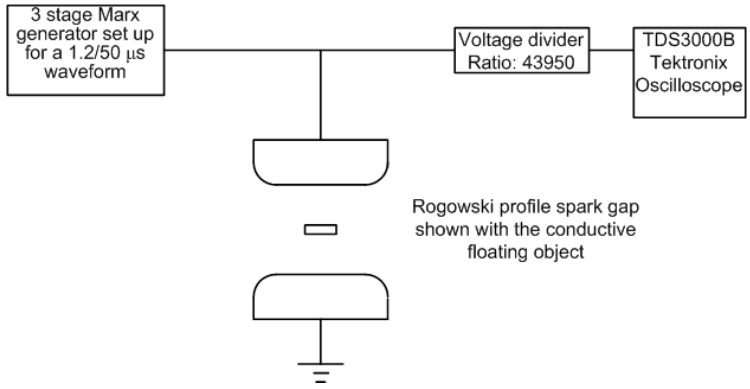


Figure 4.4: Experimental setup for 1.2/50 μs impulse experiments

An up-down U_{50} test (20 shots) was conduced on each geometry. The results showed a decrease in the breakdown voltage of the gap when the conducting object was inserted in the gap. However, the reduction was by no means as significant as that obtained in the case of the laser-triggered gap. In *Figure 4.5* and *Table 4.1* one can see the results of this set of experiments. All experiments were conduced in the following conditions: temperature: 16°C, pressure: 840 mbar and humidity: 38%, yielding a correction factor of 0.8 [2]

From these results, it can be seen that by placing the conductive body in the gap, the breakdown voltage was reduced by an average of about 6%.

These U_{50} results can be contrasted with those obtained with laser-triggering of gaps ranging from 20 to 50 mm. These were obtained by applying DC voltages to the same Rogowski profile gap using a 50 kV DC generator. These results can be seen in *Table 4.2* The maximum withstand voltage was calculated assuming an air breakdown strength of 2.7 kV/mm. In fact, this value was confirmed experimentally.

From *Table 4.2*, it can be seen that for each gap setting, the laser-induced breakdown voltage represents approximately 30% of the gap maximum withstand voltage. In other words, a reduction of about 70% in breakdown voltage was observed.

[2]These experiments were conducted in the High Voltage lab of the University of the Witwatersrand, Johannesburg at an altitude of 1740 m

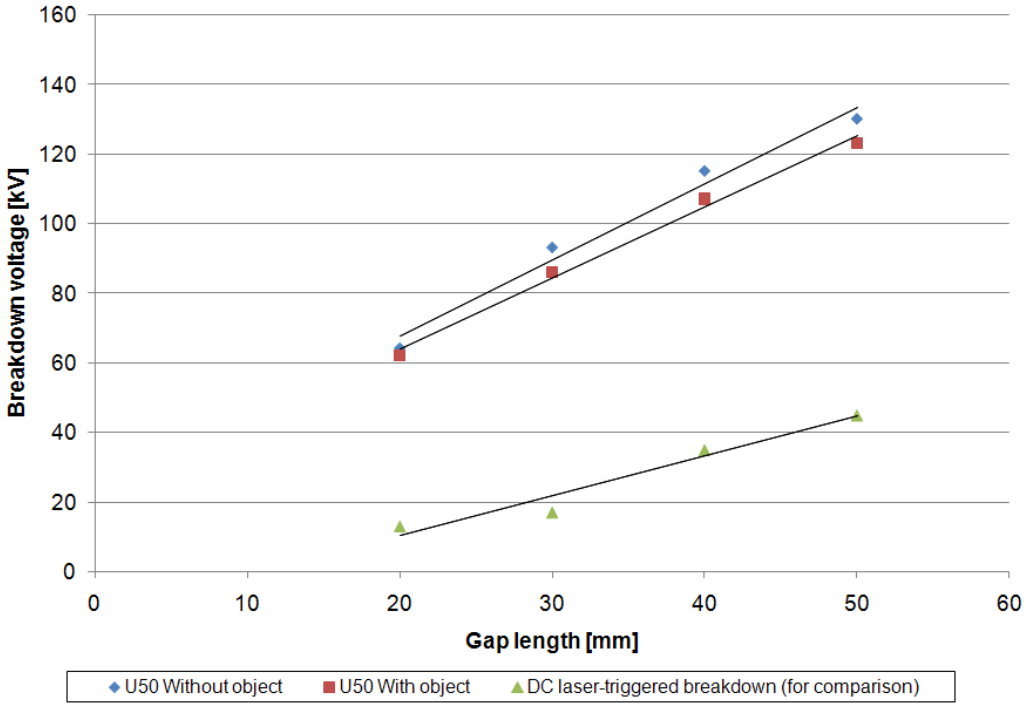


Figure 4.5: Comparison of 1.2/50 μs lighting impulse voltage breakdown levels for gaps with and without a conductive floating object with the previously obtained laser-triggered breakdown levels under DC excitation

4.4 Observation of the spatial orientation of the laser-induced plasma relative to the arc

The next set of experiments conducted, involved attempts to capture images of the laser-induced plasma and the resulting high voltage arc. As mentioned, the same setup was used as described previously, namely, the 30 mm Rogowski profile gap supplied by the 30 kV (max) half-wave rectifier circuit. As before, the beam is directed at right-angles to the gap axis (orthogonal geometry). These experiments were intended as an initial observation of the plasma-arc interaction. The temporal profile of this interaction is addressed in *Section 4.7*.

While conducting the experiments described in *Chapter 3*, it was noticed (with the naked eye) that a certain feature was visible on the resulting high voltage arc very close to the laser-induced plasma. It looked as if the arc was 'avoiding' the laser induced plasma. On closer examination (again with the naked eye) the arrangement in (*Figure 4.6*) was observed. This is very interesting since, as mentioned above, it is expected that the arc should in fact connect with the laser-induced plasma rather

Table 4.1: Tabulated results of impulse experiments for the 8 different geometries

Gap type	**Correction factor**	**U_{50} uncorrected[kV]**	**U_{50} corrected[kV]**
20 mm	0.8	51	64
20 mm + object	0.8	50	62
30 mm	0.8	75	93
30 mm + object	0.8	69	86
40 mm	0.8	92	115
40 mm + object	0.8	85	107
50 mm	0.8	104	130
50 mm + object	0.8	98	123

Table 4.2: Laser-triggered breakdown results for various gap lengths under DC excitation

Gap length [mm]	**Maximum withstand voltage [kV]**	**Laser-triggered voltage [kV]**
20 mm	54	13
30 mm	81	17
40 mm	108	35
50 mm	135	45

than go around it.

This feature, appeared each time the gap broke down and in every case it appeared as if the arc was 'avoiding' the laser-induced plasma. This was of great-interest since one would intuitively expect the high voltage arc to 'connect' with the highly conductive laser-induced plasma. For this reason, the gated camera was set up in order to closely observe the phenomenon and to obtain suitable pictures of the event. The pictures obtained confirmed what was visible with the naked eye. That is, that the arc was avoiding the laser-induced plasma. This can be seen in *Figure 4.7*

The image in *Figure 4.7* represents the head-on view of the lase-induced plasma (bright disc in centre of image) and the resulting high voltage arc. For this case, the Q-switch delay was set at 150 μs and the gap voltage at 19.4 kV. The faint shape on the top-left is the inverted image of the actual event caused by the focusing lens. The top of the image represents the anode and the bottom, the cathode. Another photo obtained showed the arc encircling the laser-induced plasma *Figure 4.8*.

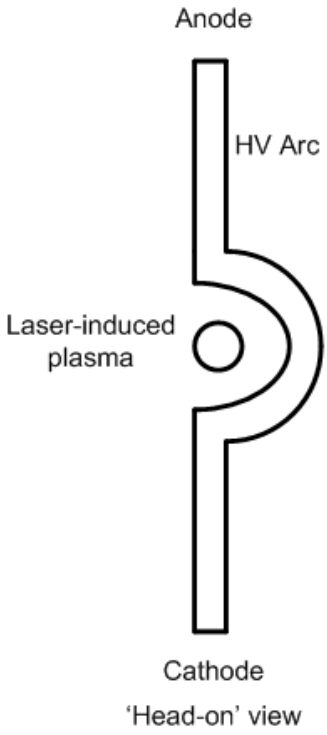


Figure 4.6: Drawing of the arc 'feature' observed with the naked eye

Once again, for *Figure 4.8*, the laser was operating at 150 μs and the voltage across the gap was set to 20 kV. For comparison, a side view of the event was also captured. This shows the laser-induced plasma arranged at right angles to the resulting arc. This can be seen in *Figure 4.9*

In figure *Figure 4.8* one can see a simple drawing showing the relative positions of the laser-induced plasma and resulting high voltage arc. The drawings are not to scale.

4.5 Description of feature

Experiments were conduced to characterise the observed breakdown arc feature in terms of shape,size and symmetry. A number of pictures were taken of the plasma from both a head-on and side view. These were then analysed and measurements were taken. In order to perform this type of analysis, a calibration shot was taken. A piece of paper, with a a carefully drawn 10 $\times$ 10 mm square was placed in the gap and photographed by the camera. This can be seen in *Figure 4.11*



Figure 4.7: Head-on view of the laser-induced plasma and the resulting arc with interesting feature – note how the arc bypasses the laser-induced plasma in the centre of the image

Appendix B shows the 59 head-on and side images taken of the feature together with the calibration image for comparison.

4.5.1 Symmetry of feature

Analysing the head-on and side images of the feature, it was noted that the feature was only clearly visible and distinguishable in the head-on views. The feature in the side views appears as a 'thickening' of the resultant high voltage arc. In other words, the feature only appears along one dimension. If the gap axis is taken as the y-axis and the the axis of symmetry of the laser-induced plasma as the z-axis, then the feature appears to be developing along the y-axis (on the positive, negative or on both sides of the y-axis). The feature always appears as a rough semi-circle (or a circle in some cases) with the laser-induced plasma at the centre.

The position of the feature (to the left or to the right of the laser induced plasma) is

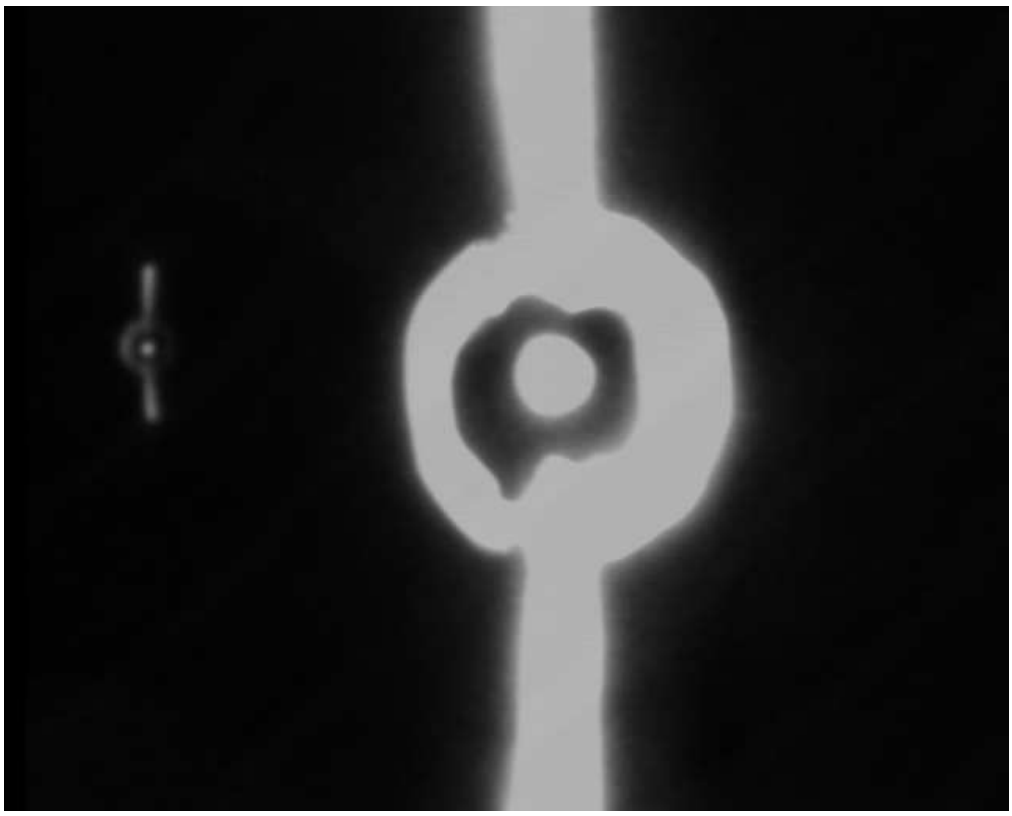


Figure 4.8: 'Head-on' view of arc encircling the laser-induced plasma

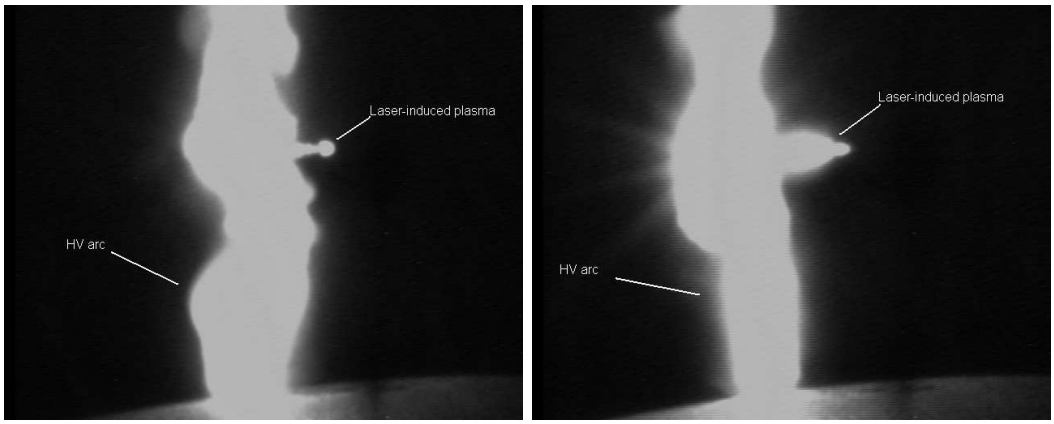


Figure 4.9: Two separate side views of arc and laser-induced plasma

random. From the 30 observed head-on images, in 12 of those, the feature appeared to the right of the plasma, 16 to the left and 2 encircled the plasma. See *Table 4.3*

This shows that there is a rough 50% split beteen the two feature-plasma positions.

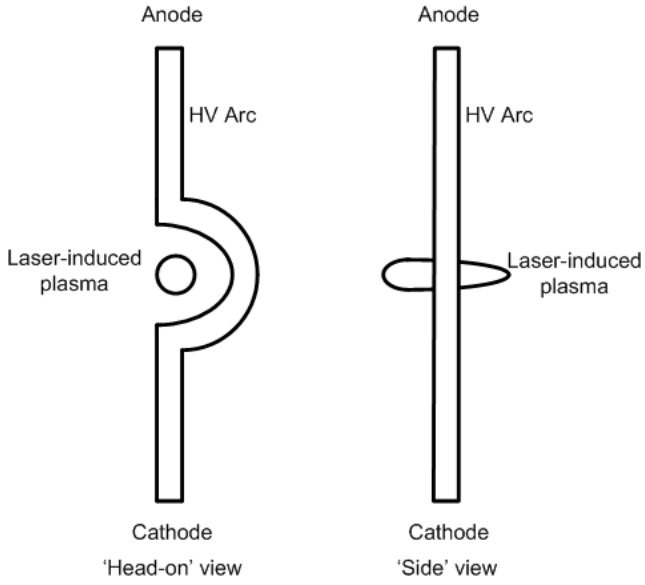


Figure 4.10: Simple drawing illustrating the relative positions of laser-induced plasma and arc

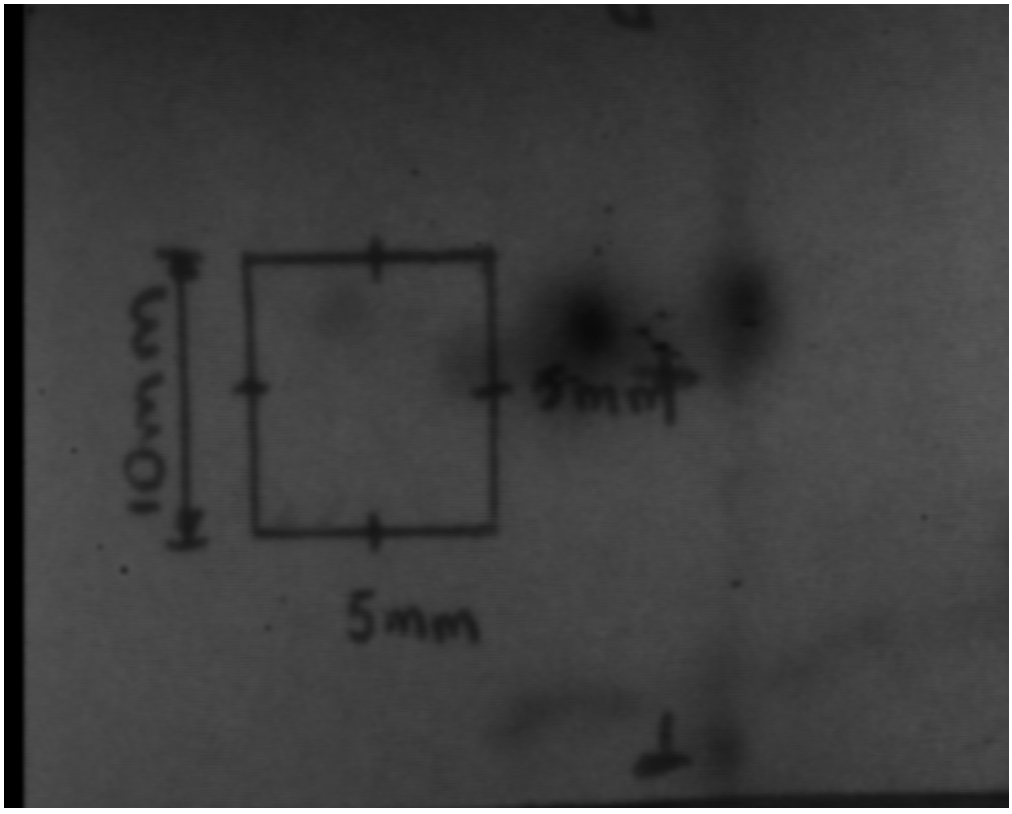


Figure 4.11: Calibration image used to measure dimensions of observed 'feature'

Table 4.3: Positions of the feature relative to the laser-induced plasma

No. of images	30
Right of plasma	12
Left of plasma	16
Encircling plasma	2

4.5.2 Size of feature

The size of the feature was measured by considering the length of the feature L and its inclination ϕ. This can be seen in *Figure 4.12*

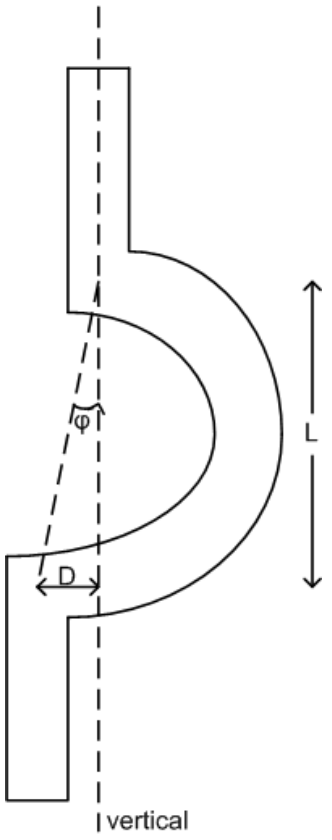


Figure 4.12: Parameters L, D and ϕ of the observed feature

These measurements were performed for both the side and head-on views. From the head-on view images, the average length of the feature was found to be about 12.4 mm. The angle of inclination varied from 0 to 19.65° with an average of 6.8°. Of the 30 images, 6 lean to the left, 17 lean to the right and 5 show no inclination.

In the case of the side view, an average length of 11.1 was measured. The angle of inclination varied from 0 to 19.98° with an average of 6.07°. Of the 29 images, 15 lean to the left, 11 lean to the right and 3 show no inclination. These results are summarised in *Table 4.4*.

Table 4.4: Average dimensions of feature

Position	**Average Length [mm]**	**Average angle ϕ [deg]**
Head-on	12.4	6.8
Side	11.1	6.07

4.6 Using the Spellman Generator and Cooke Corporation Camera

The Xybion camera used in the previous experiment, was not able to successfully provide data on the time delay before the appearance of the arc due to image capturing and triggering problems. For this reason, another camera was used (Cooke Corporation FlashCam) was used. In this case, as mentioned, the camera was triggered from the Qswitch enable line. The optical path used was approximately 6 m. The laser light took about 20 ns (c=3×10^8 m/s) to arrive at the spark gap. This meant that the camera was not able to capture the initial formation of the plasma.

At the same time, the HV generator was swapped for the Spellman DC generator. This was done in order to attain much higher voltage levels (up to 50 kV). The spark gap was initially set to 30 mm with a voltage of 30 kV across it (E=1 kV/mm).

As expected, the same type of images were obtained as before. In the experiments, the gate of the camera was set at 1 μs and the gate was shifted in time by means of the Stanford delay generator.

In *Figure 4.13* one can see again the typical observed laser-triggered discharge.

One again it is observed that the arc appeared to bypass the laser-induced plasma. All breakdown event associated with this gap configuration yielded similar images.

Since the generator was able to reach a voltage of 50 kV, an experiment was devised to check whether these discharge shapes appear at higher voltages. The gap length

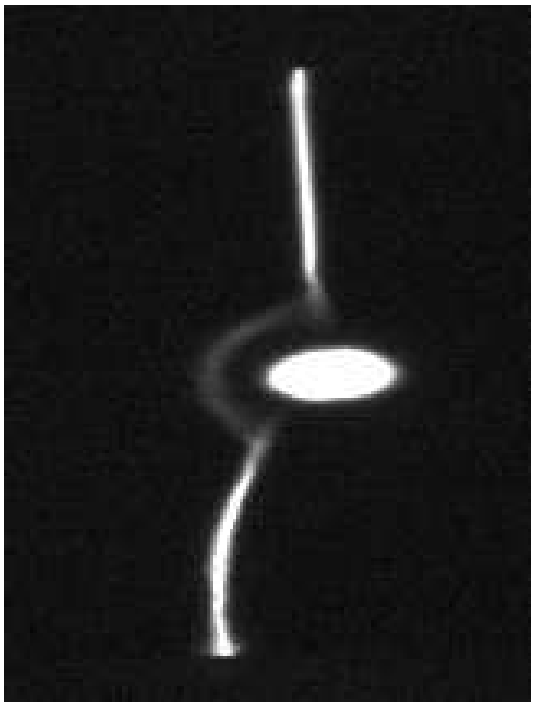


Figure 4.13: Imaged obtained with the Cooke Corporation camera for a gap of 30 mm with 30 kV across it (gate of 95 μs)

was kept at 30 mm and the voltage increased to 40 kV and then to 50 kV. This translates to the following electric field values (as seen in *Table 4.5*):

Table 4.5: Electric fields for 3 different gap geometries

Gap length [mm]	**Applied voltage [kV]**	**Electric field [kV/mm]**
30	30	1
30	40	1.3
30	50	1.7

The results obtained from this experiment were extremely interesting. They showed a marked difference in the shape of the discharge for the three different gap lengths and voltages (ultimately for three different electric field conditions). The images obtained can be seen in *Figure 4.14*.

As can be seen from *Figure 4.14*, the shape of the arc appears to depend on the applied electric field. For a 1 kV/mm field (30 kV/30 mm), the arc displays the so far observed behaviour. However, when the electric field is increased to 1.3 kV/mm (40 kV/40 mm) the arc seems to move a lot closer to the laser-induced plasma, almost

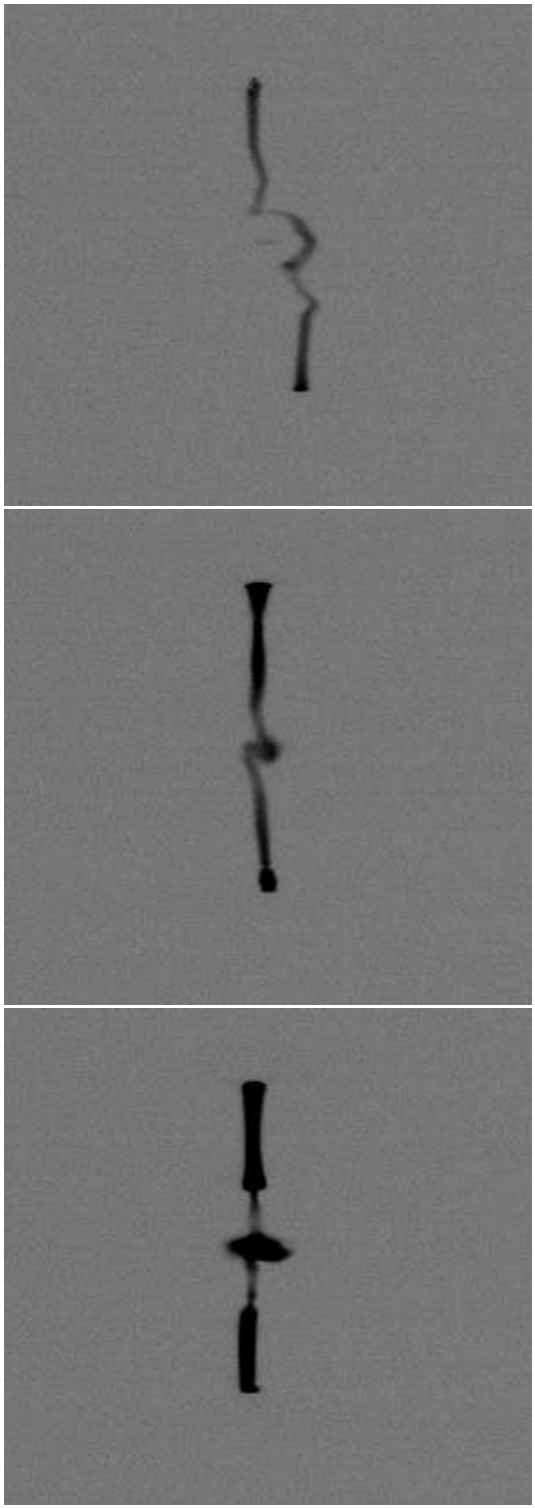


Figure 4.14: Image of arc for 30 kV (top), 40 kV (centre) and 50 kV (bottom) across a 30 mm spark gap (1, 1.3 and 1.7 kV/mm respectively)

coming into contact with it. When the field is increased further, to 1.7 kV/mm (50 kV/50 mm), the arc displays the behaviour that was initially expected: the arc treats the plasma as a conductive body and connects directly with it.

To prove this hypothesis (that the E-field plays a role in defining the shape of the laser-triggered arc) the gap was increased in length to 40 and 50 mm with a voltage of 40 and 50 kV respectively. The aim was to maintain a field of 1 kV/mm. If the hypothesis is correct, the arc is expected to exhibit the same behaviour as in the case of a 30 kV/30 mm gap. It is expected to avoid the plasma.

The experiment was conducted and the results showed what was predicted. For both cases, the arc-plasma shape was the same as in the 30 kV/30 mm case as can be seen in *Figure 4.15*

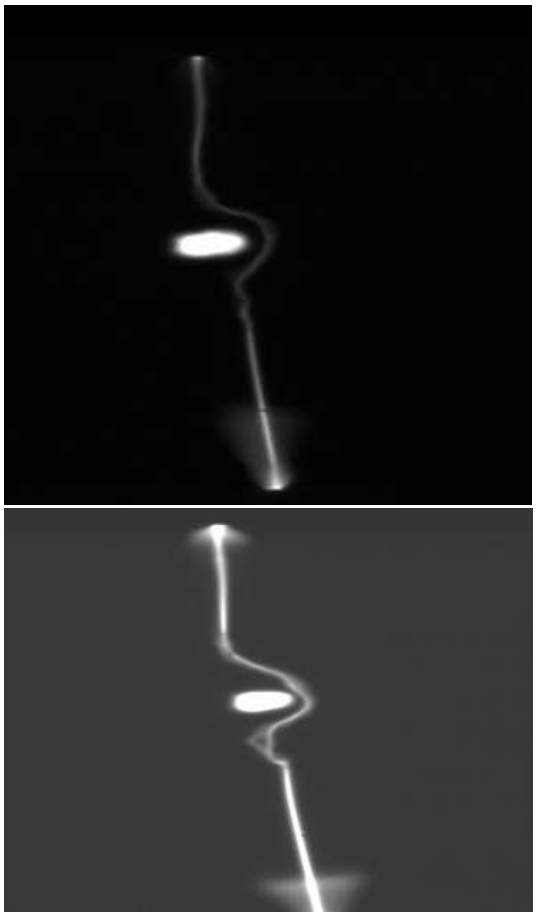


Figure 4.15: Image of arc for 40 kV, 40 mm (top) and 50 kV, 50 mm (bottom) (fields of 1 kV/mm respectively)

From the above presented experiments, it is obvious that the electric field in the gap

has an effect on the shape of the laser-triggered arc. The higher the electric field, the closer the arc moves to the laser-induced plasma. In order to get a complete picture, one must attempt to draw a time-line of events. It is important to provide the temporal relationship between the birth, formative growth and extinction of the laser-induced plasma and the appearance of the laser-triggered electrical discharge.

4.7 Time line-experiments

4.7.1 Plasma life times

It is of interest to ascertain what the plasma life time is for various Q-switch delay settings. The plasma life time is the time taken from the formation (birth) of the laser-induced plasma to the complete recombination of charge and the resulting extinction of the plasma. The plasma life time was experimentally obtained by setting the laser to a specific Q-switch delay and then using the Stanford delay generator to 'sweep' the 50 ns window (camera gate) in time until the 'start' and 'end' times (relative to the flash lamp pulse) of the plasma are found. The difference of these two times will provide the life-time of the plasma. For example:

Laser Q-switch delay of 130 μs
Plasma start time: t_{start}=126.07 μs
Plasma end time: t_{end}=156.07 μs
Plasma life time: Δt_p=t_{end}-t_{start}=30 μs

In *Figure 4.16* one can see the two images ('head-on' and 'side' view) of the laser-induced plasma [21, 24].

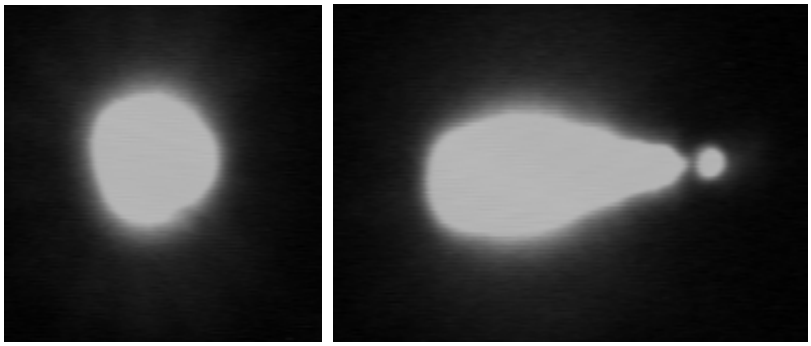


Figure 4.16: 'Head-on' and 'side' view of the laser-induced plasma

Plasma life-times were measured for Q-switch delays ranging from 90 to 270 μs. At a delay of 270 μs, the beam intensity was not high enough to cause plasma formation. The following graph can then be plotted (*Figure 4.17*).

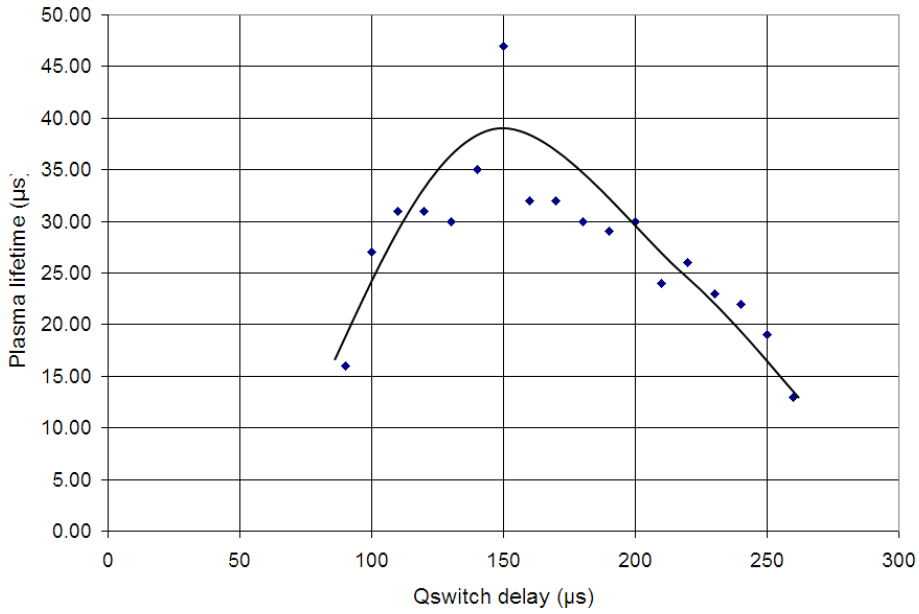


Figure 4.17: Plasma life time vs. laser Q-switch delay

This shows (as expected) that the laser life time is at its maximum round about the optimum Q-switch delay. This is due to the fact that at optimum Q-switch, the laser beam intensity is at its maximum. This in turn leads to the generation of a very intense laser-induced plasma. The higher the intensity of the plasma, the longer the extinction phase is going to be and of course the longer the plasma life-time. The maximum life time was measured at 48 μs. On average, it can be said that the duration of the plasma is approximately 30-40 μs at near optimum Q-switch delays.

4.7.2 Arc appearance

The aim of the experiments presented in this section was to try and estimate the time delay between the Q-switch trigger and the appearance of the laser-triggered arc. This was performed by shifting the camera gate forward in time (using the Stanford delay generator) until the arc was visible on the screen. This was conducted for different Q-switch values (125, 150 and 190 μs) and for 3 different voltages (30, 40 and 50 kV) while keeping the gap length constant at 30 mm. The results can be

seen in *Table 4.6* In this table, the plasma life time is defined as the time after the Q-switch trigger for which the plasma is no longer visible. The time delay is measured from the trigger pulse to the appearance of the arc.

Table 4.6: Time delays associated with the appearance of the laser-triggered arc for three different Q-switch delays

Q-switch delay [μs]	**Voltage** [kV]	**Plasma life** [μs]	**Time delay** ΔT_b [μs]
125	30	15	190
125	40	15	70
125	50	15	8
150	30	20	125
150	40	20	30
150	50	20	6
190	30	27	97
190	40	27	22
190	50	27	5

From *Table 4.6*, it can be seen that the time delay ΔT_b associated with the appearance of the arc is dependant not only on the electric field, but also on the intensity of the laser light. For low intensity light (Q-switch delay of 125 μs), the time delay ΔT_b is large (approx. 190 μs). As the applied voltage increases (and of course the electric field) so does ΔT_b. The same applies for the other two Q-switch delay cases.

Based on these results, one can modify the above-mentioned electric field hypothesis by stating that the shape of the laser-triggered arc is dependant on the level of *breakdown probability*. The higher the probability of breakdown, the lower the time delay and the closer the arc moves to the plasma. At higher probability cases, such as Q=190 μs and 50 kV (1.7 kV/mm) the time delays become very short $\sim$5 μs and the arc connects with the laser-induced plasma.

The time delays presented in *Table 4.6* were verified by measuring the time delay between the trigger pulse and current pulse through the earth wire of the spark gap using an oscilloscope. The current pulse was measured by means of a Pearson coil. The time delays obtained can be seen in *Table 4.7*. These time delays presented are average values.

Table 4.7: Time delays associated with the appearance of the laser-triggered arc at optimum Q-switch delay

Gap length [mm]	**Voltage [kV]**	**E-field [kV/mm]**	**Time delay ΔT_b [μs]**
30	30	1	90
40	40	1	150
50	50	1	260
30	30	1	90
30	40	1.3	20
30	50	1.7	2

In *Figure 4.18* one can see an example of the waveforms obtained from the oscilloscope showing the time delay. In this figure, Q=190 μs, 30 kV, 30 mm. In this figure, the top plot shows the current pulse through the earth wire and the bottom trace shows the Q-switch trigger pulse.

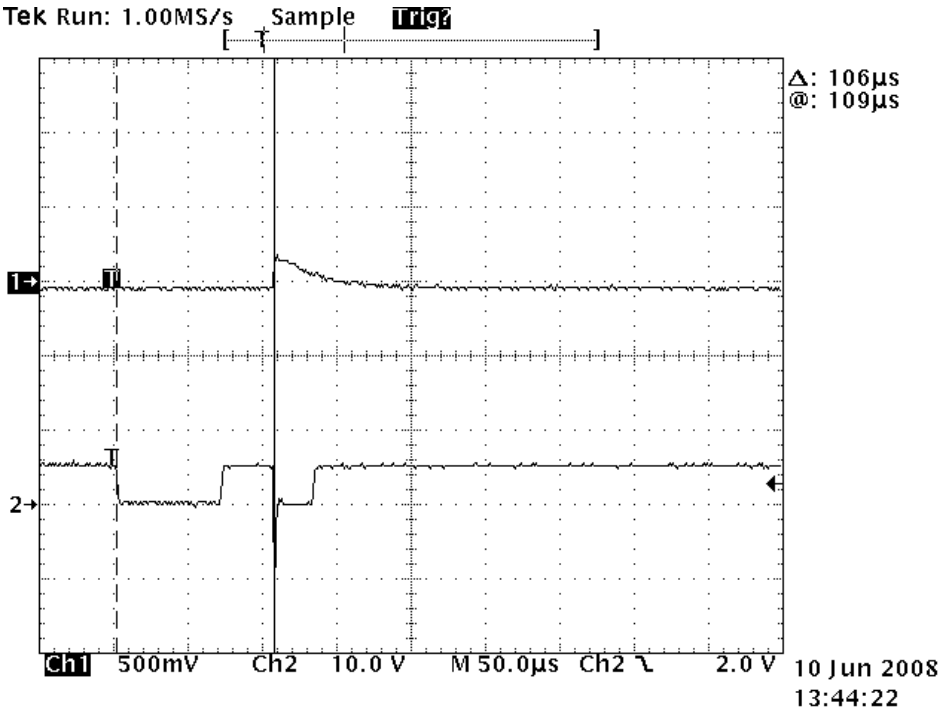


Figure 4.18: Breakdown time delay: Bottom trace shows the laser Q-switch trigger pulse and the top trace shows the current pulse through the earth wire representing electrical breakdown. Time delay is measured between the falling edge of the trigger and the rising edge of the current waveform

From these results, it is now possible to plot a simple timeline of events for the laser-triggered spark gap. In *Figure 4.19* one can see the sequence of events for a Q-switch of 190 μs and a voltage of 30, 40 and 50 kV (gap length of 30 mm).

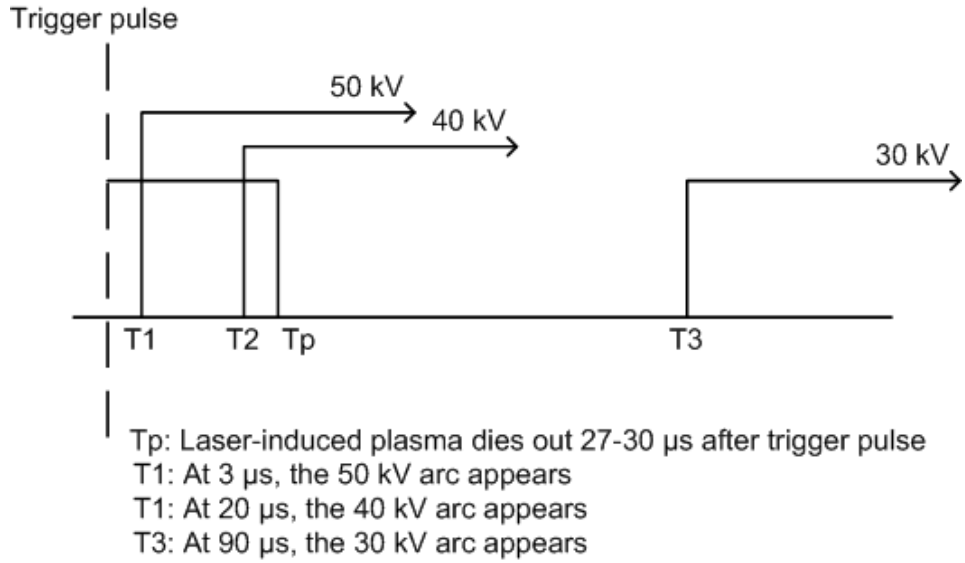


Figure 4.19: Time-line of events for a 30 mm gap and laser at 190 μs Q-switch

4.8 Explanation of arc shape

The above time-line can be used now to explain the different shapes of the laser-triggered arc under various conditions. From this time-line it is evident that when the breakdown probability is very low (voltages of 30 kV or electric fields of about 1 kV/mm), the time delay is far greater than the duration of plasma. This means that the arc appears long after the plasma has died away.

It is well known that during the initiation of the laser-induced plasma, two wavefronts develop: A very fast moving shock wave, and a slower moving thermal wave [18]. The shock wave expands symmetrically in all directions. However it has been found to move towards the focusing lens. The thermal wave on the other hand expands very asymmetrically. The velocity of this wave is much greater in the direction towards the focusing lens and very much slower in the opposite direction. It is also known [18] that during the formation of a laser-induced plasma, temperatures of 10^4 to 10^5 K are developed. These are enough to cause thermal ionisation of air (see *Appendix A.2.4*). Thus, as the thermal wave expands, it ionises the air it passes

through leaving behind it charge carriers. These of course will recombine after a certain time, resulting in once again a neutral gas.

The arc shape observed in the case of the 30 kV/ 30 mm gap can be attributed to the interaction of one of these (or both) wavefronts. In both cases, the wavefront in question (shock or thermal) may very well be either pushing charged particles outwards thus developing a conductive ring around the original plasma or (especially in the case of the strong fast moving shock wave), forcing the arc away from the plasma. This ring of charge carriers can be attributed to the expansion of the thermal shock wave. The relative velocities, however, of these waves are very important to the discussion.

From the images obtained, it was noted that the distance between the arc and the laser-induced plasma is on average about 5 ± 1 mm. Measurements conducted on these waves show that in the first 1 μs the shock and thermal velocities are about 460 and 40 m/s respectively [18]. This means that if a linear approximation is to be taken, after a time t=90 μs, the shock wave would have moved 41 mm away and the thermal wave 3.6 mm away. This means that the shock wave is long gone by the time breakdown occurs. At the same time, if the shock wave was responsible for the observed arc shape, then the shape should also appear in the 40 and 50 kV cases. This is not the case. This means that the shock wave theory can be discarded.

In the case of the thermal wave, measurements showed that that after 150 μs, the thermal wave expands to a radius of about 3.5 mm. This is in good agreement with the observed radius of 5 ± 1 mm. At 2 and 20 μs the thermal wave would have expanded by 80 and 800 μm respectively. This means that the thermal wave would not have an effect on the arc for the cases where the time delay ΔT_b is small (as in the 40 and 50 kV cases).

These observations so far can be summarised in *Table 4.8*

Table 4.8: Shock and thermal wave velocities and expansion

Wave type	**Velocity [m/s]**	**Expansion at 2 μs [mm]**	**Expansion at 90 μs [mm]**
Shock wave	460	0.9	41
Thermal wave	40	0.08	3.5

A simplified explanation of the phenomenon can be seen in *Figure 4.20*

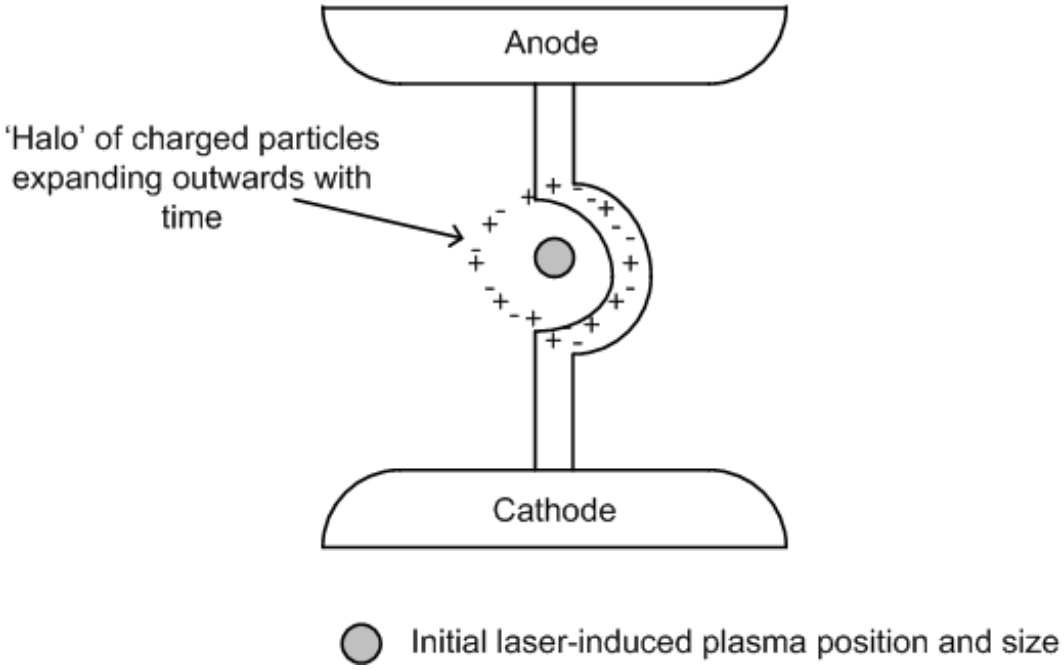


Figure 4.20: Simple drawing explaining the formation of the observed arc shape at 30 kV/30 mm

4.9 Conclusion

In this chapter, the results of the experiments involving capturing images of laser-induced breakdown with two gated cameras are presented. The aim was to explore the spatial and temporal relationship between the laser-induced plasma and the resulting laser-induced arc. During the experiments presented in the previous chapter, it was noted that the arc tended to avoid the laser-induced plasma. This was of great interest, since it was expected that the arc should attach itself to the highly conductive laser-induced plasma. In fact, three main parameters were isolated that can be used to describe the behaviour of a laser-triggered arc. These are:

- Spatial relationship between the plasma and the arc
- Temporal relationship between these two parameters
- Electric field applied to the gap electrodes

The gated camera experiments confirmed that the laser-induced arc did in fact avoid (or move around) the laser-induced plasma. However, it was found that this behaviour was linked to the breakdown probability of the gap and hence on the time delay between the appearance of the laser-induce plasma and the triggering of the main gap discharge. The higher the time delay (the lower the breakdown probability), the more the arc avoided the plasma. The life-time of the plasma was found to be on average 27 μs. For time delays of about 2 μs (corresponding to electric fields of 1.7 kV/mm - a 50 kV/30 mm gap), the arc clearly attached itself to the plasma. For delays of 100-200 μs – long after the plasma has died out (fields of 1 kV/mm - gaps of 30 kV/30 mm, 40 kV/40 mm and 50 kV/50 mm) the arc avoided the plasma. In the case however of a 40 kV/30 mm gap having an electric field of 1.3 kV/mm and an associated time delay of 20 μs – very close to the end of the plasma life, the arc tended to move very close to the plasma, but not attach to it every time. This behaviour can be explained by considering that the laser-induced arc encounters charge carriers at different points in time and space and can be linked to the action of the thermal wave generated by the laser-induced plasma.

Chapter 5

Conclusion

In the work presented, it has been shown than an orthogonal geometry is indeed a very practical and effective way of triggering a spark gap by means of a focused laser beam. A wide range of breakdown voltages was obtained. In particular a reduction in breakdown voltage of almost 70% was observed for a 50 mm gap (from 135 to 45 kV). It was noted that parameters such as the beam intensity, the gap length used and the position of the laser-inducuced plasma in the gap play an important role in the breakdown process. During laser-triggered breakdown events, it was noted that the triggered high voltage arc did not always attach itself to the hightly conductive plasma as expected. This anamalous behaviour can be explained by taking into account the spatial and temporal relation between the laser-induced plasma and the resulting laser-triggered arc. In fact, this attachment depends on the breakdown probabilty of the spark gap. This represents a unique and valuable contribution to the field of laser-triggered spark gaps and to the knowledge base of high voltage discharges.

Appendix A

Electrical breakdown in gases

A.1 Introduction

Air, being an insulator, has a dielectric strength that can be calculated from the following 2 equations:

$$U_d = 24.5kV \times s + 7kV\sqrt{s} \tag{A.1}$$

$$E_d = 24.5kV/cm + 7kV/cm \times \frac{1}{s} \tag{A.2}$$

For uniform fields and short gaps of a couple of cm, breakdown occurs at approximately 2.7 kV/mm. When the applied electric field exceeds this value, electrical breakdown occurs. There are various types of electrical breakdown with different mechanisms. In the case of short gaps (gaps in the region of a couple of centimetres) the streamer mechanism is used to explain breakdown. In the cases of much larger gaps (in the order of a couple of meters) the leader mechanism is used. In this chapter, the main 2 mechanisms for electrical breakdown in short gaps are presented. These are the Townsend and streamer breakdown theories. At the same time, topics such as the various ionisation methods and types of time lags associated with electrical breakdown are discussed. These concepts are important in order to understand the experiments described and analysed in the following chapters.

A.2 Ionisation methods

As mentioned above, the key process that allows electrical breakdown to occur, is ionisation. Ionisation can happen in many different ways. Irrespective of the

mechanism though, as the name implies, ionisation is the production of ions. Ions are produced when electrons are stripped from neutral atoms or molecules. In essence there are four main mechanisms that enable ionisation to take place. These are:

1. Ionisation by collision
2. Photoionisation
3. Ionisation by metastable atoms
4. Thermal ionisation
5. Radioactivity of the earth and cosmic radiation

The ionisation forms that are important in the case of laser triggering of spark gaps are:

A.2.1 Ionisation by collision

This is the most common form of ionisation. It is the principle of the Townsend ionisation process. Electrons with high enough energies are able to strip other electrons off neutral atoms. The number of electrons produced through collision depends on the type of atoms or molecules and the mean free path between them. It also depends on the average velocity of the electrons. This process is very important when the electric field is very high. This is because electrons do not lose too much energy through collisions, but they are able to build up their kinetic energy supplied by the electric field. To cause ionisation through impact, the transferred energy must be equal to, or greater than the ionisation potential of the molecule. For example, the ionisation energy of an Oxygen atom is 13.6 eV, whereas for Nitrogen it is 14.5 eV. The transferred energy is closely related to the mean free path λ between atoms ($\delta W = e\lambda$). It must be mentioned though, that ionisation by electron collision is a probabilistic phenomenon. In some cases ionisation does not take place even though the colliding electron my have the required energy [25].

Another important factor that determines how easy a gas is ionised, is the ionisation cross section of the molecules or atoms in question.

A.2.2 Photoionisation

In many cases, a low energy electron may on collsion with a neutral gas atom exite it to a higher energy state. When the atom returs to is relaxed state, a photon is emitted. This photon may be able to ionise another atom whose ionisation energy is lower than the photon energy. The process can be symbolically written as $A + hf = A^* + e$, where A and A^* represent the neutral and exited atom of the gas. hf is the photon energy. As mentioned, for photoionisation to occur, the photon energy hf must be greater than the atom ionisation energy. The photon energy depends on the photon wavelength. The shorter the wavelength, the higher the photon energy.

This means that the breakdown process can be assisted by irradiating the electrodes with a light source whose photons have a high energy. The commonest way is to user a source of Ultraviolet light.

A.2.3 Ionisation by metastable atoms

Another ionisation process, is ionisation due to metastable atoms. Metastable atoms are atoms whose lifetime in the exited state can last up to a couple of seconds. The result of this is that their energy is high enough to cause ionisation of neutral atoms. Depending on the metastable energy (V_m), The following situations can arise:

1. If $V_m > V_i$ (where V_m refers to atom A^m and V_i refers to atom B). In this case, the process can be written as

$$A^m + B \rightarrow A^+ + B + e \tag{A.3}$$

2. If $V_m > V_i$ (where V_m refers to atom A^m and V_i refers to atom B). The process is be expressed as

$$A^m + B \rightarrow A + B^* + e \tag{A.4}$$

3. In the case where $2V_m > V_i$ (where both V_m refers to A^m and V_i refer to atom A). The reaction that happens can be written as

$$2A^m \rightarrow A^+ + A + e + KE \tag{A.5}$$

4. Finally, in some cases the following may occur:

$$A^m + 2A \rightarrow A_2^* + A \tag{A.6}$$

and

$$A_2^* \rightarrow A + A + hf \tag{A.7}$$

The photon emitted does not usually have enough energy to cause ionisation in a gas. It way though induce electrons to be emitted form the cathode.

It is interesting to note that ionisation by metastable atoms is more effective in gas mixtures.

A.2.4 Thermal ionisation

Thermal ionisation is a form of ionisation that is not often observed. The basic principle is that when the temperature of a gas is sufficiently high, the vibration of the molecules become very significant. These vibrations can result in ionisation due to molecules colliding with each other. Thermal ionisation becomes significant at temperatures above 1000 K.

A.3 The Townsend Mechanism

The Townsend mechanism is the simplest model that is used to describe electrical breakdown across a gap. The model in essence describes ionization by electron collision (between atoms and molecules in the gas and collision with the surface of the electrodes) [26].

The starting point for this model is to assume two electrodes (an anode and a cathode) that set up a high electric field as can be seen in *figure A.1.*

The gap distance is d. The model assumes that there are N_0 free electrons at the cathode. These free electrons start a series of collisions and at distance from the cathode, the electron number has increased to N. An increase in distance dx will produce an increase in electron numbers of $dN = \alpha dx$. Integration of this relationship across the gap gives the following relationship:

$$N = N_0 e^{\alpha d} \tag{A.8}$$

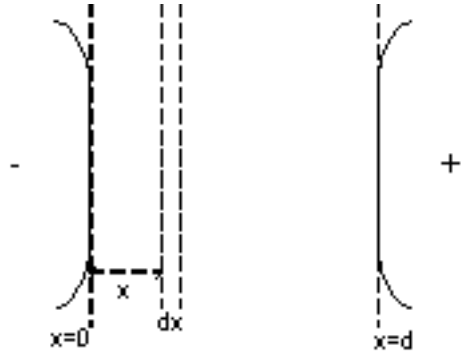


Figure A.1: Townsend mechanism [26]

This Shows that the initial free electrons start an avalanche (through collision) that expands exponentially across the gap. The quantity is known as the first ionization coefficient. It is defined as the number of electrons produced by an electron collision per unit length of path in the direction of the field.

Generation of free electrons through electron collision with gas atoms and molecules is not the only process that happens in the gas. At the same time, electrons are emitted through impact with the electrode surface (secondary emission). Assuming that $\alpha N dx$ electrons are emitted by the primary ionization process, then $\omega N dx$ electrons are emitted from the cathode. These electrons are emitted due to the impact of the much heavier positive ions that are created by the electron collision process. The total number of electrons emitted from the cathode is then:
$N_0{}' = N_0 + \int_0^d \omega N dx$. At the same time, it is known that $N = N_0 \acute{e}^{\alpha d}$. Therefore,
$N_0{}' = N_0 + \int_0^d \omega N_0 \acute{e}^{\alpha x} dx = N_0 + \frac{\omega}{\alpha} N_0{}' \left[e^{\alpha d} - 1\right] \Rightarrow N_0 = N_0{}' \left\{1 - \frac{\omega}{\alpha}\left[e^{\alpha d} - 1\right]\right\}$
From this relation it can be seen that the total number of electrons arriving at the anode is therefore:

$$N_a = N_0 \acute{e}^{\alpha d} = N_0 \frac{e^{\alpha} d}{\left\{1 - \left(\frac{\omega}{\alpha}\right)\left[e^{\alpha d} - 1\right]\right\}} \tag{A.9}$$

The term $\frac{\omega}{\alpha}$ is known as the second ionisation coefficient γ. This number expresses the number of electrons emitted from the cathode per incident ion [25]. It can be also seen that the number of electron charges arriving at the anode per unit time (in other words the current detected by the external circuit) can be written as:

$$I = eN_d = I_0 \frac{e^{\alpha d}}{1 - \gamma \left(e^{\alpha d} - 1\right)} \tag{A.10}$$

As the voltage (and hence the field) increases, the term $e^{\alpha d}$ increases until $\gamma e^{\alpha d} \rightarrow 0$.At this point, the denominator tends to zero and therefore, the current tends to infinity [27]. This is the condition for which we get electrical breakdown. In general terms, the Townsend criterion for breakdown can be expressed as:

$$\left(\gamma e^{\alpha d} - 1\right) = 1 \tag{A.11}$$

The Townsend mechanism is the simplest theory that describes electrical breakdown across a gap. It is interesting to state that for both the first and second ionisation coefficients (α and γ respectively) it has been found experimentally that they are dependent on the ratio $\frac{E}{p}$ where E and p are the electric field and pressure of the gas respectively. It has been found that the following relationships exist [25]:

$$\frac{\alpha}{p} = f\left(\frac{E}{p}\right) \tag{A.12}$$

$$\gamma = g\left(\frac{E}{p}\right) \tag{A.13}$$

where f and g are two arbitrary functions

When a high intensity laser beam is focused in the region of a spark gap (between the two electrodes), the following two event occur: Due to the high photon energy, the phenomenon of photoionisation occurs. This means that there is an abundance of free electrons at the focal point of the beam. At the same time, a very high local electric field is developed. The fact that a large number of free electrons are available, means that that more electron collisions can occur thus generating a large electron avalanche.

A.4 The Streamer mechanism

The Townsend mechanism is a very simple way of describing the breakdown process. It is unable, though, to explain phenomena like the irregular and random formation of a discharge in long gaps. That is why the streamer (or Kanal) processes is used. In essence, the streamer mechanism describes the development of a spark from a single electron avalanche. This is because, as the avalanche progresses and grows

across the gap, a space charge is formed at the head of the electron cloud as can be seen in *figure A.2*.

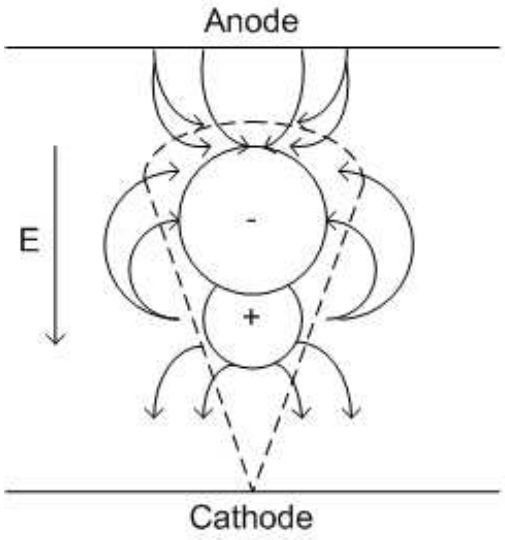


Figure A.2: Field distortion caused by electron avalanche [26]

The result of this space charge, is the conversion of the electron avalanche into what is known as a plasma streamer. There are two main features that are related to the streamer process. The first one is that there is a large amount of photo-ionisation present. In essence, it can be thought that the avalanche emits high energy photons from the head of the process.These photons are absorbed not too far away from the ion space charge. The newly created electron in their turn contribute to the production of more photons and so the process continues. The second point is that there is a localised enhancement of the electric field between the two electrodes. This is due to the space charge that has been formed again at the head of the streamer[26, 27]. The approximate value of the space charge field can be evaluated by assuming that the total charge Q is contained within a sphere of radius r at the head of the avalanche. The charge Q is in Coulombs (C) and the radius r is in meters (m). It is known that the electric field is given by $E_r = k\frac{Q}{r^2}$ where $k = \frac{1}{4\pi r^2}$. At the same time, the charge Q can be expressed as $Q = Ne$ where N is the number of ions per unit volume and e is the electron charge. From this information the field equation can be rewritten as:

$$E_r = \frac{(4/3\pi r^3)Ne}{4\pi\epsilon_0 r^2} \Rightarrow E_r = \frac{rNe}{3\epsilon_0} \tag{A.14}$$

As the avalanche moves forward a distance dx, the number of electrons produced will be $\alpha e^{\alpha x} dx$. This means that N can be written as $N = \frac{\alpha e^{\alpha x} dx}{\pi r^2 dx}$ (assuming a cylindrical volume). Therefore $E_r = \frac{\alpha e^{\alpha x}}{3\epsilon_0 \pi r} e$. The radius r can be obtained by considering the diffusion expression which is $r = \sqrt{2Dt}$ where D is the diffusion coefficient and $t = x/u_a$. u_a is the speed with which the avalanche progressed across the gap. Combining the above equations, the electric field due to the space charge can be expressed as:

$$E_r = \frac{\alpha e^{\alpha x} e}{3\epsilon_0 \pi \sqrt{2D\frac{x}{u_a}}} \tag{A.15}$$

With the streamer mechanism, a criterion exists that explains the transition from an electron avalanche to a streamer. This criterion is that $E = kE_r$ where $k \approx 1$. In other words, an electron avalanche develops into a streamer when the field at the head of the avalanche is approximately equal to the total electric field applied between the electrodes.

The strength of the streamer mechanism lies in the fact that it is able to explain breakdown in non-uniform fields such as point-to-plane or point-to-point gaps. It fails though to explain the breakdown process in long gaps. That is why the leader mechanism was developed [28].

A.5 Electronegative gases

A.5.1 Mechanisms and applications

There are a certain category of gases that have the ability to readily acquire electrons from stable negative ions. These are known as electronegative gases. These gases lack one or two electrons in their outer shells. Such gases include the halogens (F, Cl, Br, I, At) and gases such as oxygen (O) or sulphur (S).

A very important parameter associated with electronegative gases, is their electron affinity. This quantity is defined as the change in energy that occurs when en electron is attached to the gaseous form of the atom. For example, the electron affinity for Hydrogen is $-72\ kJ/mole$. where as the electron affinity for Fluorine is

$-330\ kJ/mole$.

Electronegative gases are used quite often as insulators. The most potent electronegative gas used in this capacity if sulphur hexafluride (SF_6). As a gas, SF_6, has an excellent dielectric strength. It is about 2.5 times that of air. It also has the ability (as an electronegative gas) to quench arcs very effectively. The gas is obtained from molten sulphur and gaseous fluorine. It is refined to 99.9% purity [29]. Electron detachment is the main mechanism associated with electronegative gases. Abdel-Salam and Turkey in 1988[1] ascribed the detachment process to the following events [28]:

1. Photodetachment. In this situation, a quantum of energy (in the form of a photon) is absorbed by the negative ion. This can be written as follows:

$$A^- + hf \rightleftharpoons A + e \tag{A.16}$$

2. Ion collision with fast atoms:

$$A^- + A \rightleftharpoons 2A + e \tag{A.17}$$

3. Collision and association with a neutral atom. This process normally leads to the loss of an excessive electron.

$$A^- + B \rightleftharpoons AB + e \tag{A.18}$$

4. A molecular negative ion may at some point collide with a fast excited atom. This results in the negative ion becoming excited:

$$A_2^- + B^* \rightleftharpoons A_2^* + e \tag{A.19}$$

5. Finally, recombination can occur between negative and positive ions of atoms. The result is the formation of a diatomic molecule:

$$A^- + B^- \rightleftharpoons AB^+ + e \tag{A.20}$$

A.5.2 The attachment coefficient

In analogy to the first ionisation coefficient (α) that expressed the number of electrons released for per electron collision, a similar coefficient exists for the case of

[1] M. Abdel-Salam, A. Turkey, (1988), IEEE Trans., IA-24: 1031

electronegative gases. This coefficient expresses the number of attachments produced in a path of a single electron travelling a distance of 10 mm in the direction of the field. In this case, the electron current will decrease in accordance with the relationship:

$$I_{loss} = I_0 e^{-\eta d} \tag{A.21}$$

where d is the gap distance.

Considering the two basic mechanisms (electron multiplication through electron collision and electron attachment) one can say that the two processes complement each other. Therefore, breakdown will occur if the number of electrons produced is more than the number of electrons attached. One can express this mathematically as follows:

Let the number of electrons produced via electron collision by $dn_c = n\alpha dx$ (From Townsend). At the same time, let n_a be the number of electrons attachted by the electronegative gas. In other words, $dn_a = -n\eta dx$. From this we can calculate the number of electrons that are still free in the gas. This number can be given by: $dn = dn_c + dna = n(\alpha - \eta)dx$. By Integration (from $x = 0$ to $x = d$) the number at any point in the gap can be expressed as

$$n = n_0 e^{(\alpha-\eta)} d \tag{A.22}$$

where n_0 is the number of electrons at the cathode. The total current that is observed, has two components: One resulting from ionisation be collision and one resulting from deionisation by attachment. The latter can be expressed as $dn_{neg} = n\eta dx = n_0 \eta e^{(\alpha-\eta)dx}$. By integrating across the gap,

$$n_{neg} = \frac{n_0 \eta}{\alpha - \eta}[e^{(\alpha-\eta)d} - 1] \tag{A.23}$$

The overall current can be expressed as follows:

$$\frac{n + n_{neg}}{n_0} = \frac{\alpha}{\alpha - \eta} e^{(\alpha-\eta)d} - \frac{\eta}{\alpha - \eta} \tag{A.24}$$

The final equation is therefore:

$$I = I_0[\frac{\alpha}{\alpha - \eta}e^{(\alpha-\eta)d} - \frac{\eta}{\alpha - \eta}] \tag{A.25}$$

A.6 Time lags in electrical breakdown

One of the most important parameters in electrical breakdown situations, is time. In some applications, it is very important to know when exactly breakdown phenomena take place. If a step voltage is applied to a gap, then there will be a finite time before the gap actually breaks down. This time t is made up of two components. These are the formative (t_f) and the statistical (t_s) time lags.

The statistical time lag is the most problematic of the two. It is the time taken for a free electron to become available at the cathode and start the electron avalanche that will lead to electrical breakdown across the gap. As the name implies, this time lag is variable. On average it is about $0.1\,ms$ [30]. The statistical time lag can be controlled (or eliminated completely) by providing the free electrodes required. This can be done by irradiating the cathode with ultraviolet (UV) light. Because of the short wavelength, electrons become available through photoionisation.

The formative time lag on the other hand is much faster than the statistical time lag and more importantly it is relatively constant. The formative time lag is the time taken for the avalanche to cross the gap. The formative time lag is dependant on the percentage overvoltage under impulse conditions. In other words, as the ratio $\frac{V_a - V_b}{V_b}$ increases. Where V_a is the applied voltage and V_b is the breakdown voltage of the gap. On average it is in the region of $0.01\mu s$

The above mentioned parameters (ionisation mechanisms, attachment coefficient and breakdown under pressurised conditions) and their affect on the phenomenon of laser-triggered breakdown will be further discussed in chapters 3 and 7.

A.7 Conclusion

There are three main mechanisms that are used to describe electrical breakdown in gases. These are the Townsend, Streamer and Leader mechanism. The leader

mechanism is used to describe breakdown across long gaps (over a meter). The streamer process s able to explain breakdown across gaps where the electric field is not uniform. For example a plane to point gap.

There are many ways by which electrical breakdown can occur. The most important of these process is ionisation by electron collision. At the same time processes such as photoionisation, ionisation by metastable atoms and to a lesser degree thermal ionisation become important.

In some cases gases such as the halogens are able to attach free electrons and form negative ions. These gases are known as electronegative and the process of electron attachment counteracts that of ionisation. Therefore, the breakdown of a gap depends on the combination of ionisation and attachment.

The phenomenon of electrical breakdown is dependent on the pressure of the gas and the electric field applied to the gap. The law that describes the relationship between the breakdown voltage and the gap pressure and electric field, is known as Paschen's Law ($V = f(pd)$).

There are two types of time lag that are associated with gap breakdown. These are the statistical and formative time lag. The statistical time lag is the time taken for an electron to become available and start the breakdown process, whereas the formative time lag is the time taken for the electron avalanche to cross the gap. The first, as the name implies is highly variable, whereas the formative time lag remains relatively constant.

Appendix B

Head-on and Side images of observed 'feature'

Presented here are the head-on and side view images of the observed 'feature'. These images were used together with the calibration image in order to measure the dimensions of this feature.

B.1 Head-on view of 'feature'

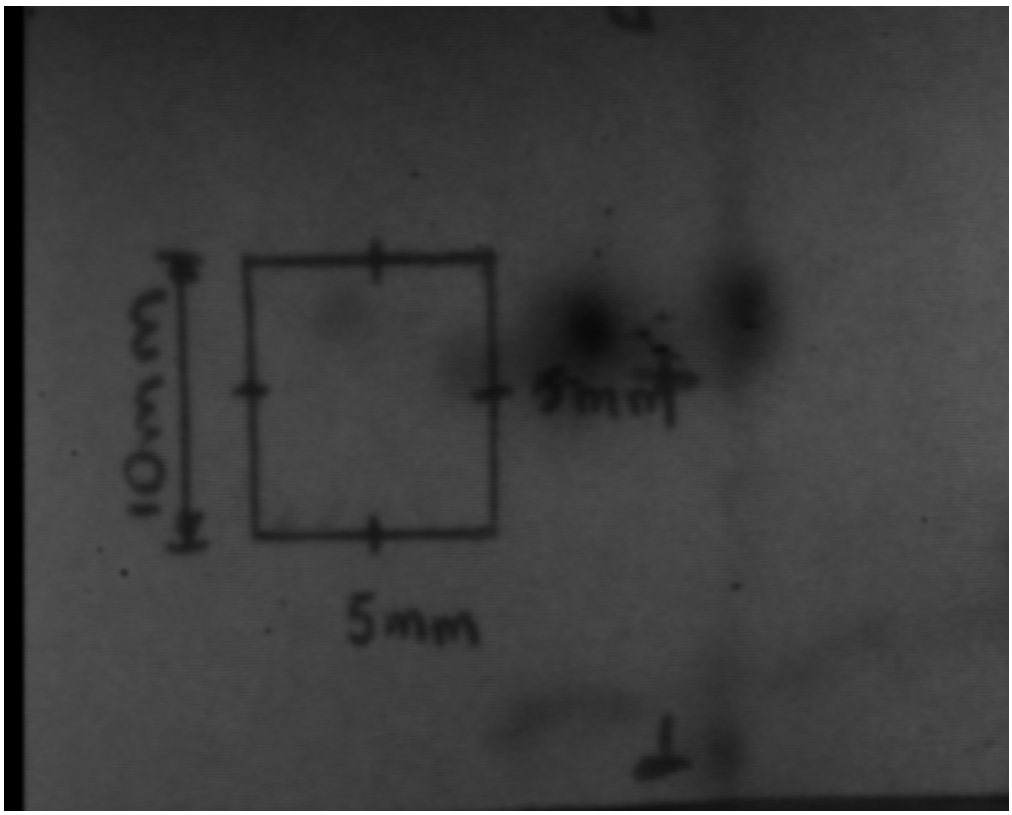


Figure B.1: Calibration image used to measure dimensions of observed 'feature'



Figure B.2: Feature 1 L=14 mm $\phi = 8.13°$

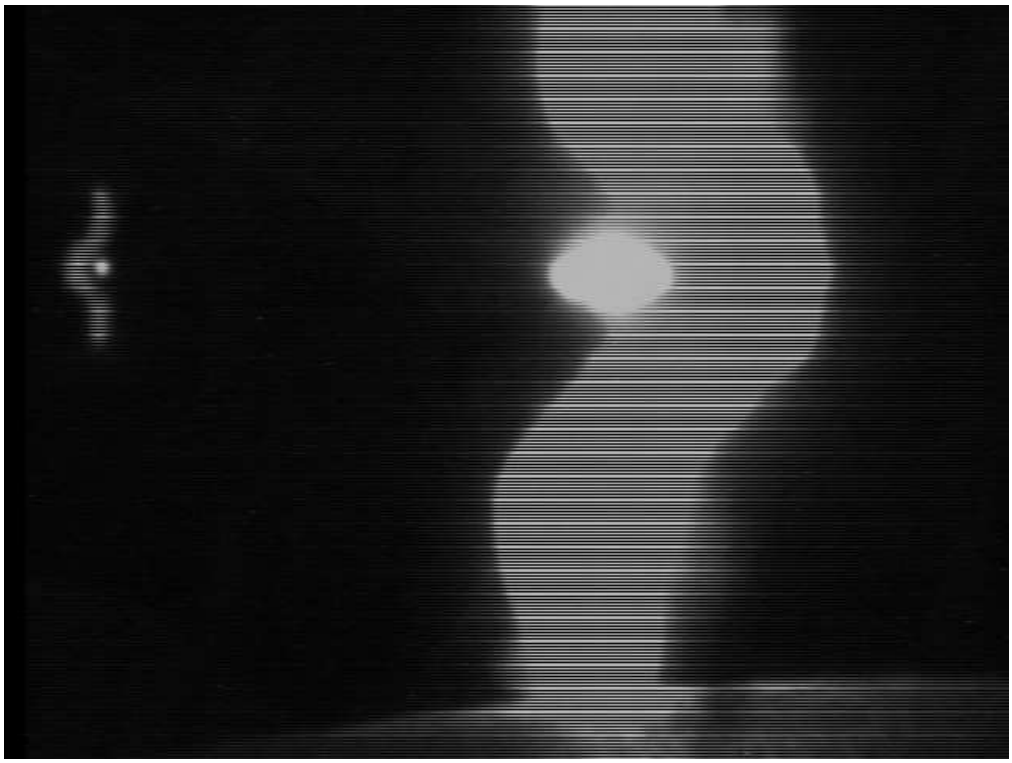


Figure B.3: Feature 2 L=12 mm $\phi = 4.46°$

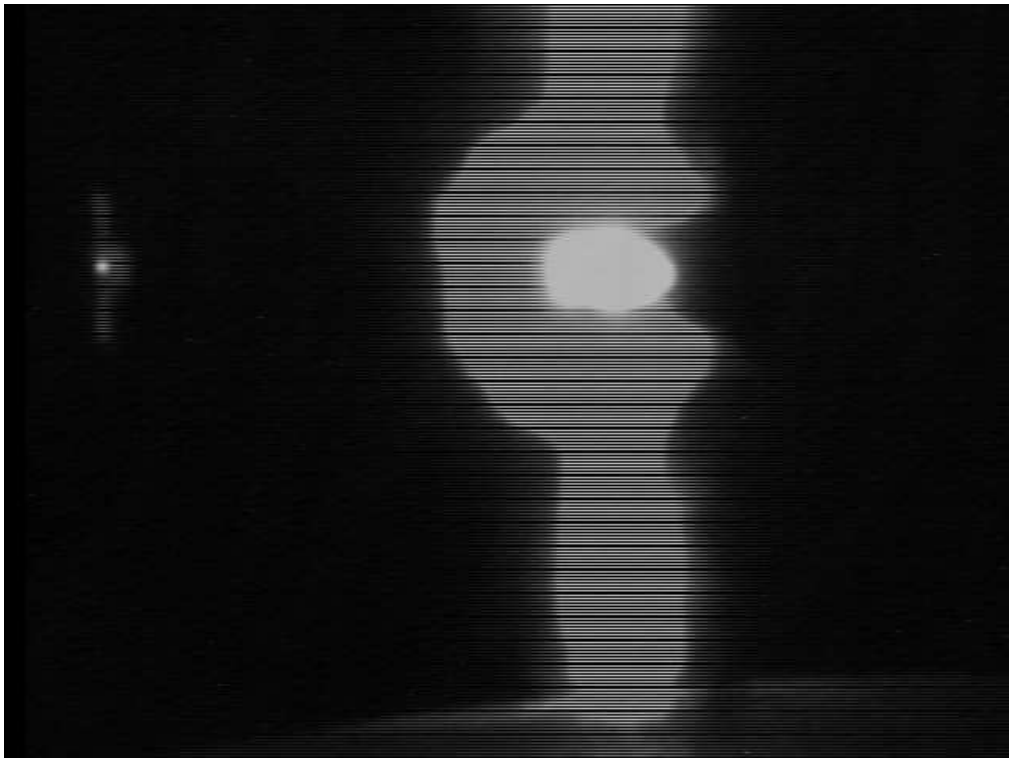


Figure B.4: Feature 3 L=12 mm $\phi = 0°$

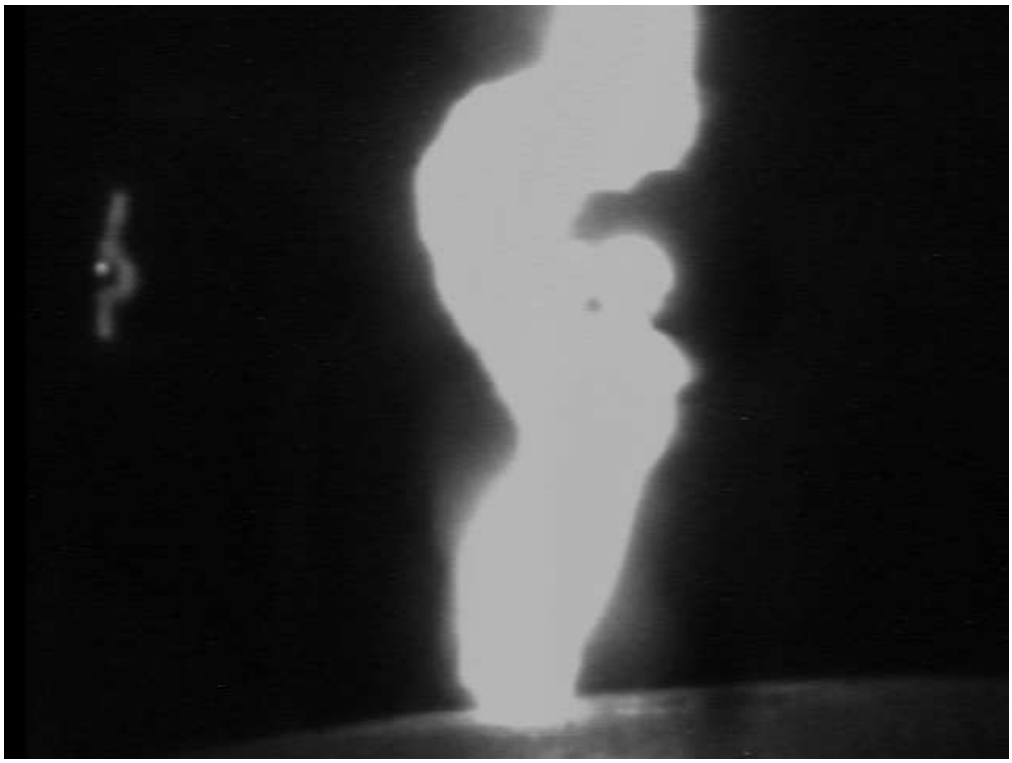


Figure B.5: Feature 4 L=13 mm $\phi = 0°$

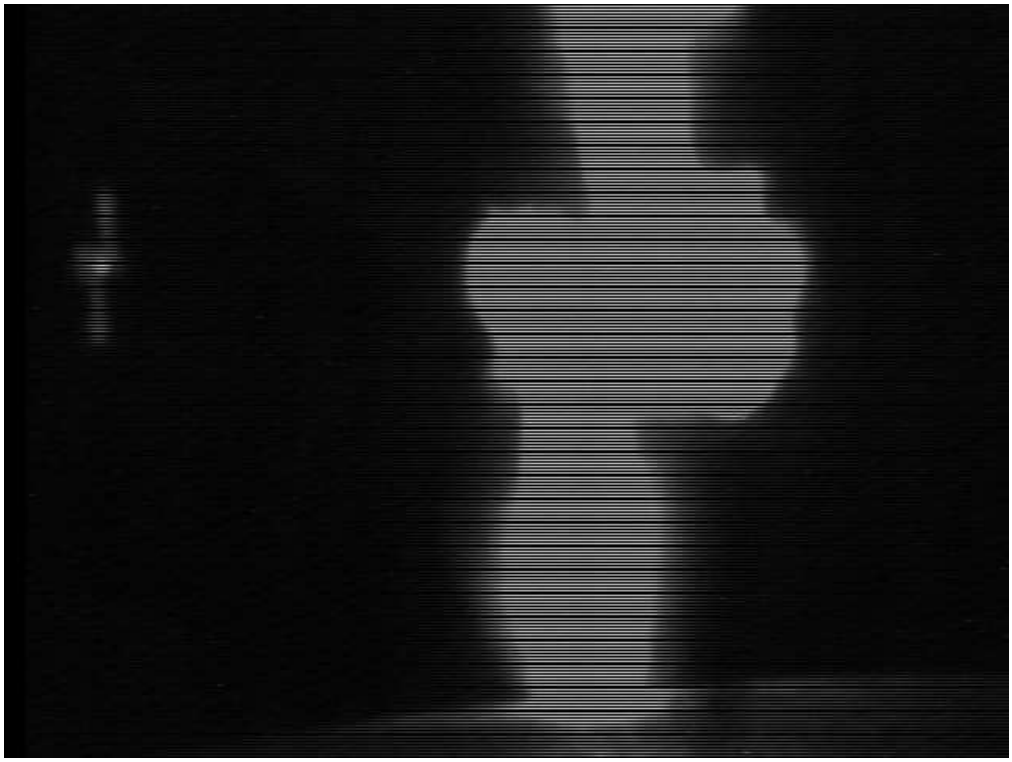


Figure B.6: Feature 5 L=11 mm $\phi = 10.3°$



Figure B.7: Feature 6 L=14 mm $\phi = 4.09°$

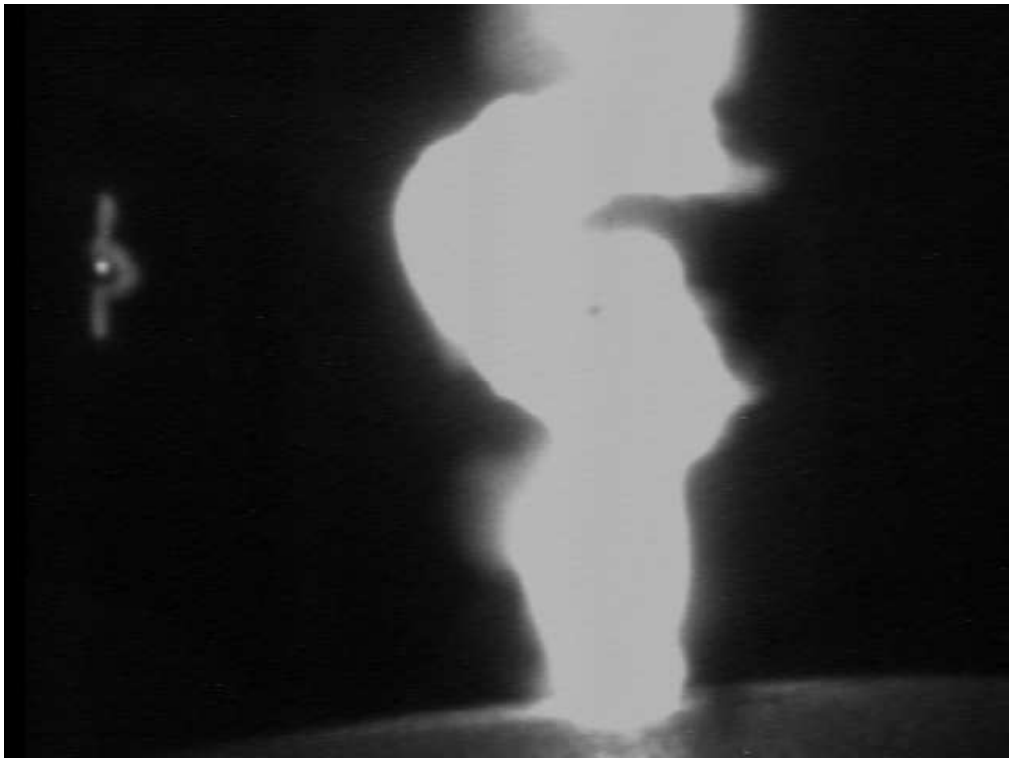


Figure B.8: Feature 7 L=14 mm $\phi = 4.9°$

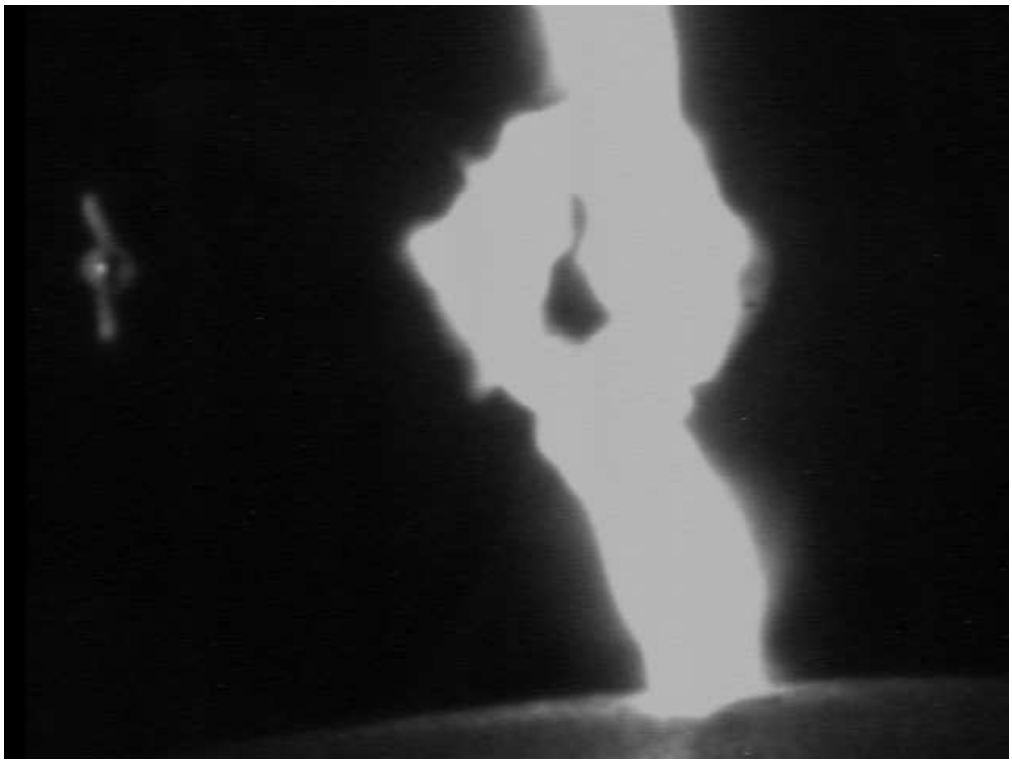


Figure B.9: Feature 8 L=13 mm $\phi = 0°$



Figure B.10: Feature 9 L=14 mm $\phi = 4.09°$



Figure B.11: Feature 10 L=12 mm $\phi = 2.39°$

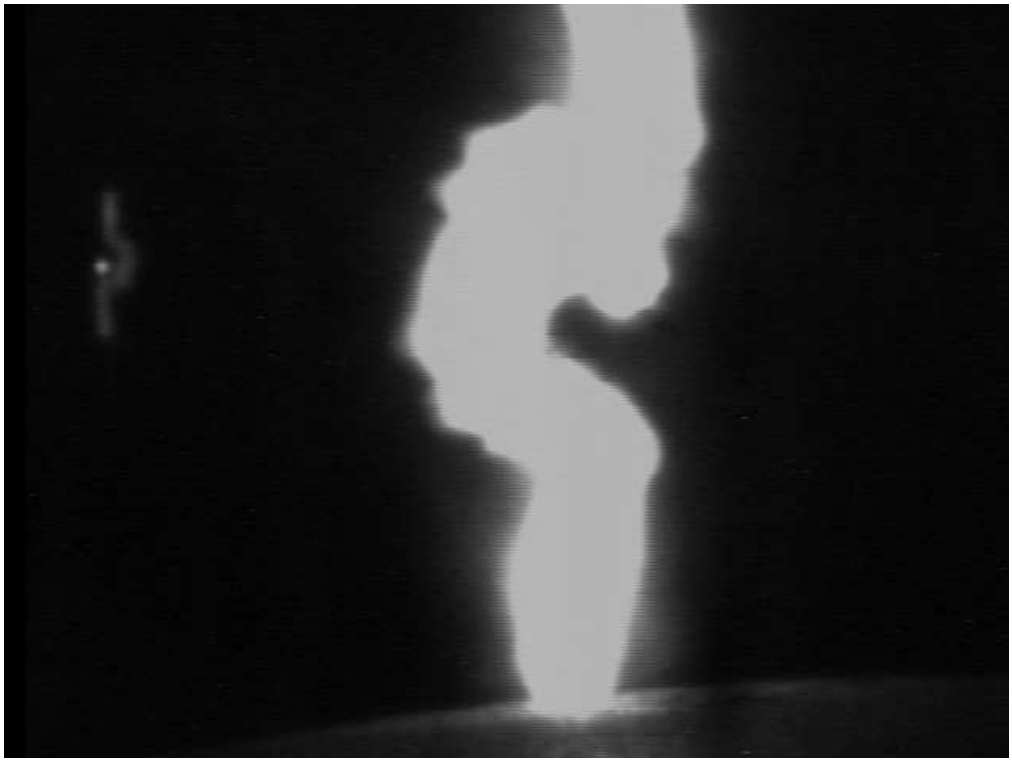


Figure B.12: Feature 11 L=14 mm $\phi = 8.13°$

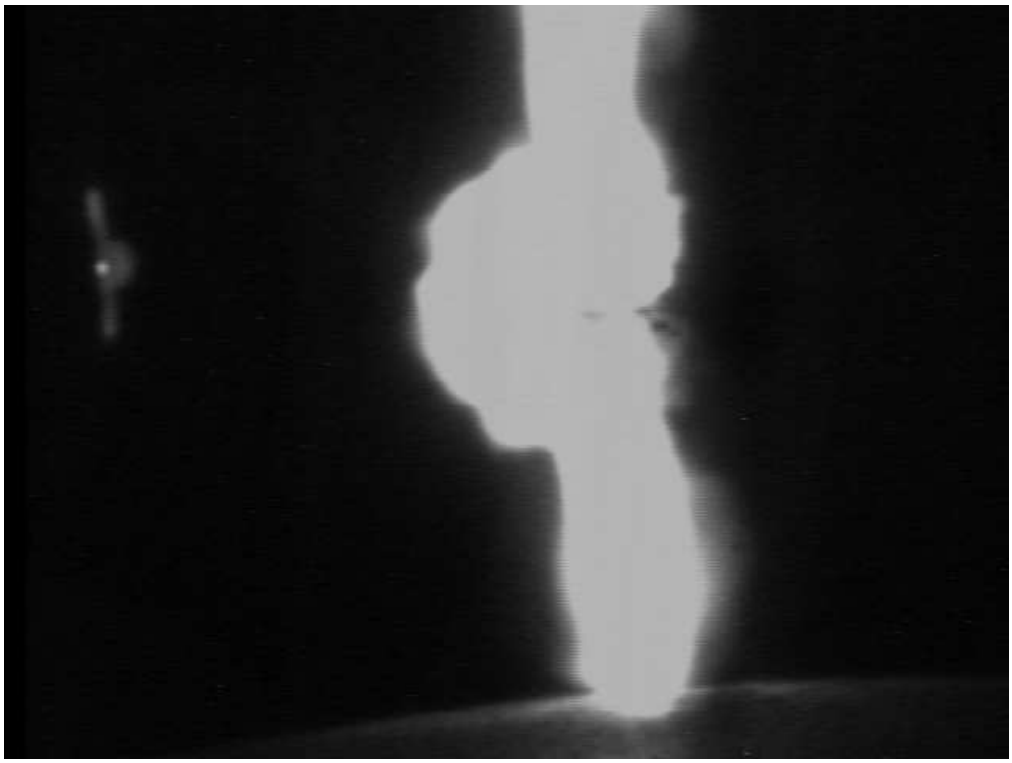


Figure B.13: Feature 12 L=12 mm $\phi = 4.76°$

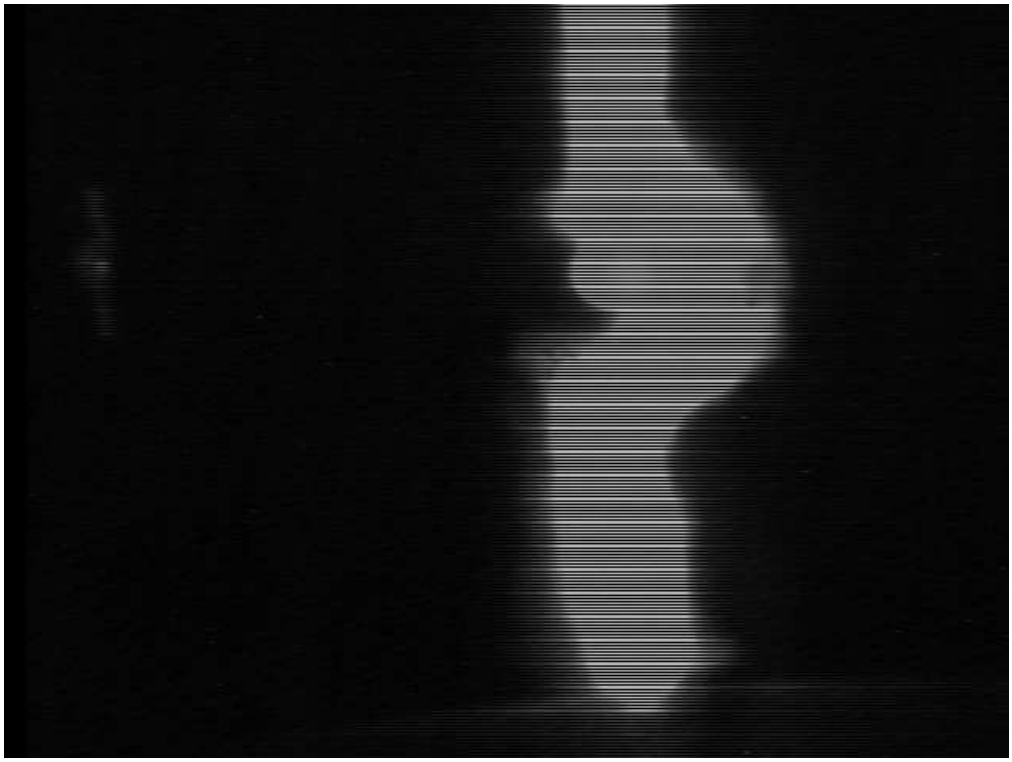


Figure B.14: Feature 13 L=12 mm $\phi = 0°$

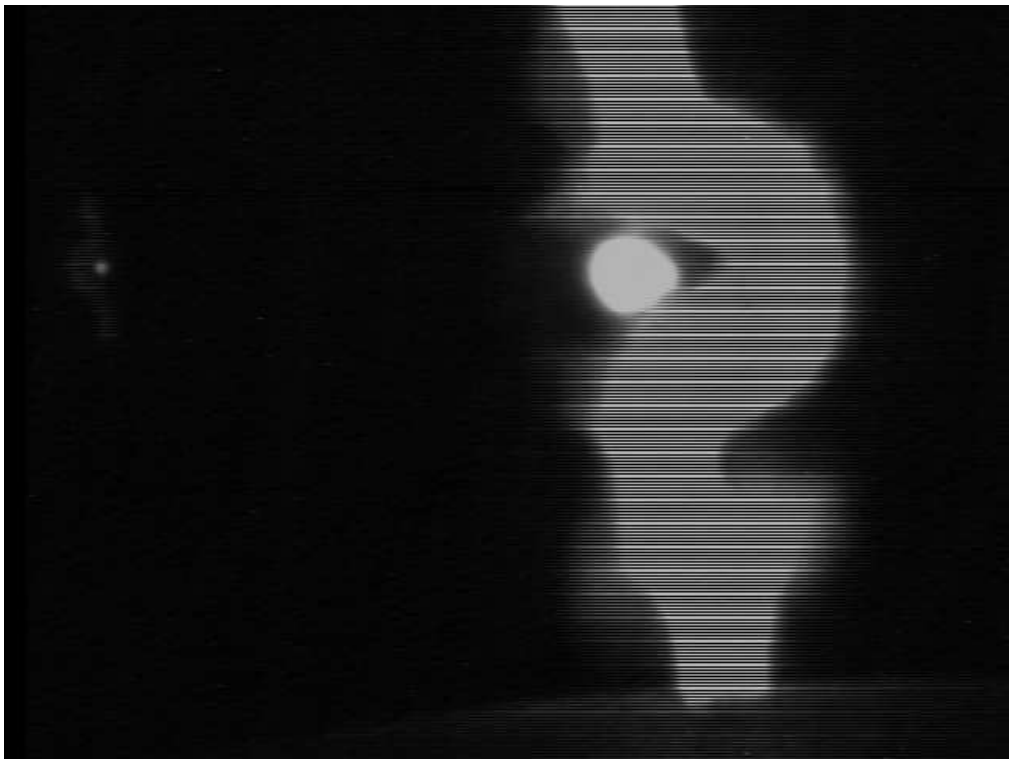


Figure B.15: Feature 14 L=13 mm $\phi = 4.4°$

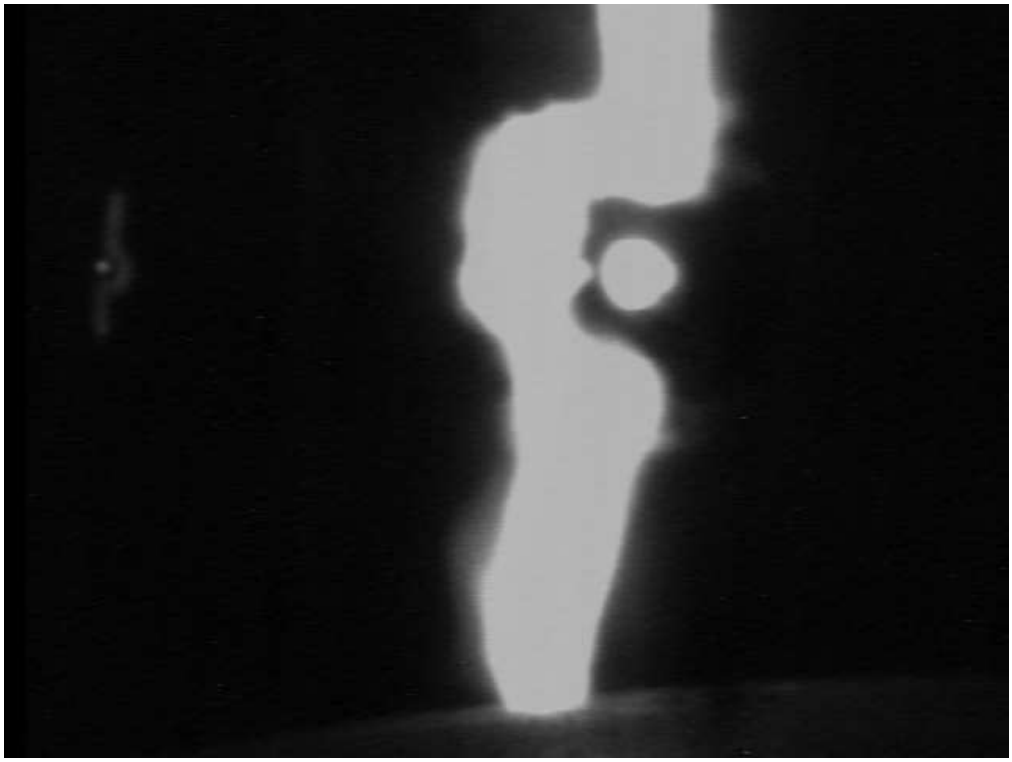


Figure B.16: Feature 15 L=14 mm $\phi = 12.09°$

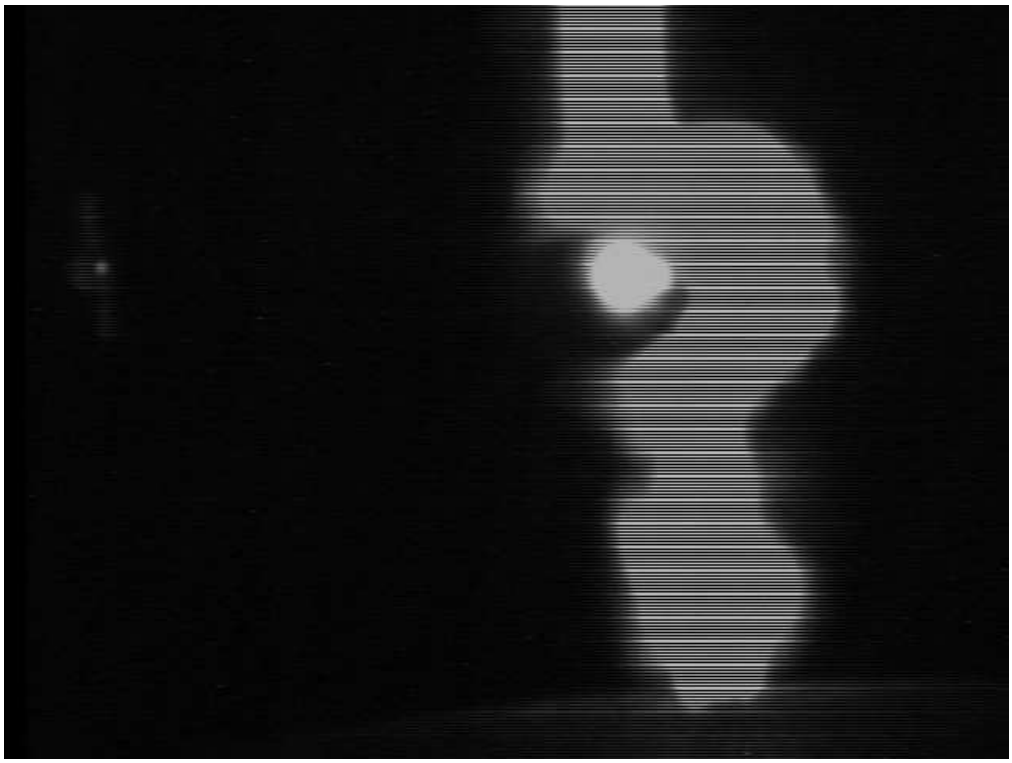


Figure B.17: Feature 16 L=13 mm $\phi = 12.99°$

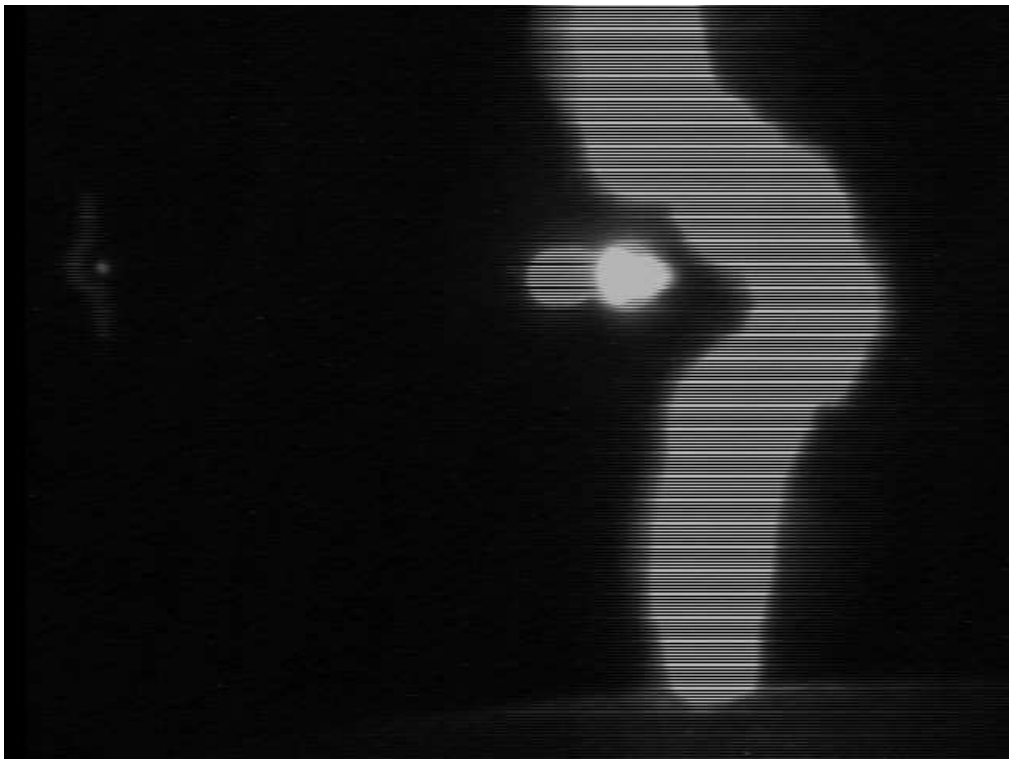


Figure B.18: Feature 17 L=10 mm $\phi = 16.7°$

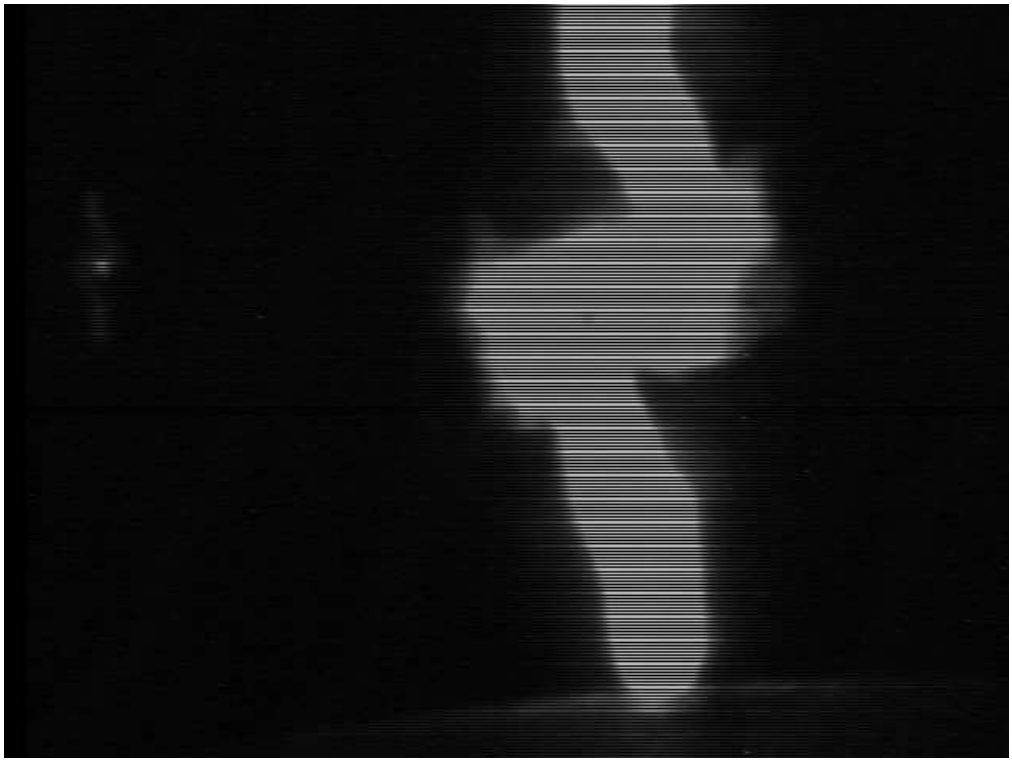


Figure B.19: Feature 18 L=10 mm $\phi = 16.7°$

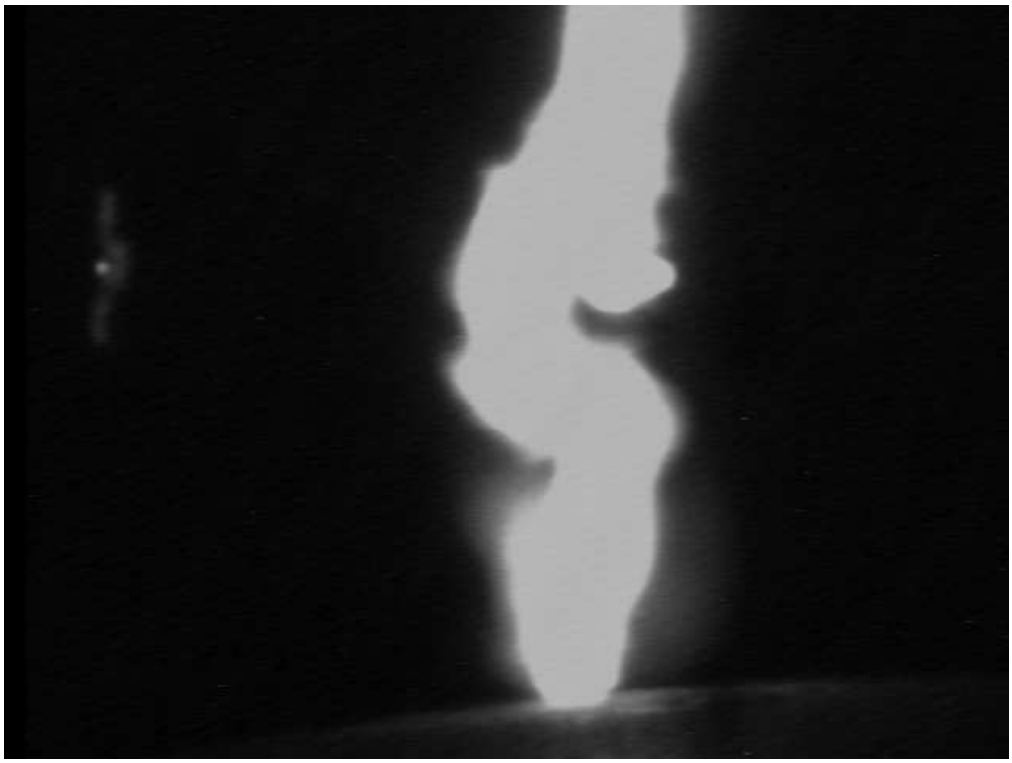


Figure B.20: Feature 19 L=13 mm $\phi = 4.4°$

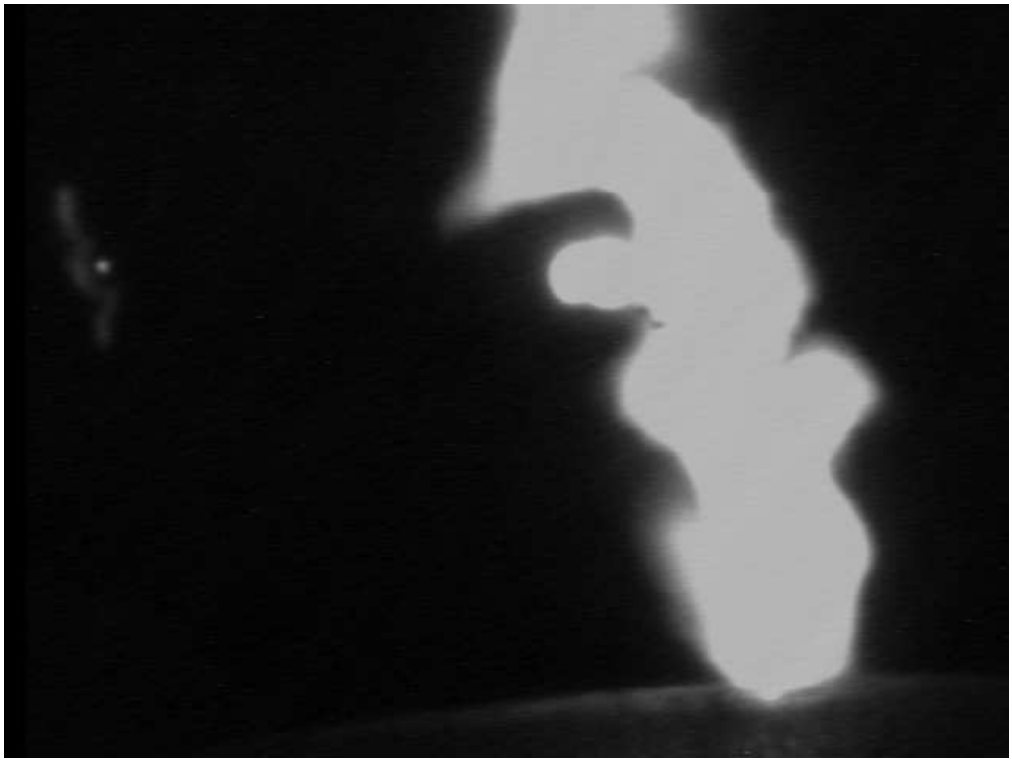


Figure B.21: Feature 20 L=10 mm $\phi = 14.3°$

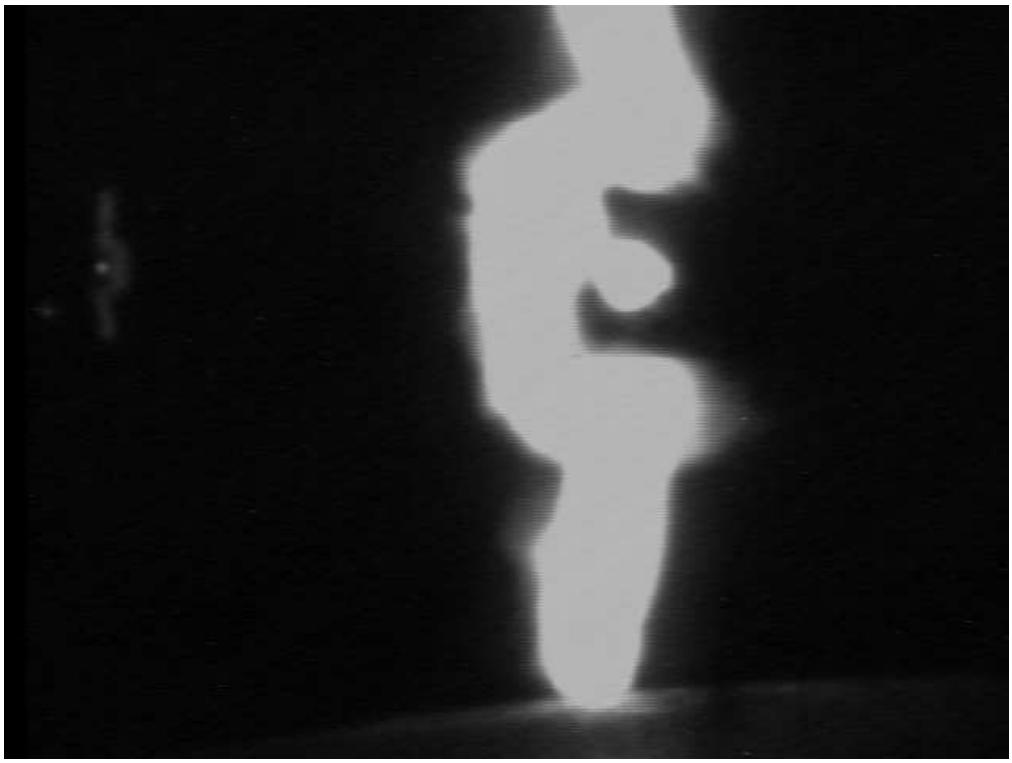


Figure B.22: Feature 21 L=15 mm $\phi = 3.81°$

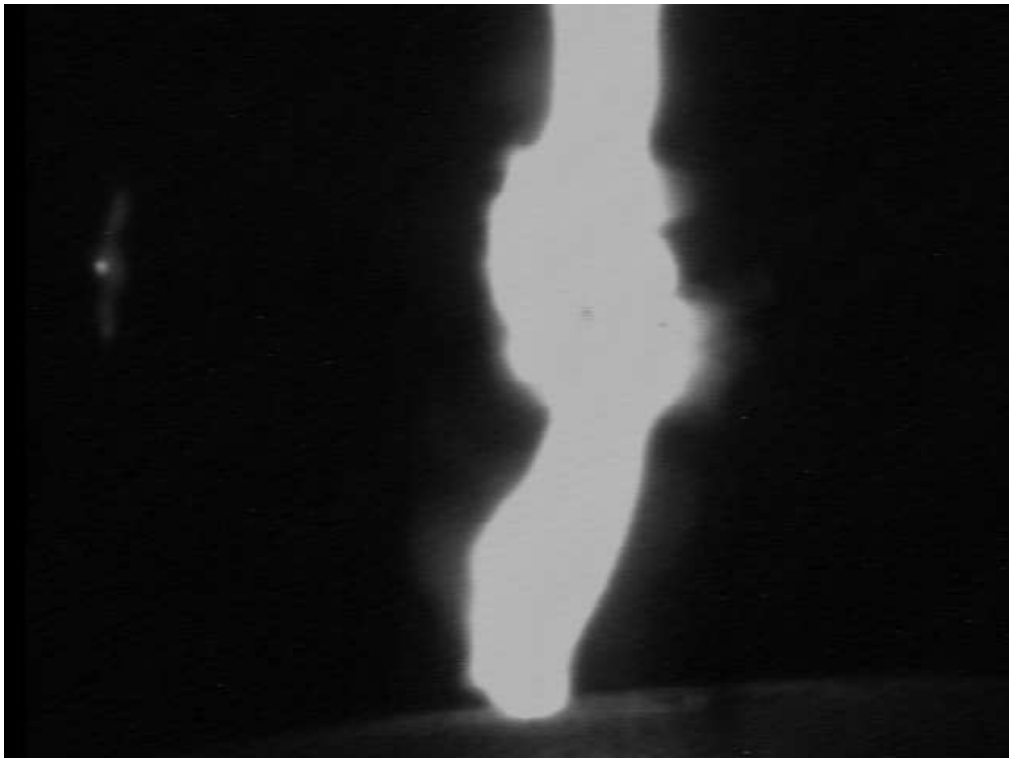


Figure B.23: Feature 22 L=12 mm $\phi = 3.39°$

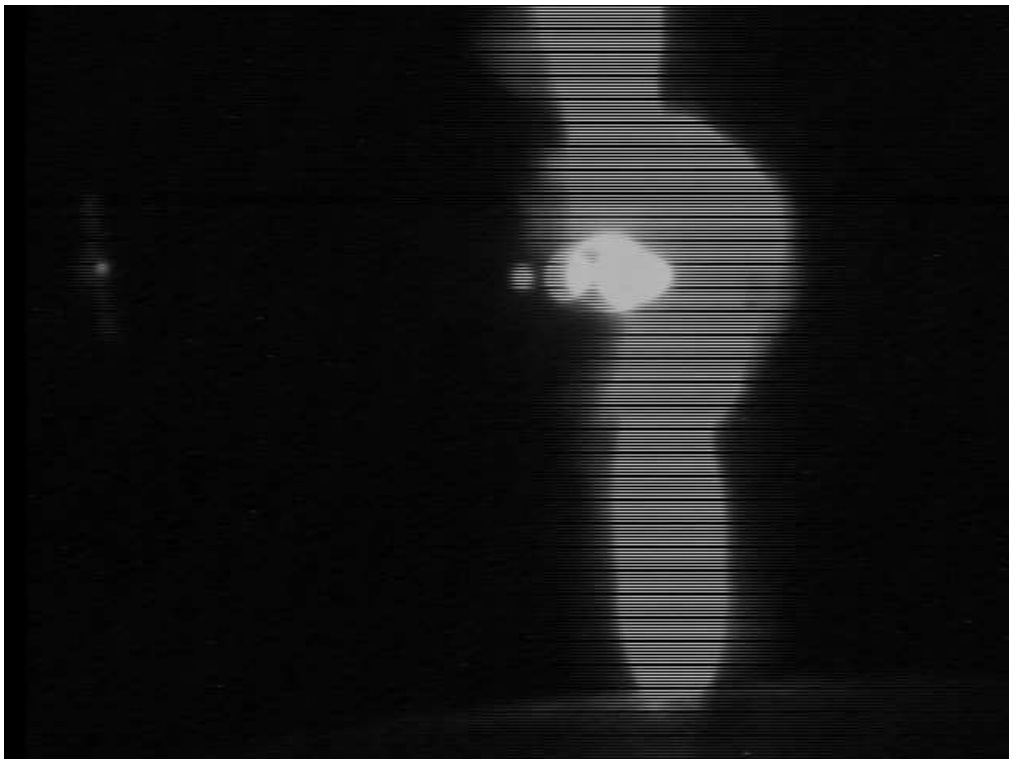


Figure B.24: Feature 23 L=11 mm $\phi = 10.3°$

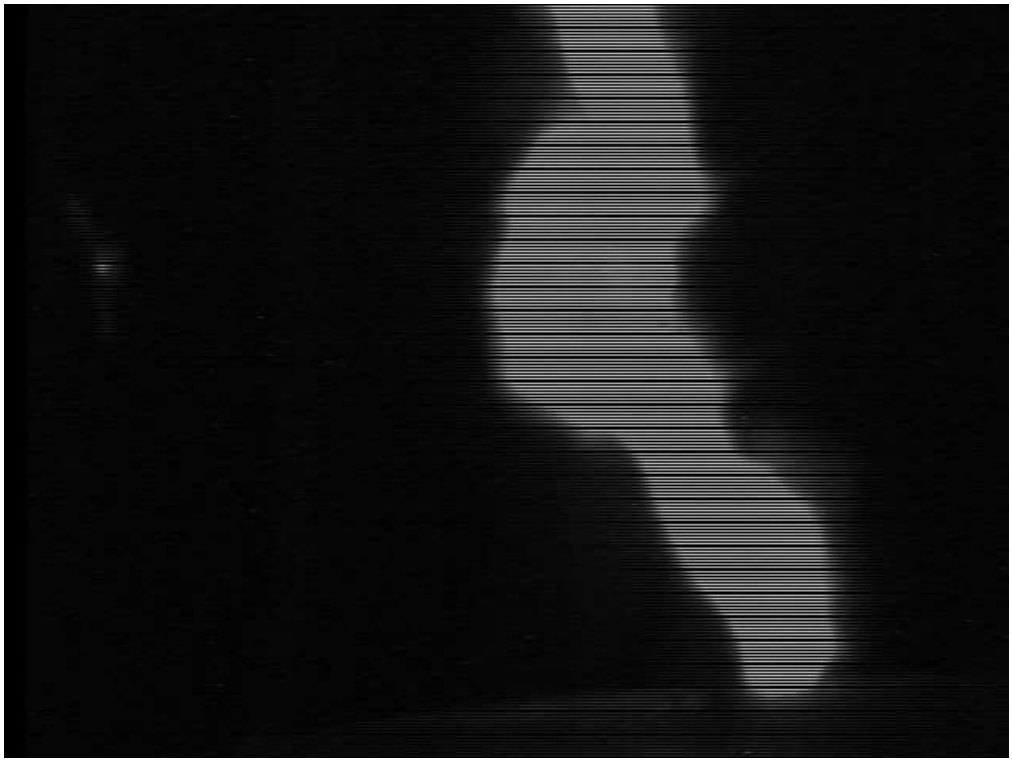


Figure B.25: Feature 24 L=12 mm $\phi = 9.46°$

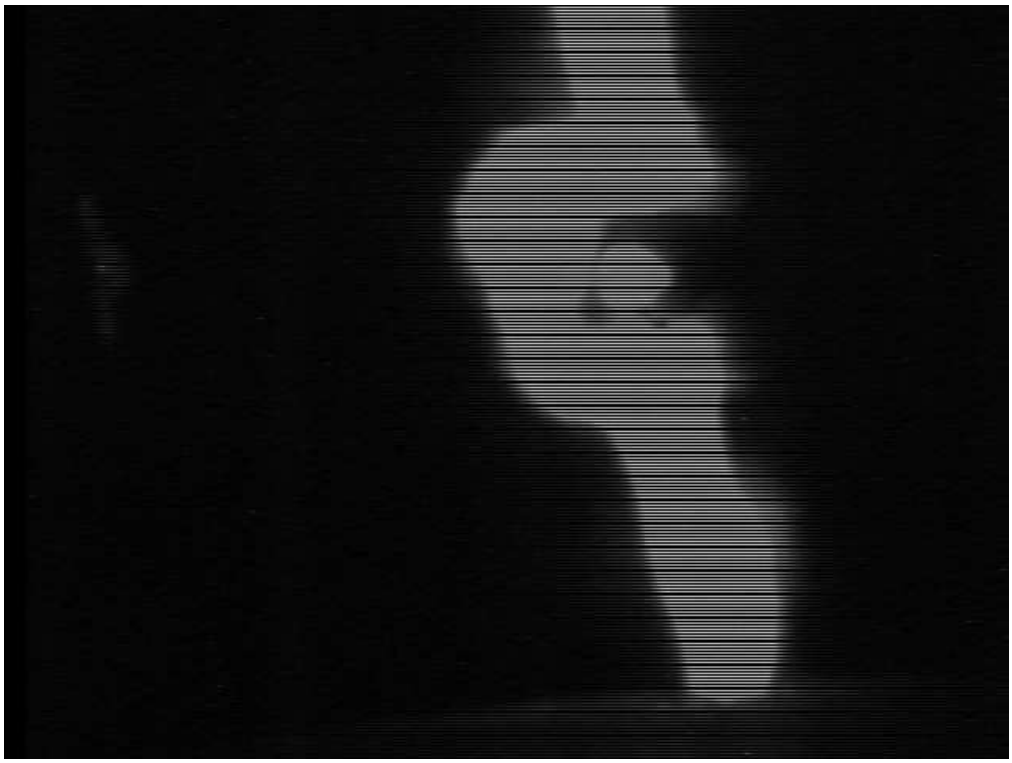


Figure B.26: Feature 25 L=13 mm $\phi = 8.75°$

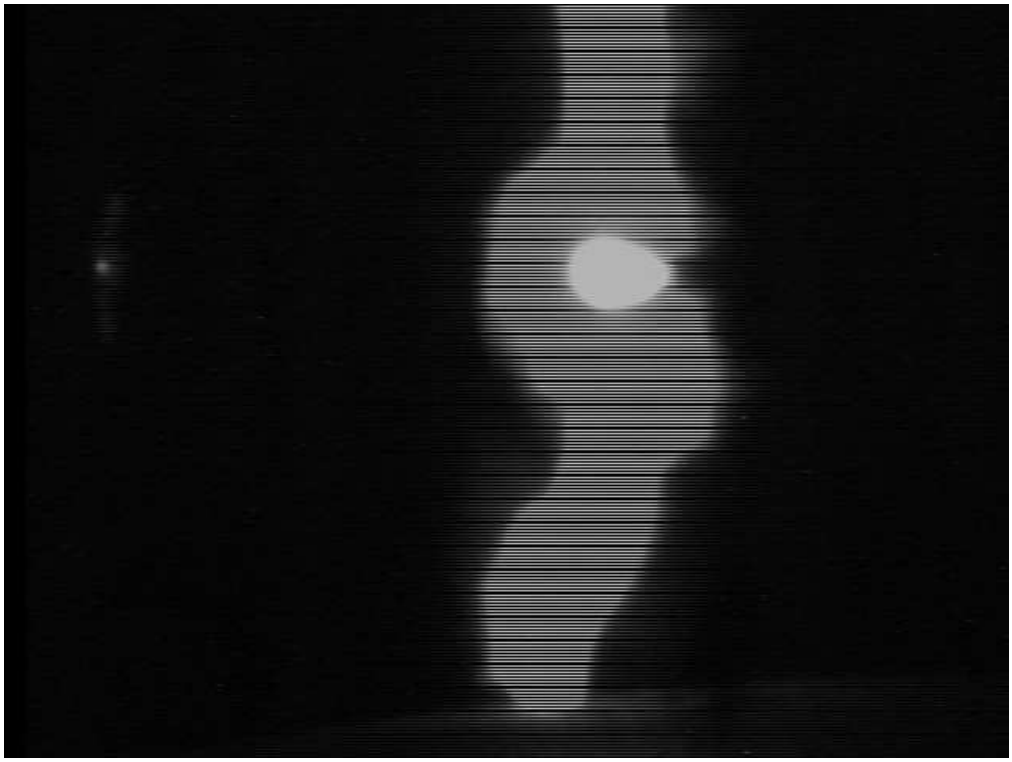


Figure B.27: Feature 26 L=13 mm $\phi = 0°$

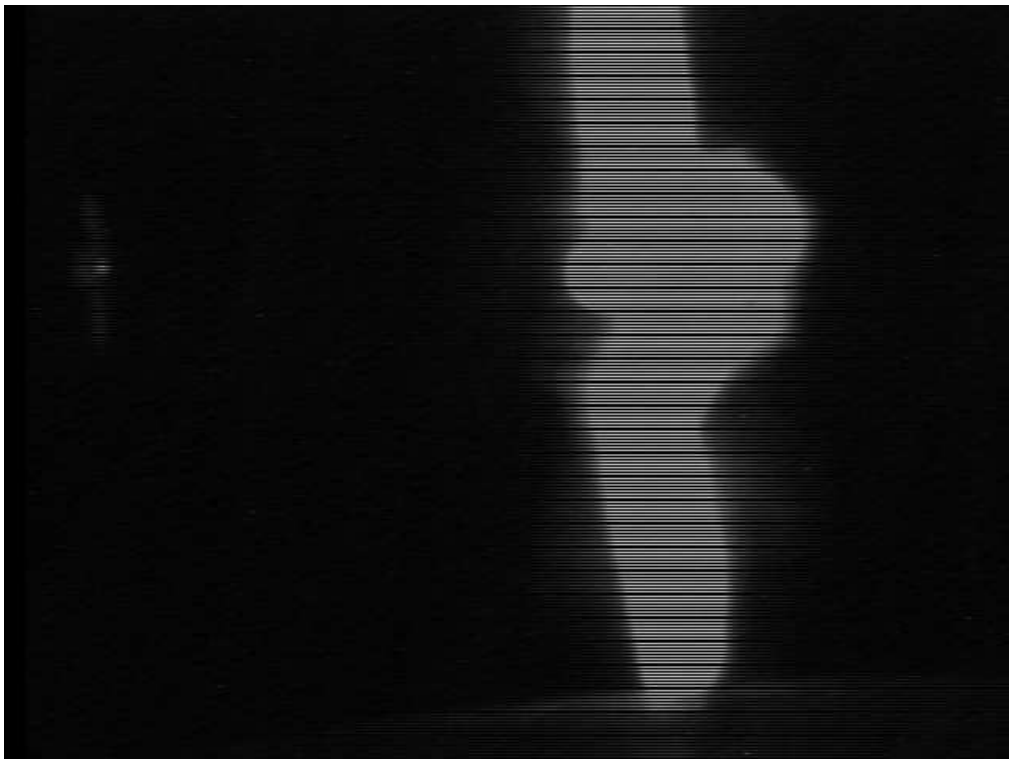


Figure B.28: Feature 27 L=10 mm $\phi = 5.71°$

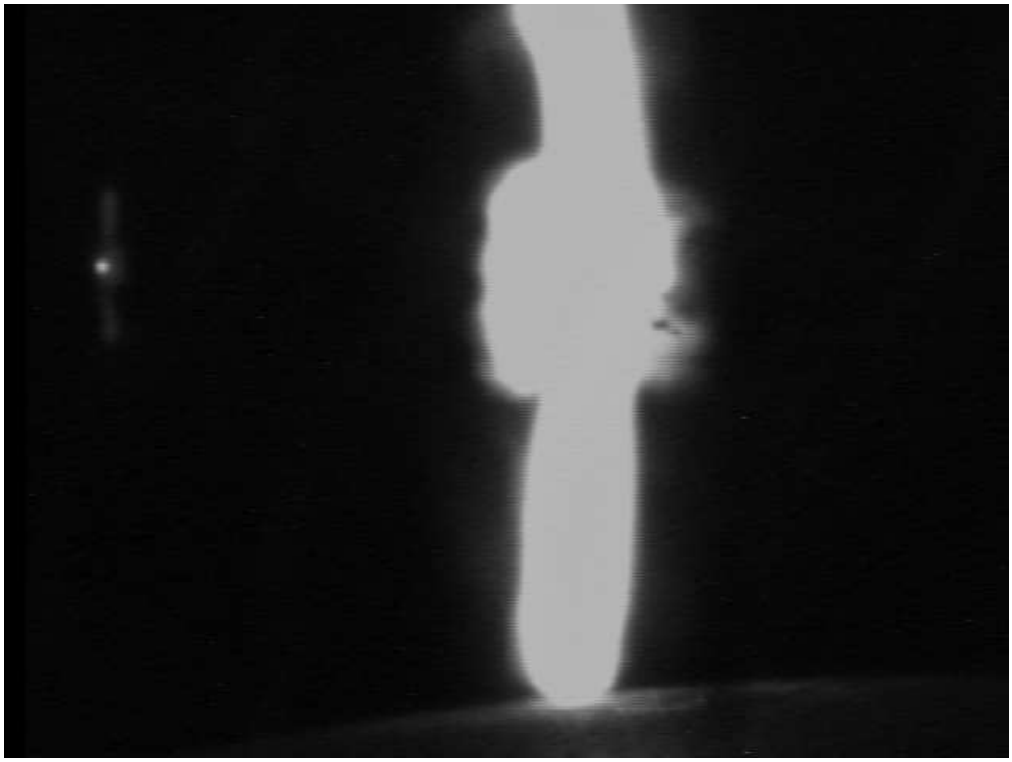


Figure B.29: Feature 28 L=10 mm $\phi = 0°$

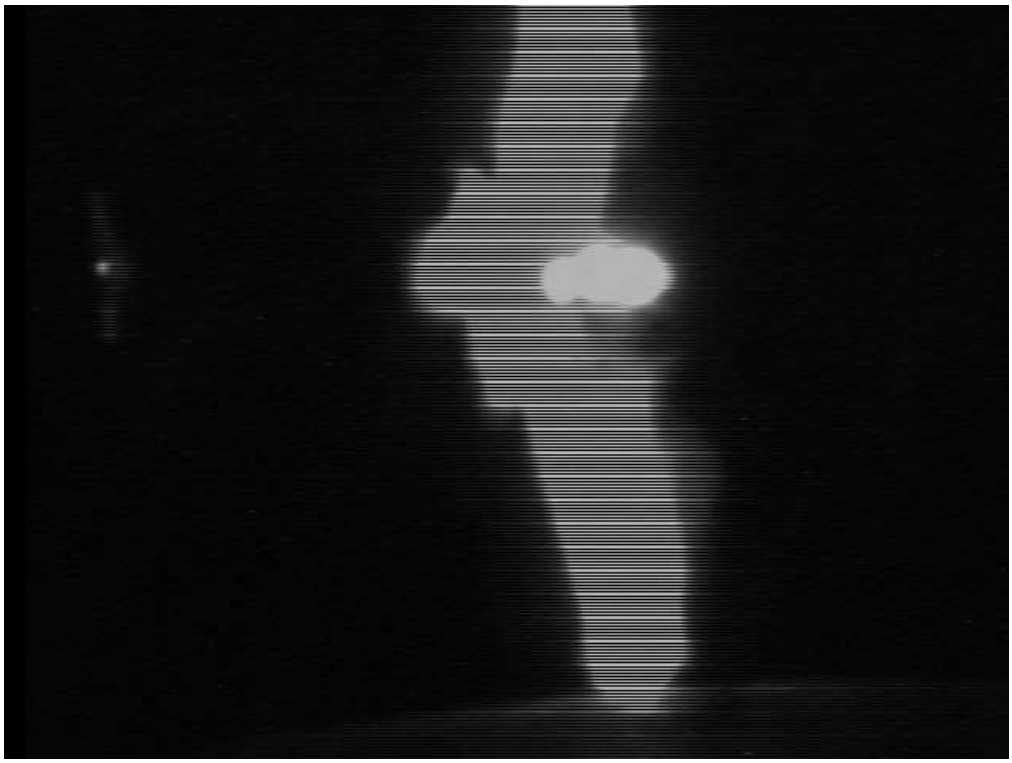


Figure B.30: Feature 29 L=12 mm $\phi = 9.46°$

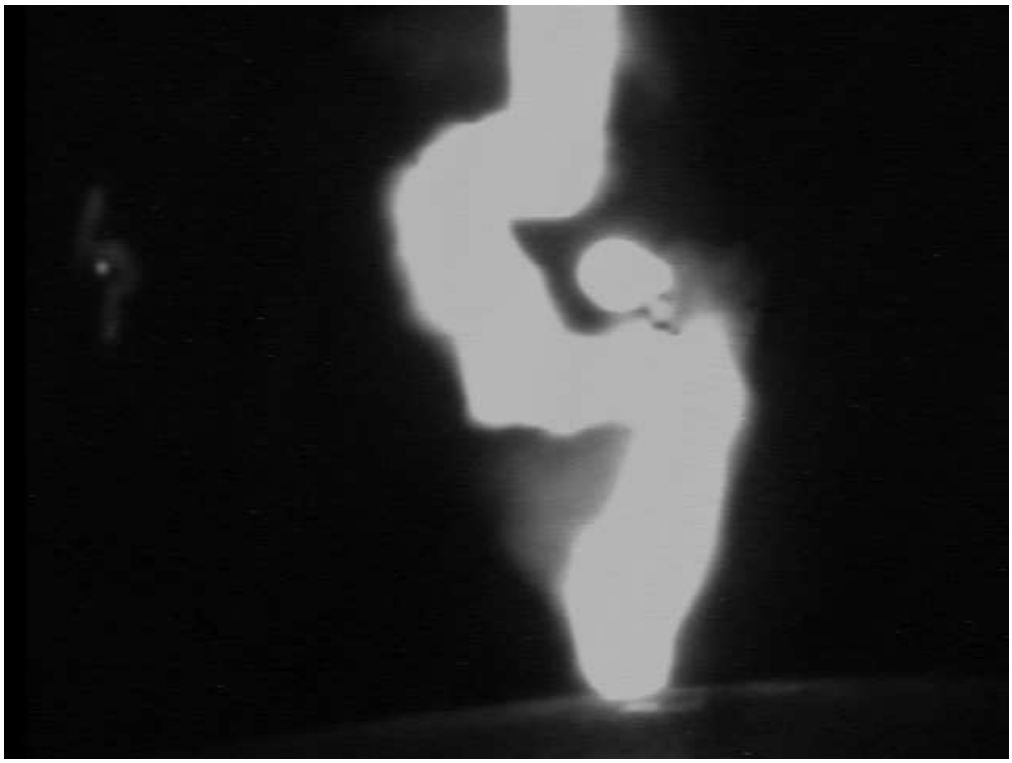


Figure B.31: Feature 30 L=14 mm $\phi = 19.65°$

B.2 Side view of 'feature'

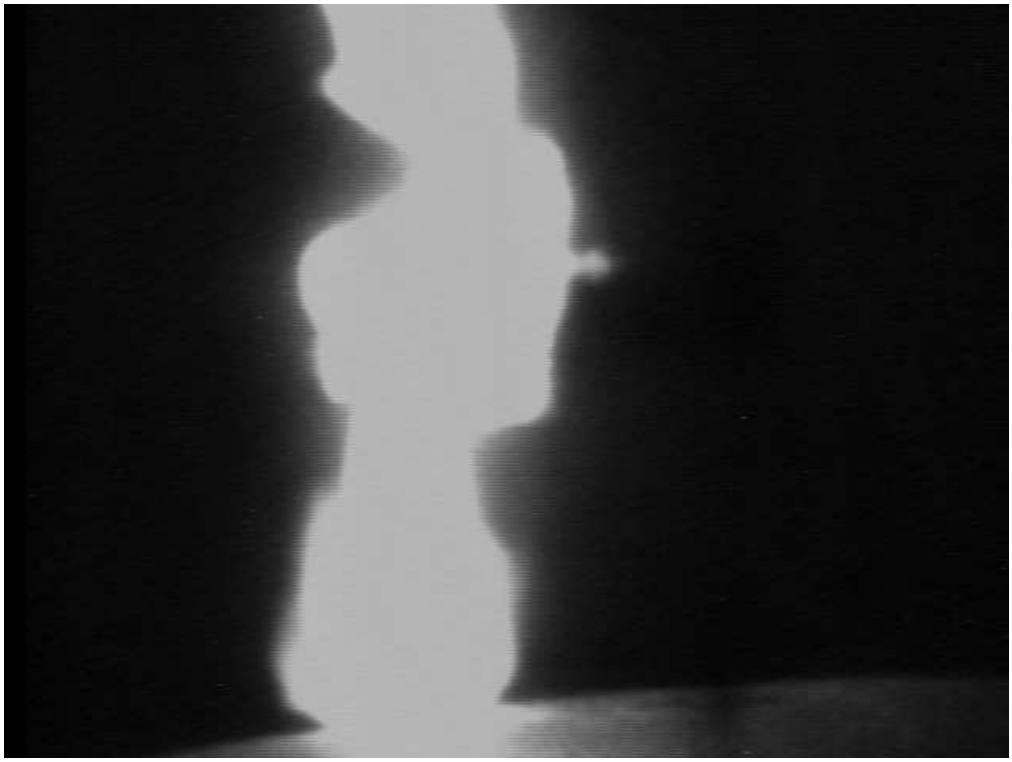


Figure B.32: Feature 31 L=11 mm $\phi = 10.3°$

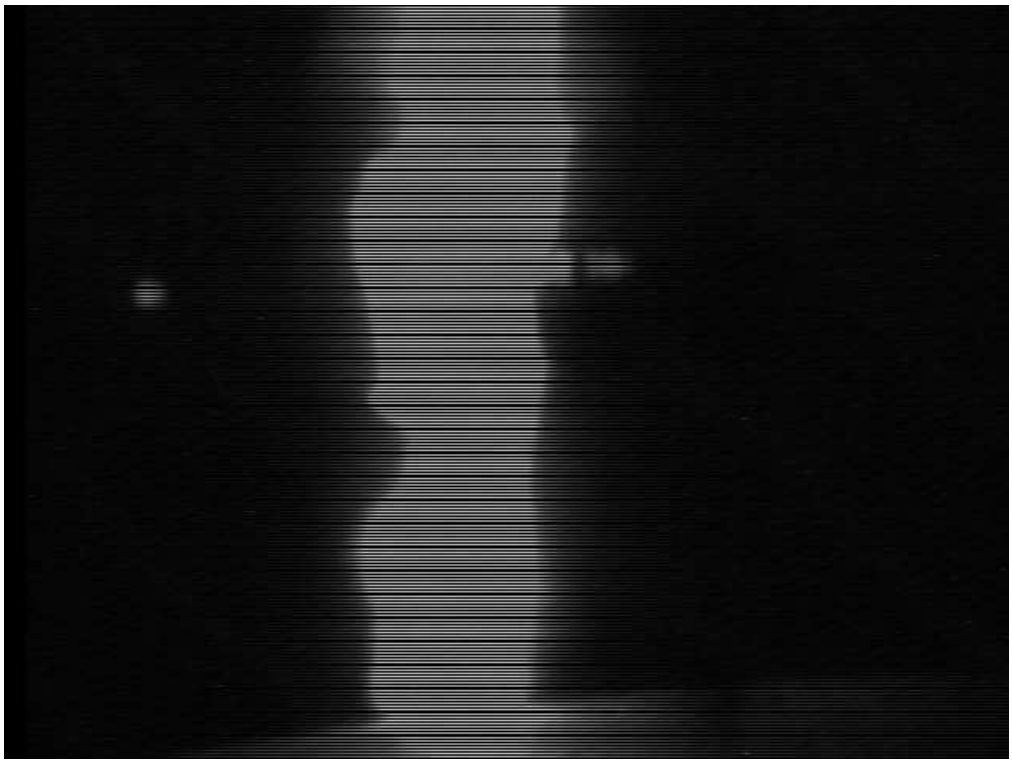


Figure B.33: Feature 32 L=10 mm $\phi = 5.71°$

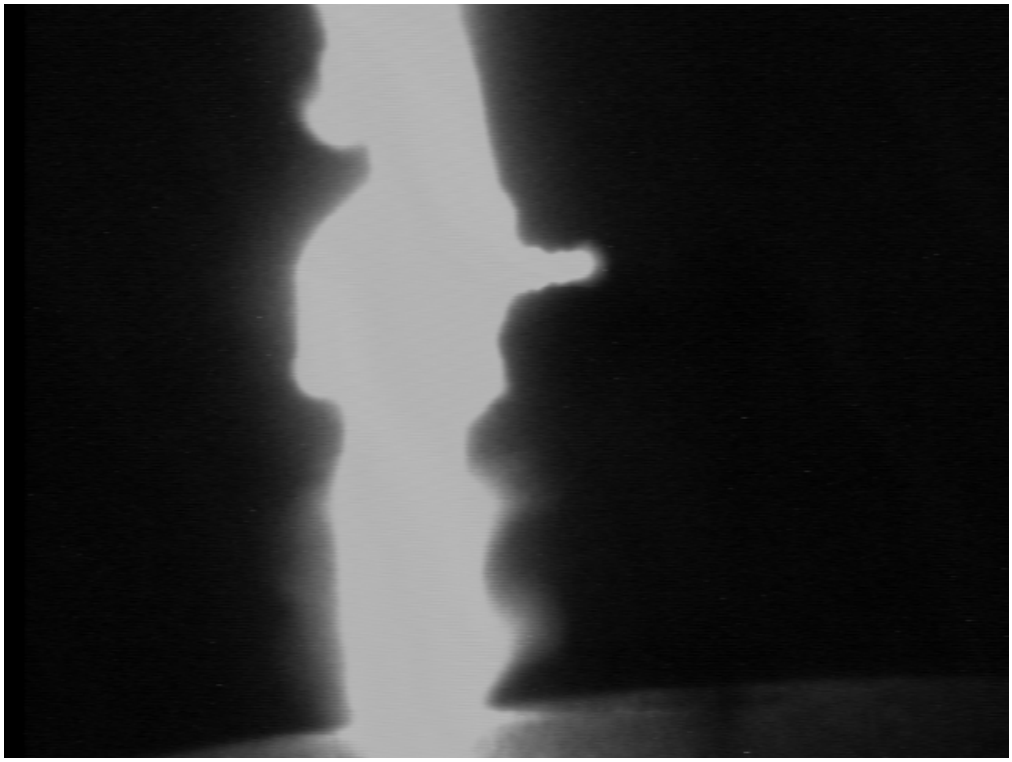


Figure B.34: Feature 33 L=10 mm $\phi = 5.71°$

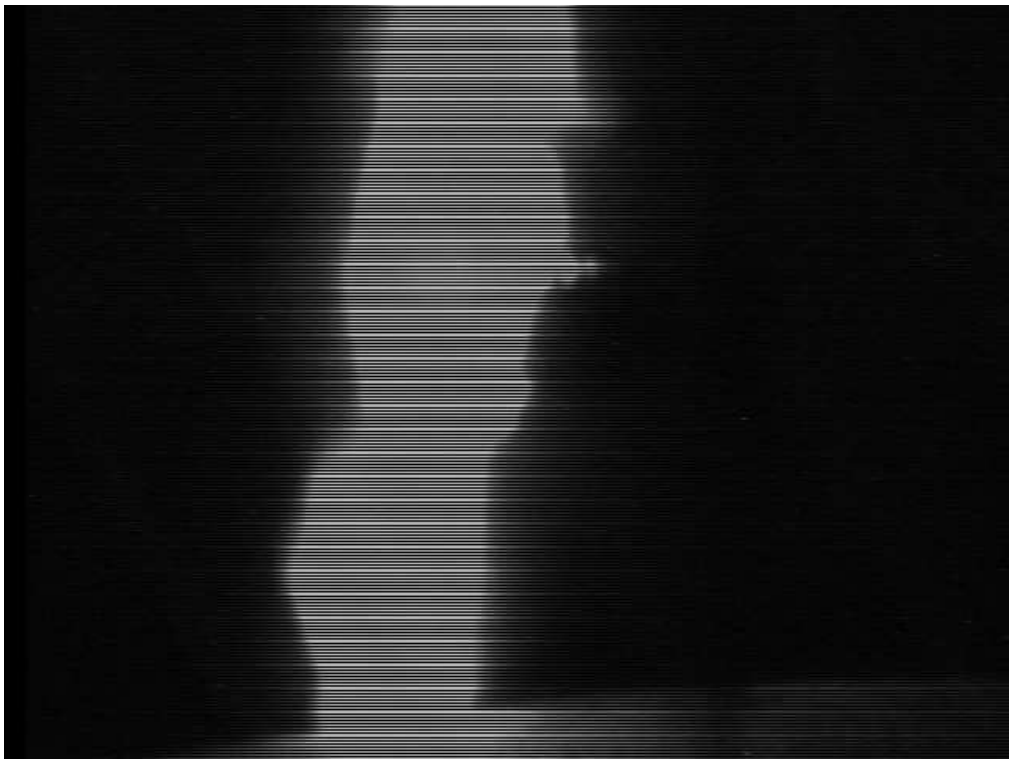


Figure B.35: Feature 34 L=9 mm $\phi = 6.34°$

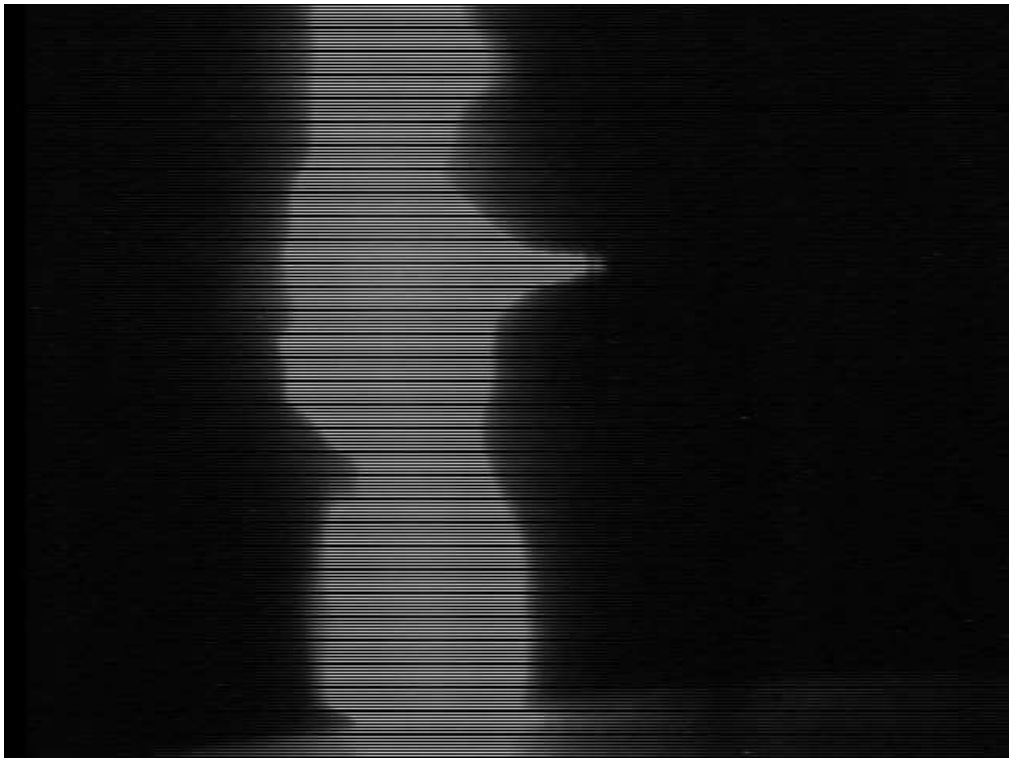


Figure B.36: Feature 35 L=13 mm $\phi = 2.2°$

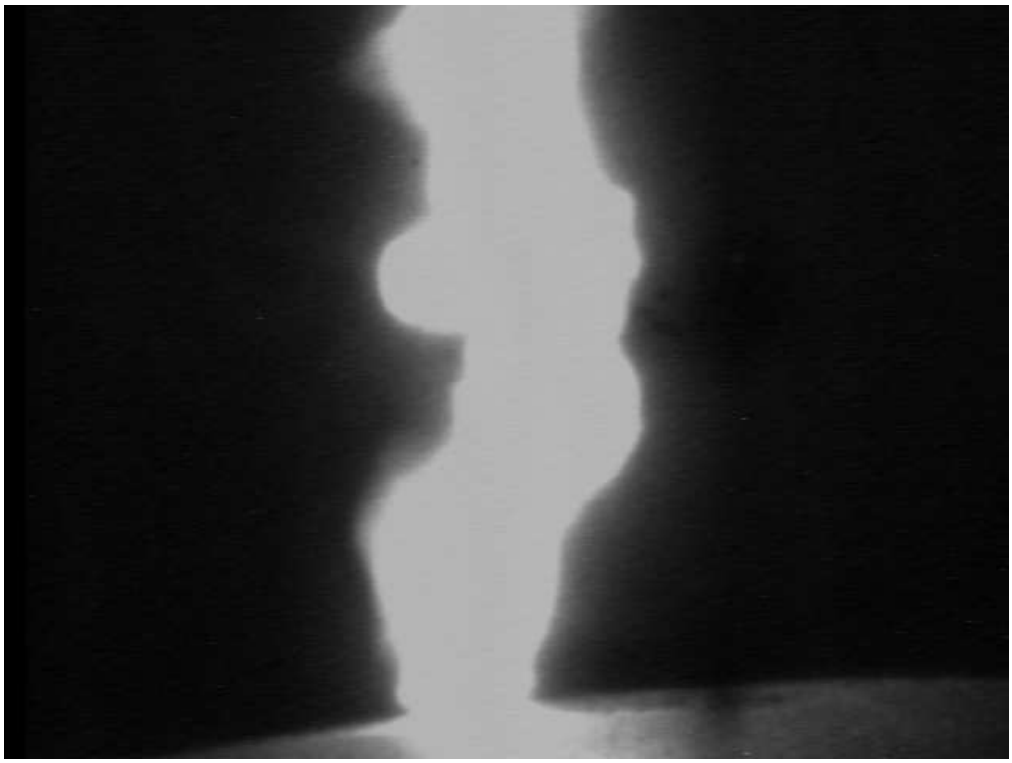


Figure B.37: Feature 36 L=11 mm $\phi = 2.6°$

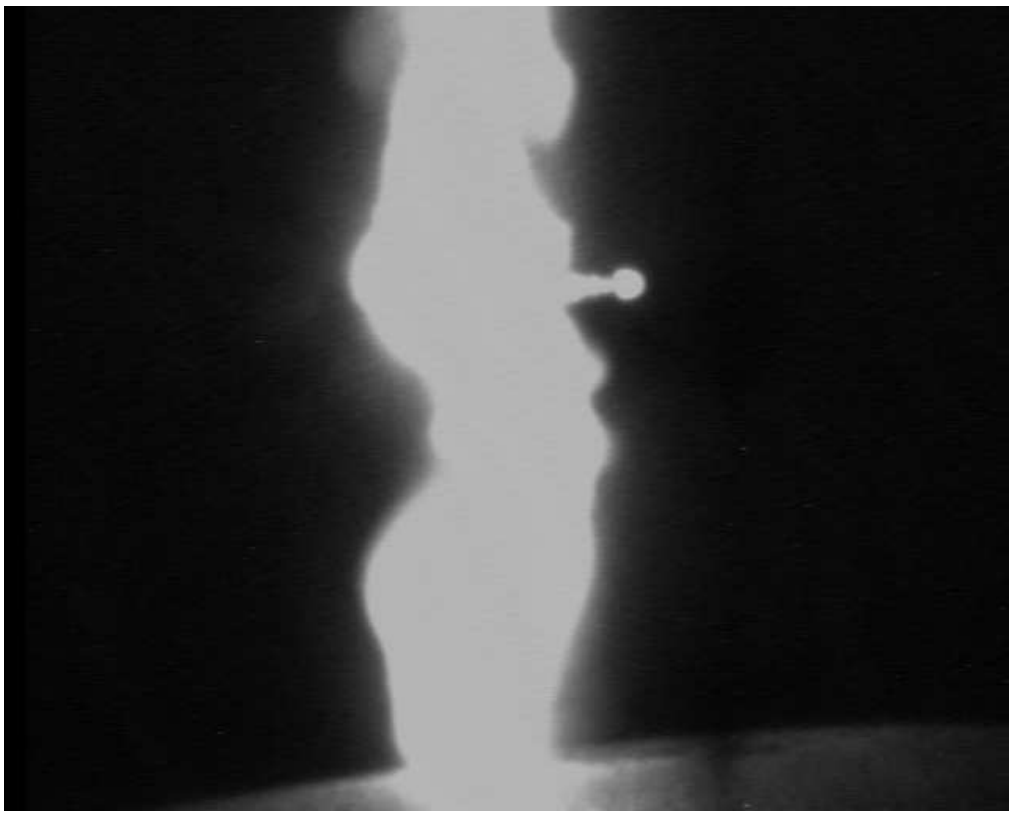


Figure B.38: Feature 37 L=11 mm $\phi = 12.8°$

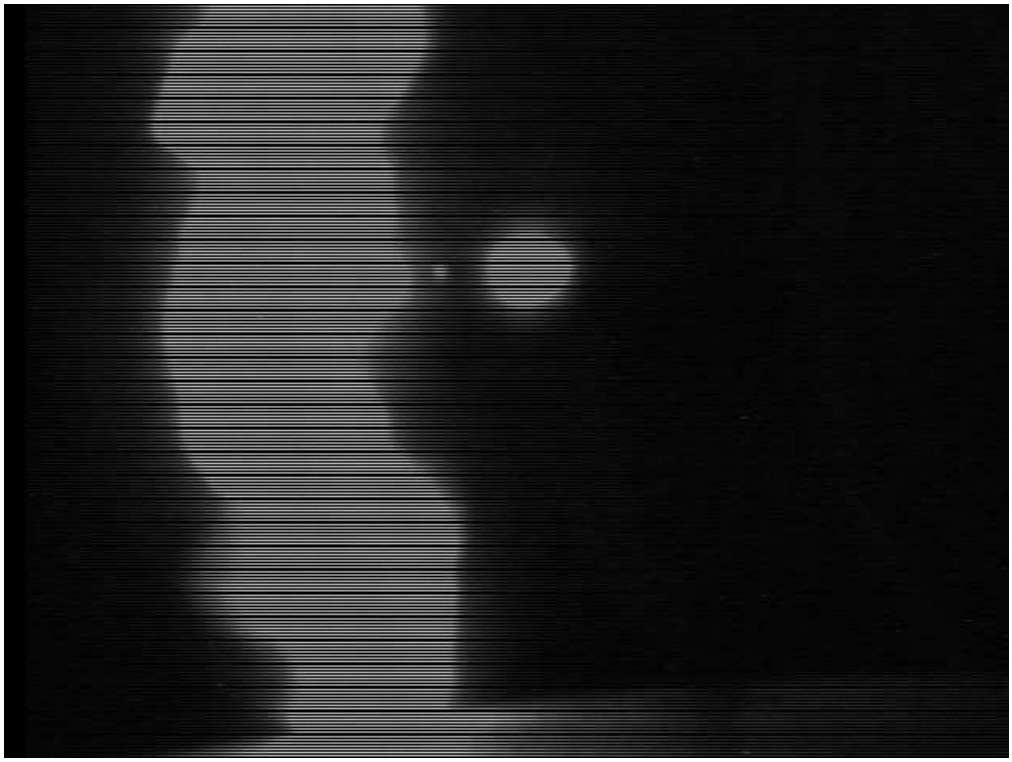


Figure B.39: Feature 38 L=11 mm $\phi = 19.98°$



Figure B.40: Feature 39 L=11 mm $\phi = 2.6°$

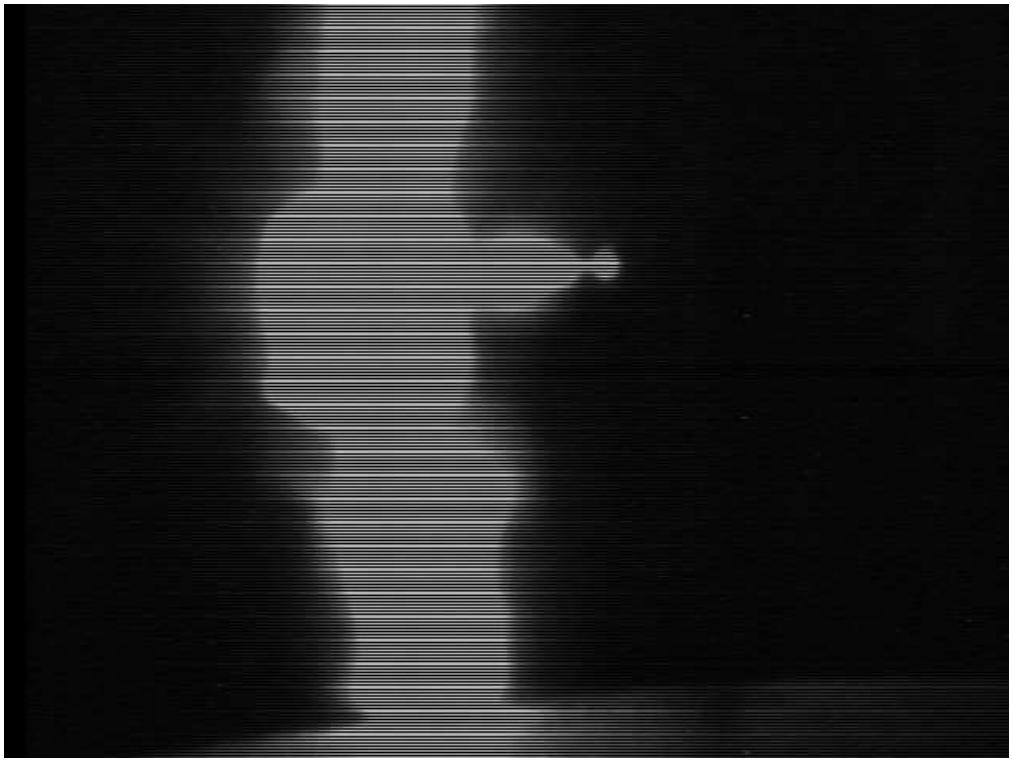


Figure B.41: Feature 40 L=11 mm $\phi = 5.19°$

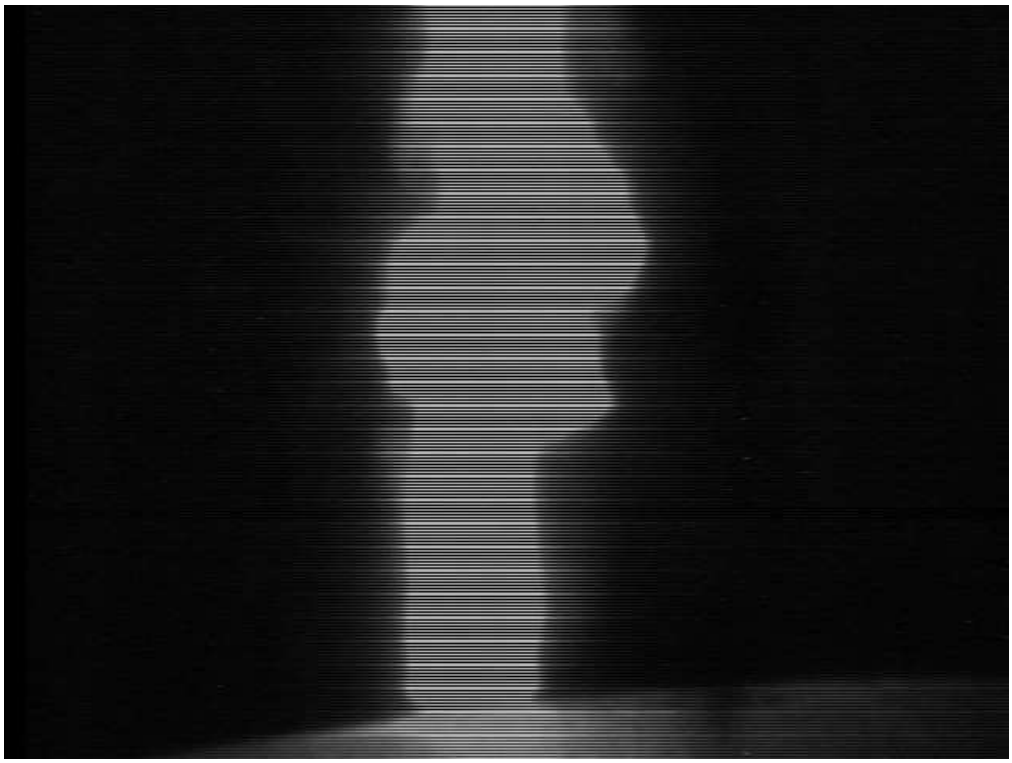


Figure B.42: Feature 41 L=13 mm $\phi = 8.5°$

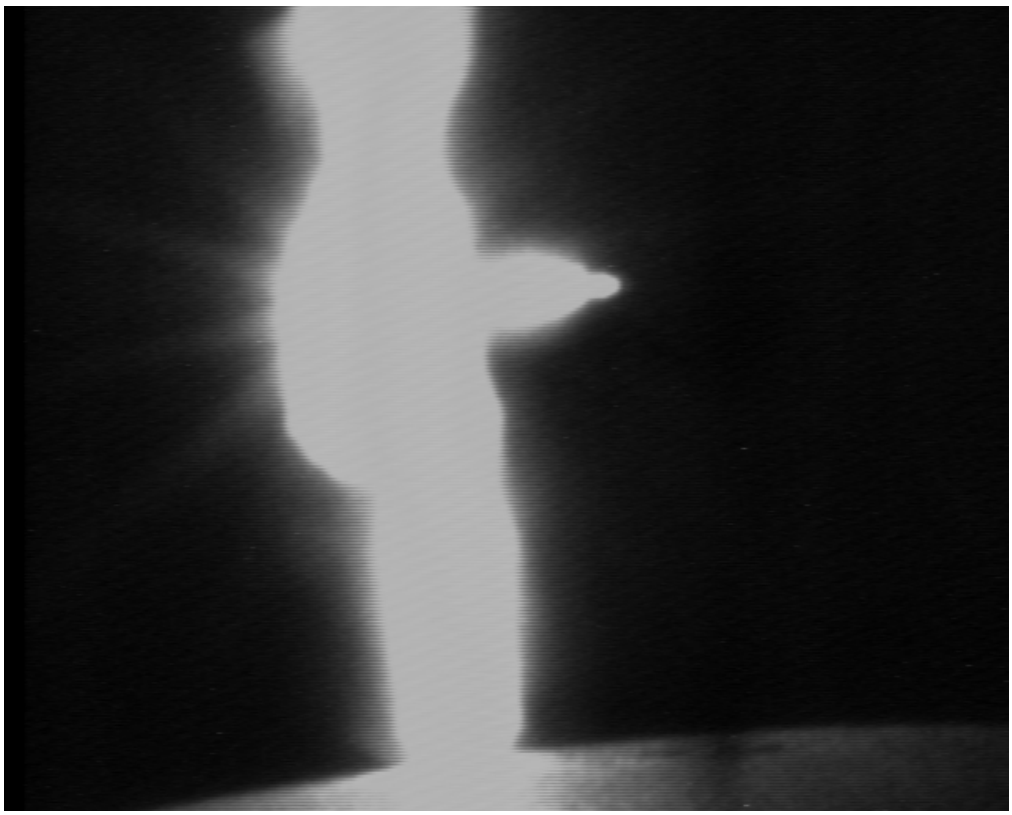


Figure B.43: Feature 42 L=12 mm $\phi = 9.46°$

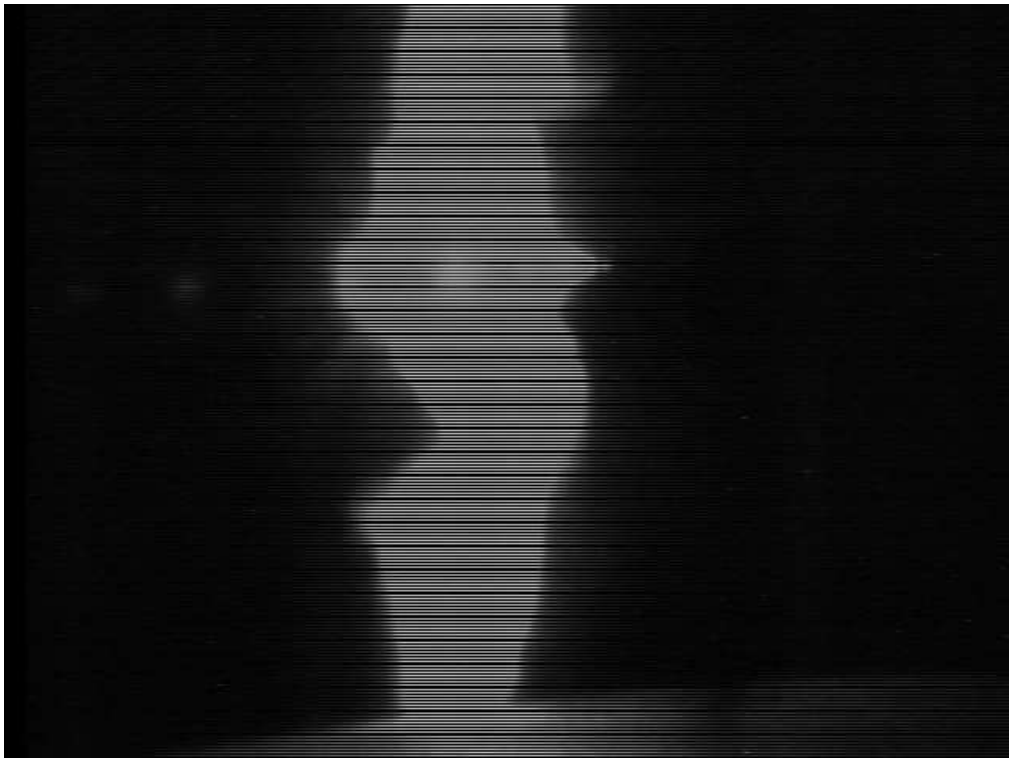


Figure B.44: Feature 43 L=11 mm $\phi = 2.6°$

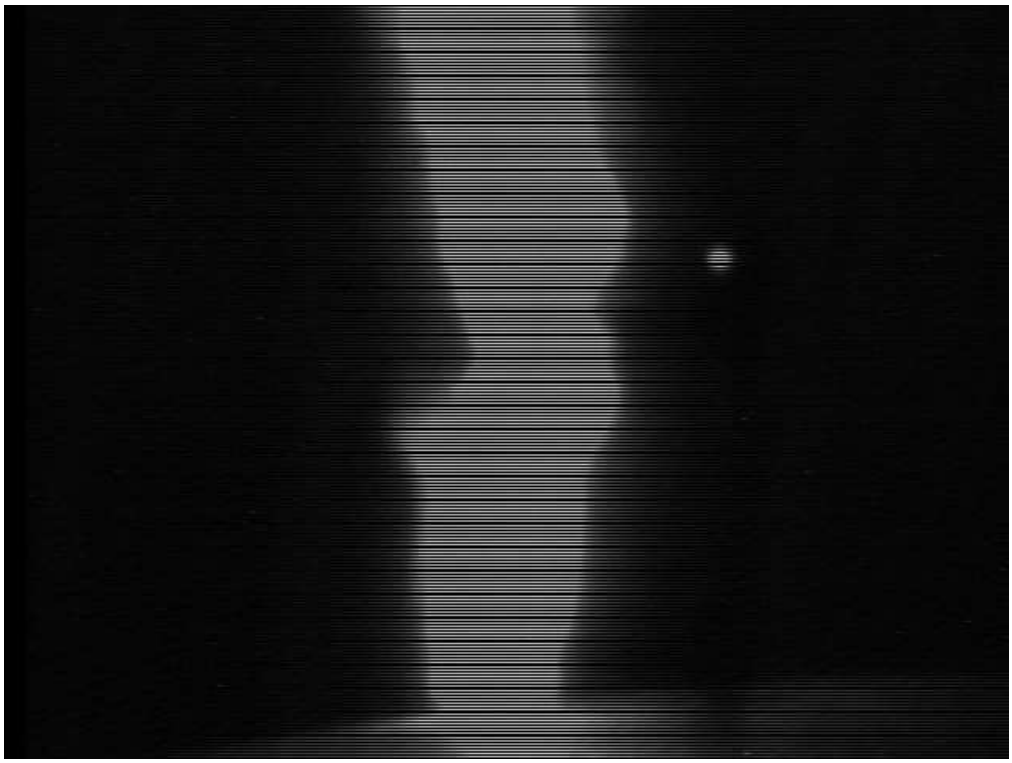


Figure B.45: Feature 44 L=10 mm $\phi = 0°$

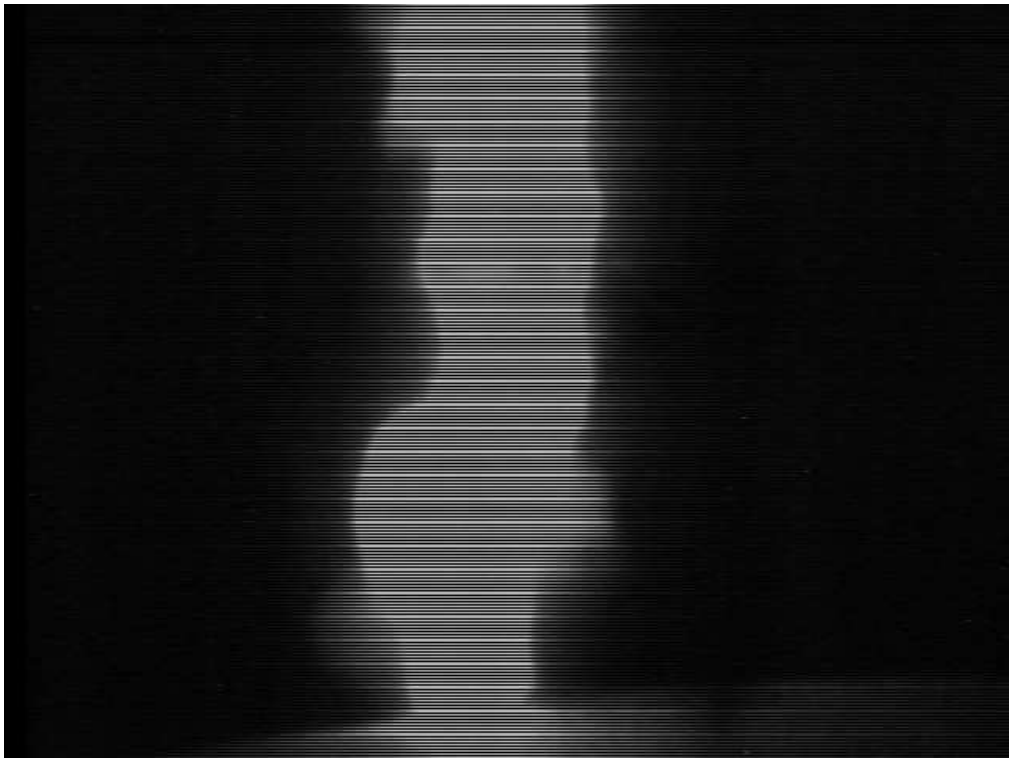


Figure B.46: Feature 45 L=12 mm $\phi = 0°$

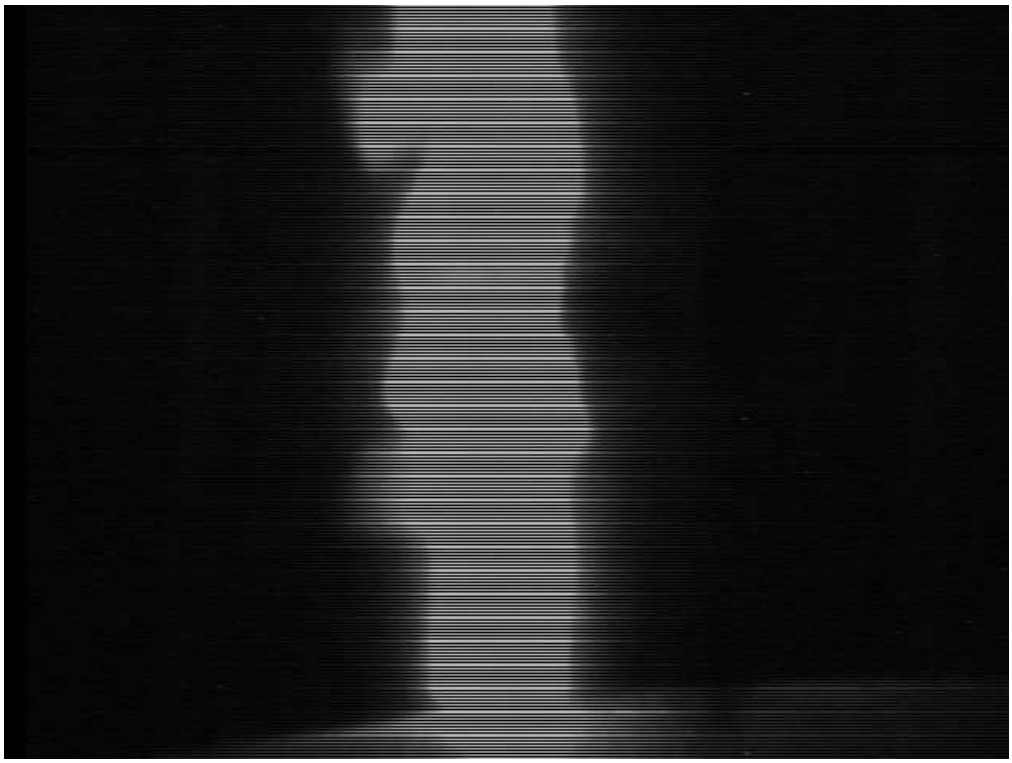


Figure B.47: Feature 46 L=10 mm $\phi = 5.71°$

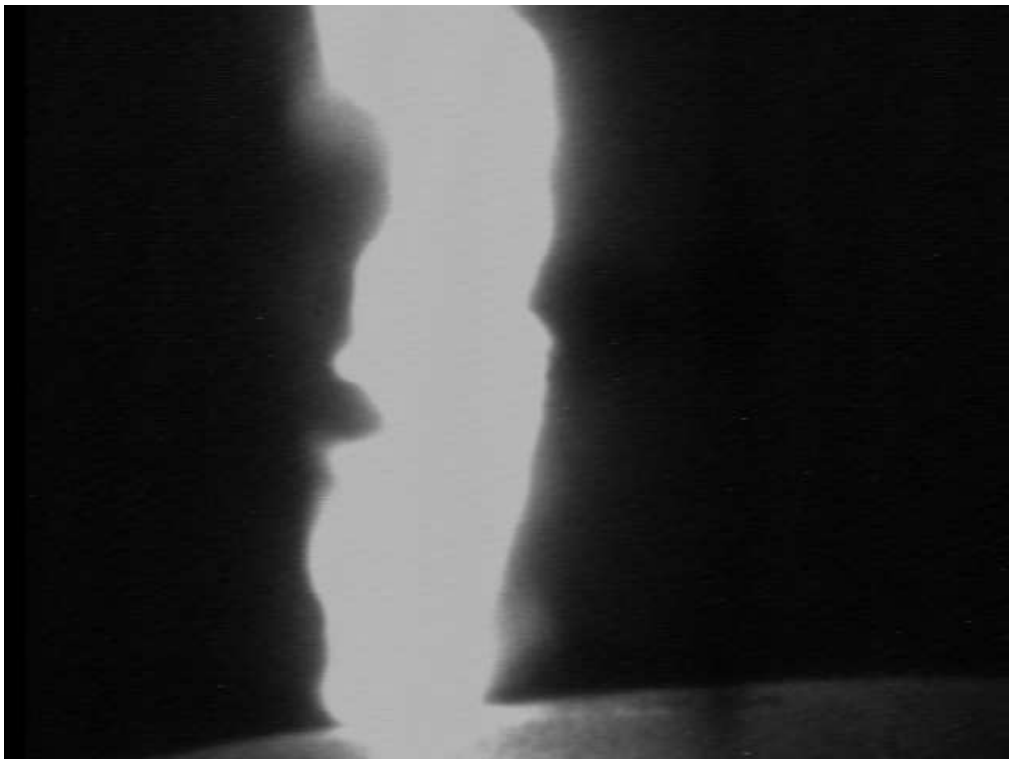


Figure B.48: Feature 47 L=9 mm $\phi = 12.3°$

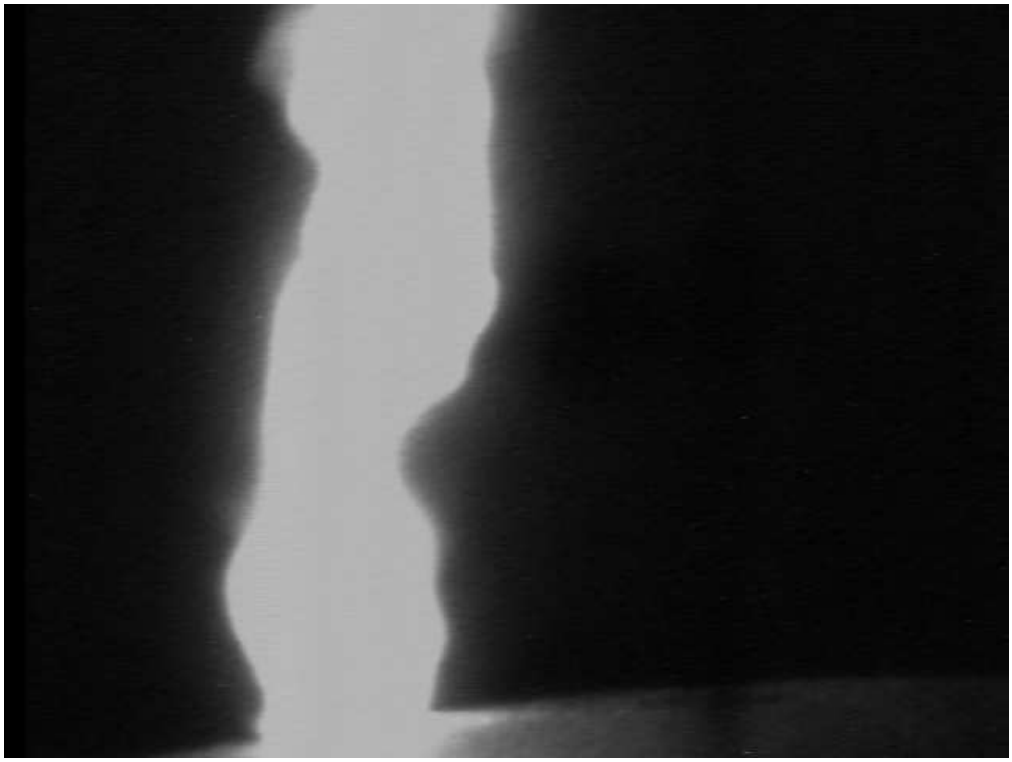


Figure B.49: Feature 48 L=11 mm $\phi = 2.6°$

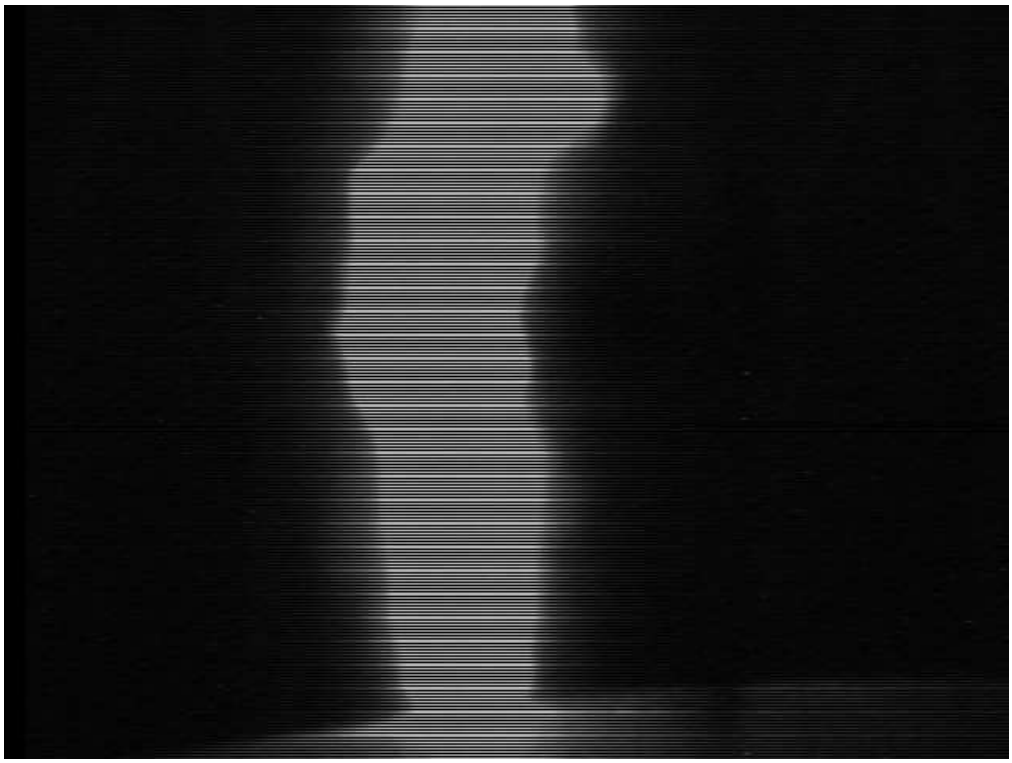


Figure B.50: Feature 49 L=12 mm $\phi = 4.76°$

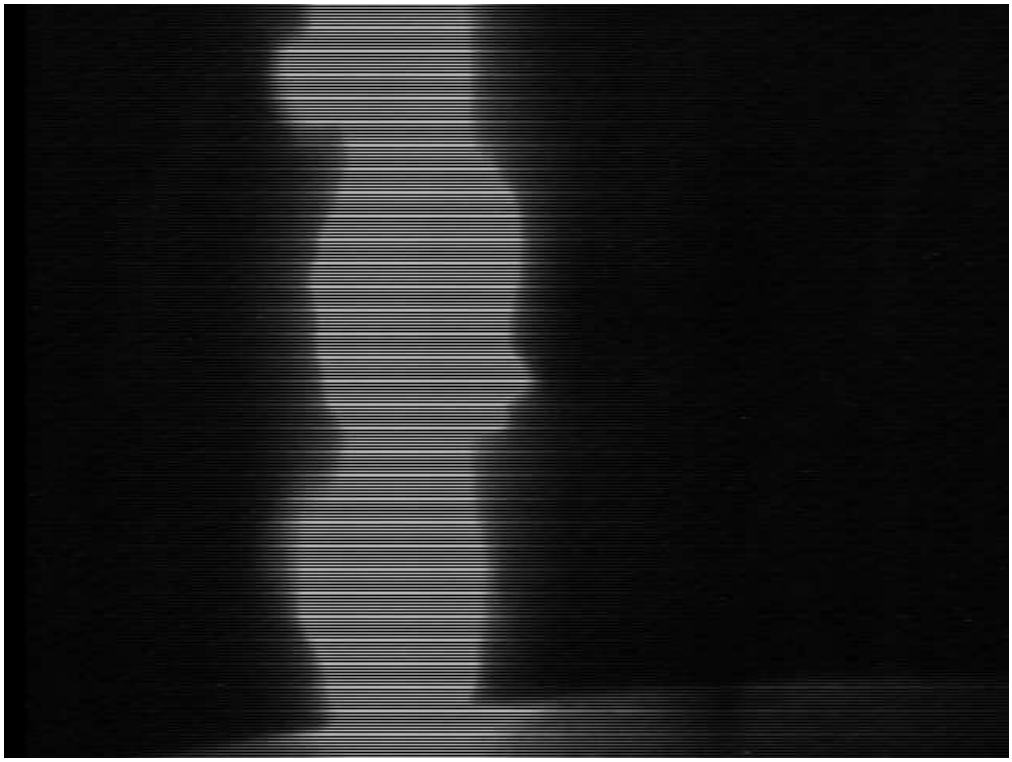


Figure B.51: Feature 50 L=12 mm $\phi = 2.39°$

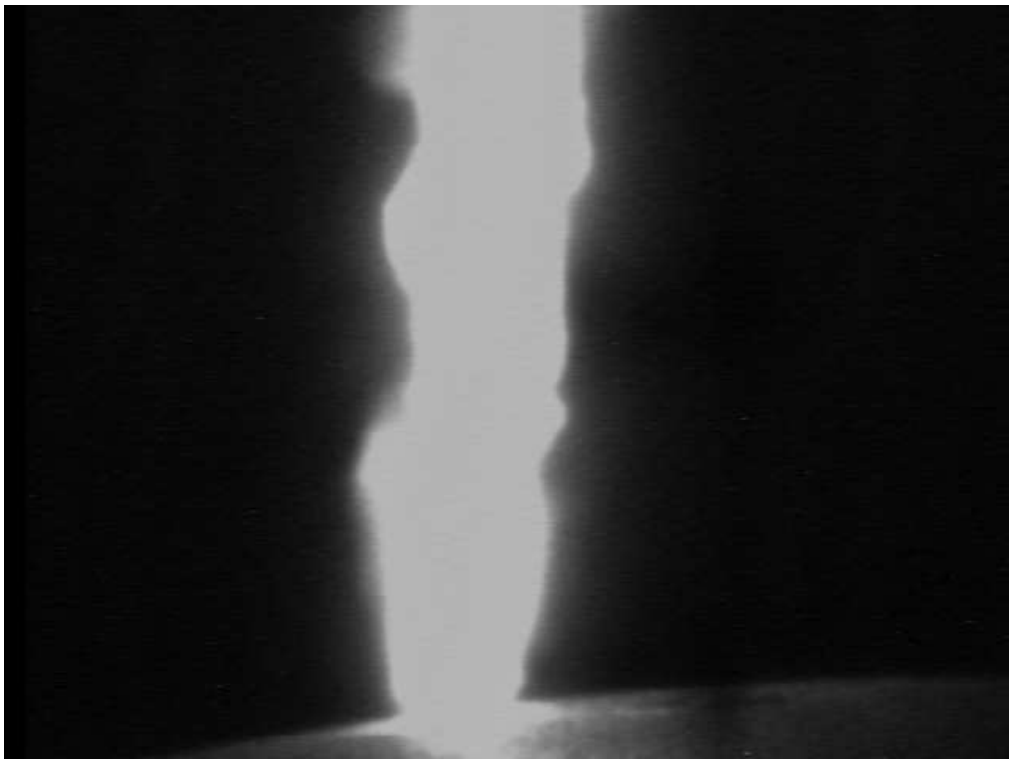


Figure B.52: Feature 51 L=10 mm $\phi = 11.3°$

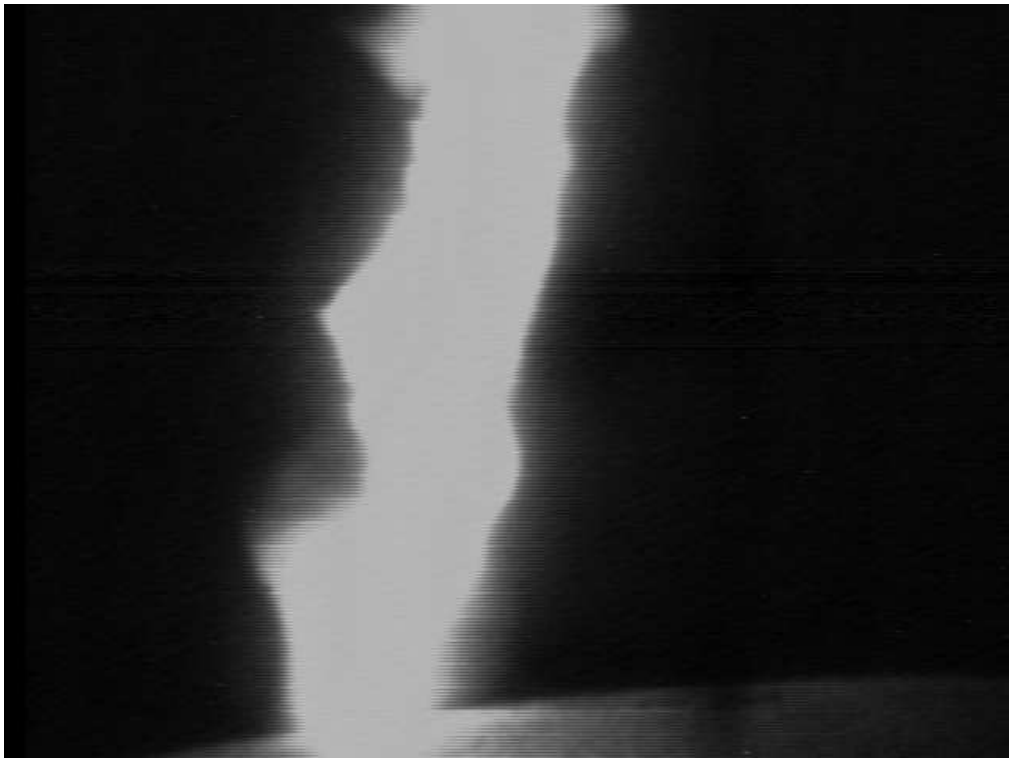


Figure B.53: Feature 52 L=12 mm $\phi = 9.46°$

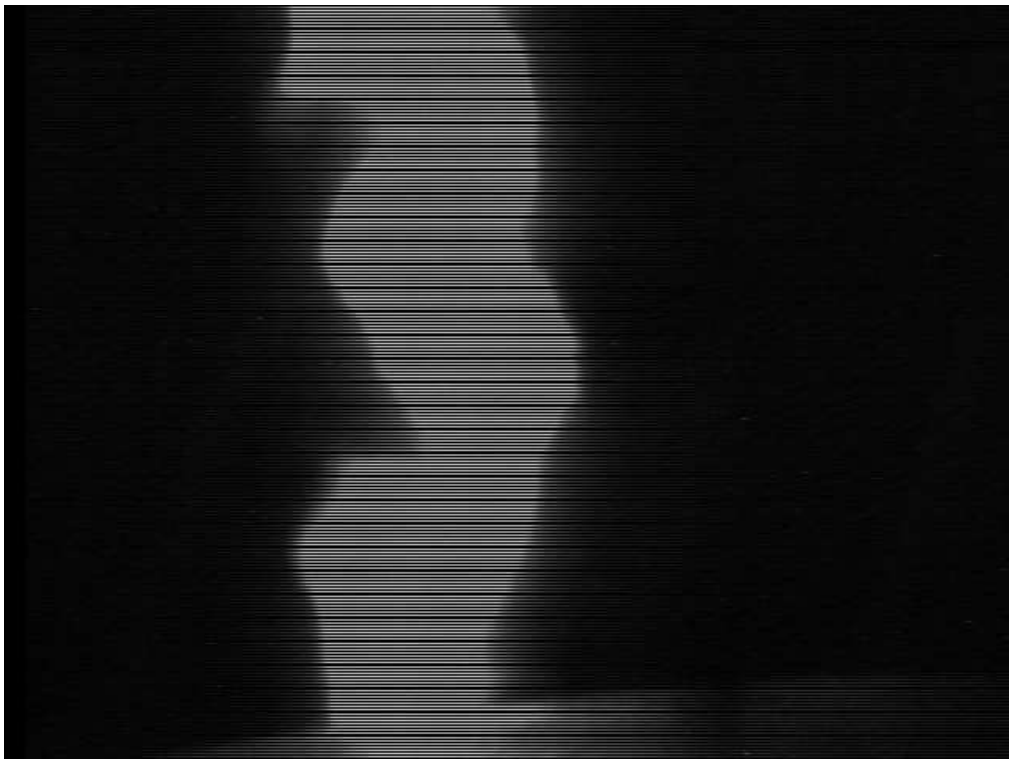


Figure B.54: Feature 53 L=11 mm $\phi = 10.3°$

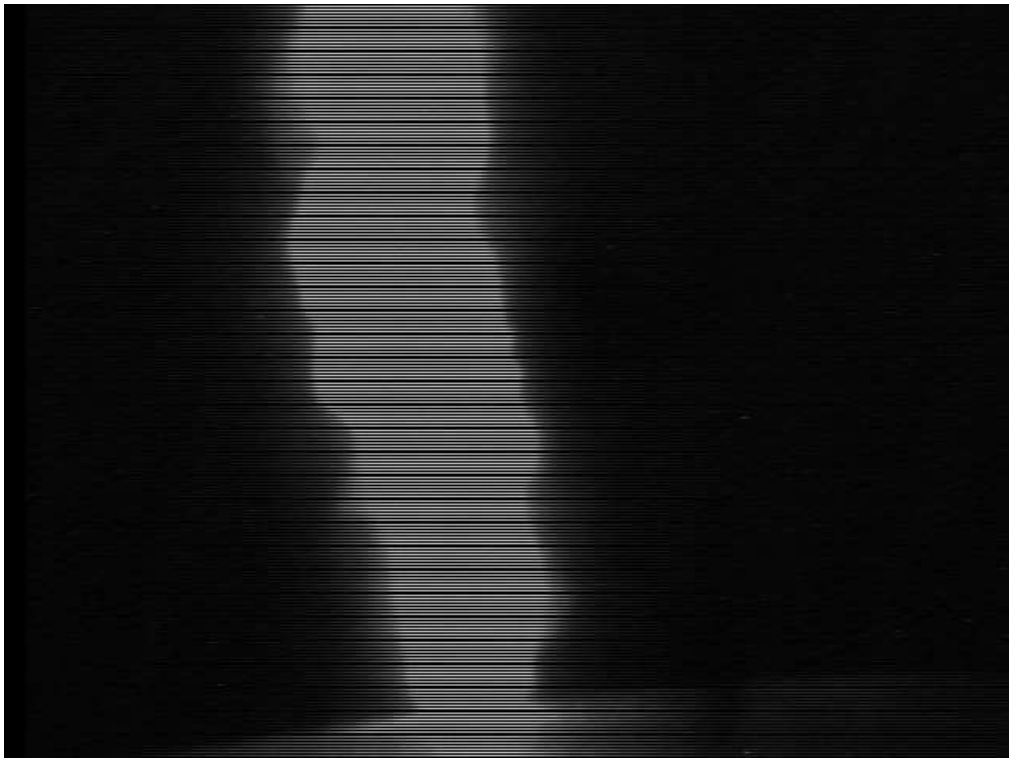


Figure B.55: Feature 54 L=13 mm $\phi = 4.4°$

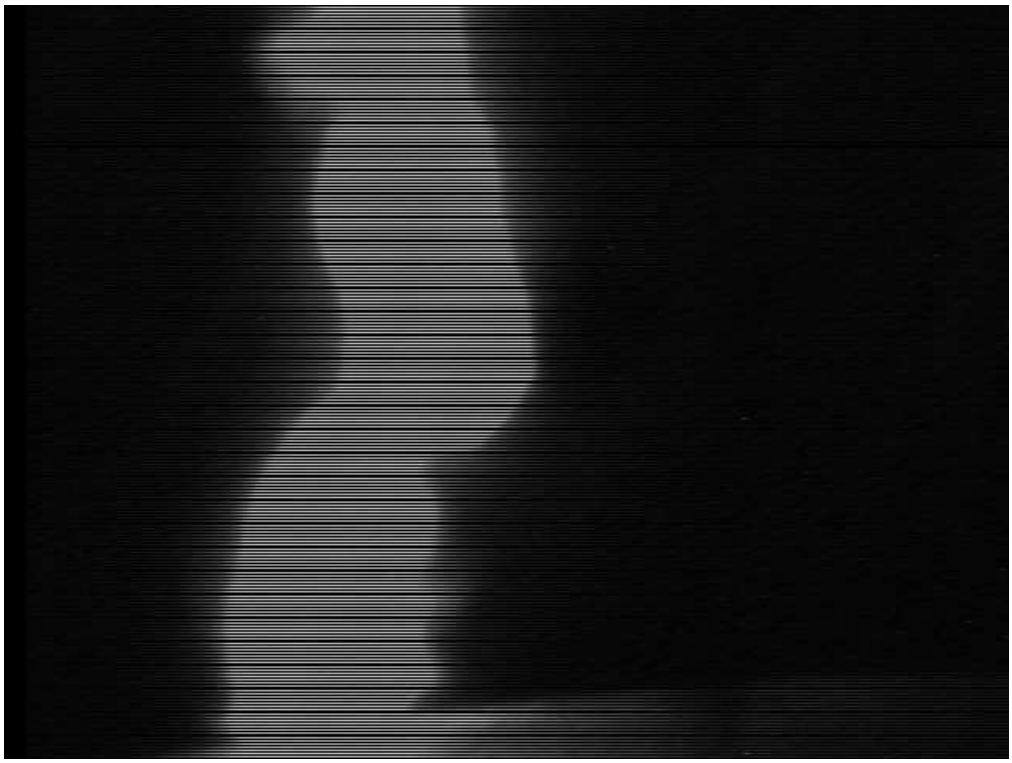


Figure B.56: Feature 55 L=11 mm $\phi = 5.19°$

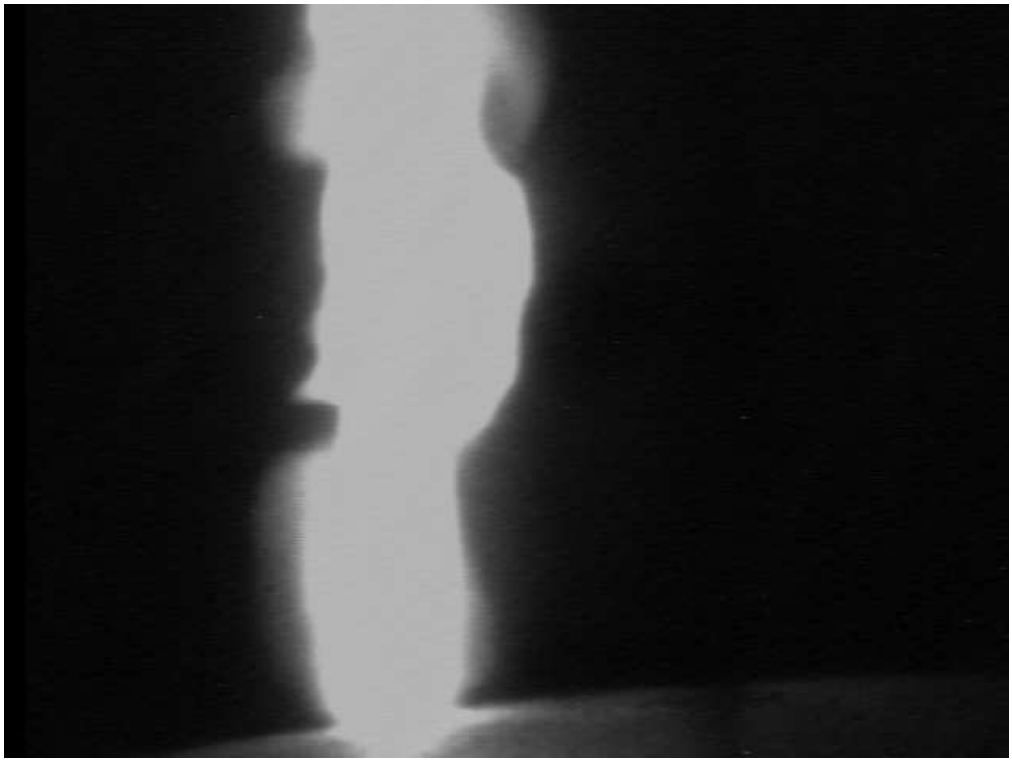


Figure B.57: Feature 56 L=10 mm $\phi = 5.71°$

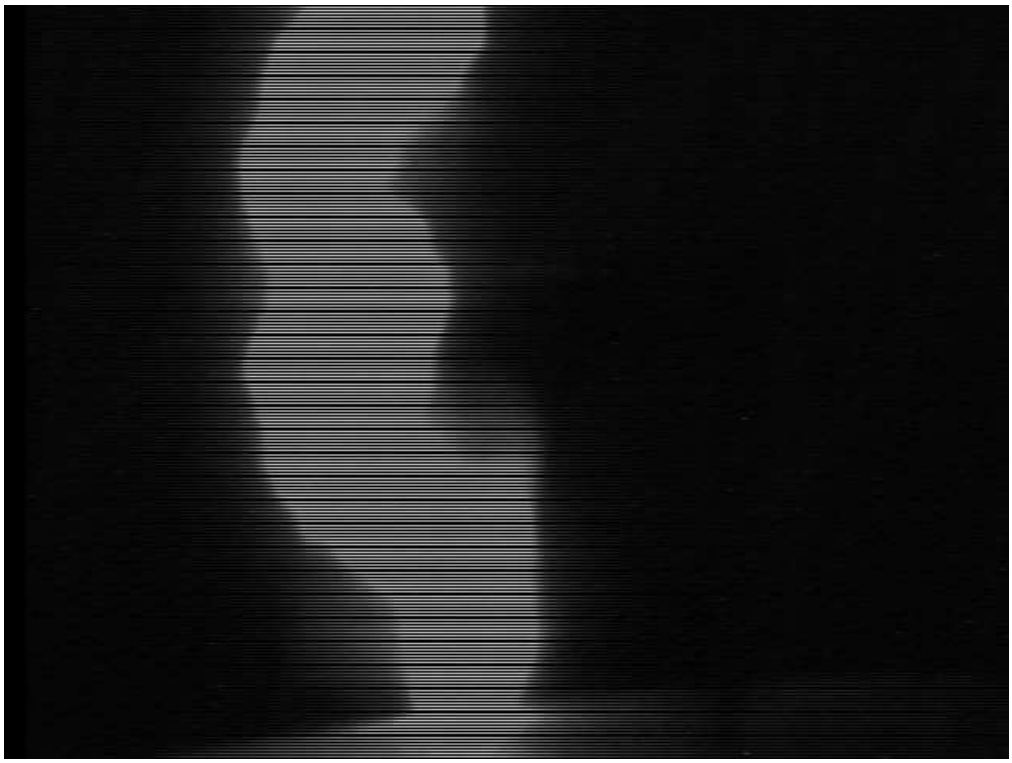


Figure B.58: Feature 57 L=12 mm $\phi = 4.76°$

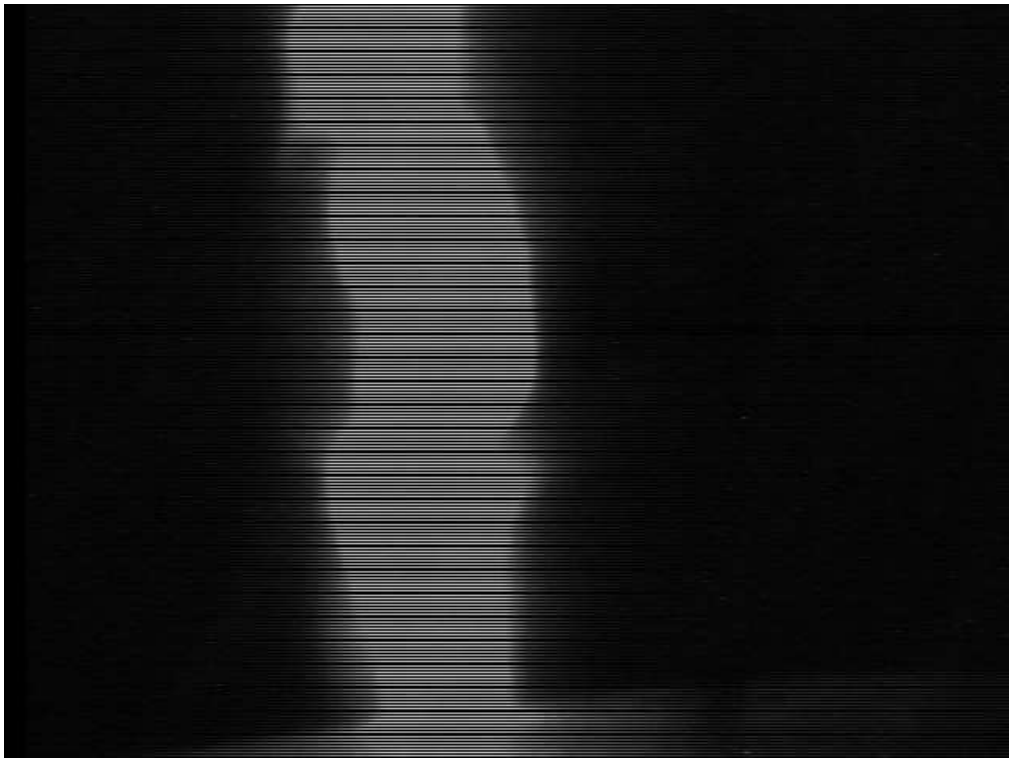


Figure B.59: Feature 58 L=11 mm $\phi = 0°$

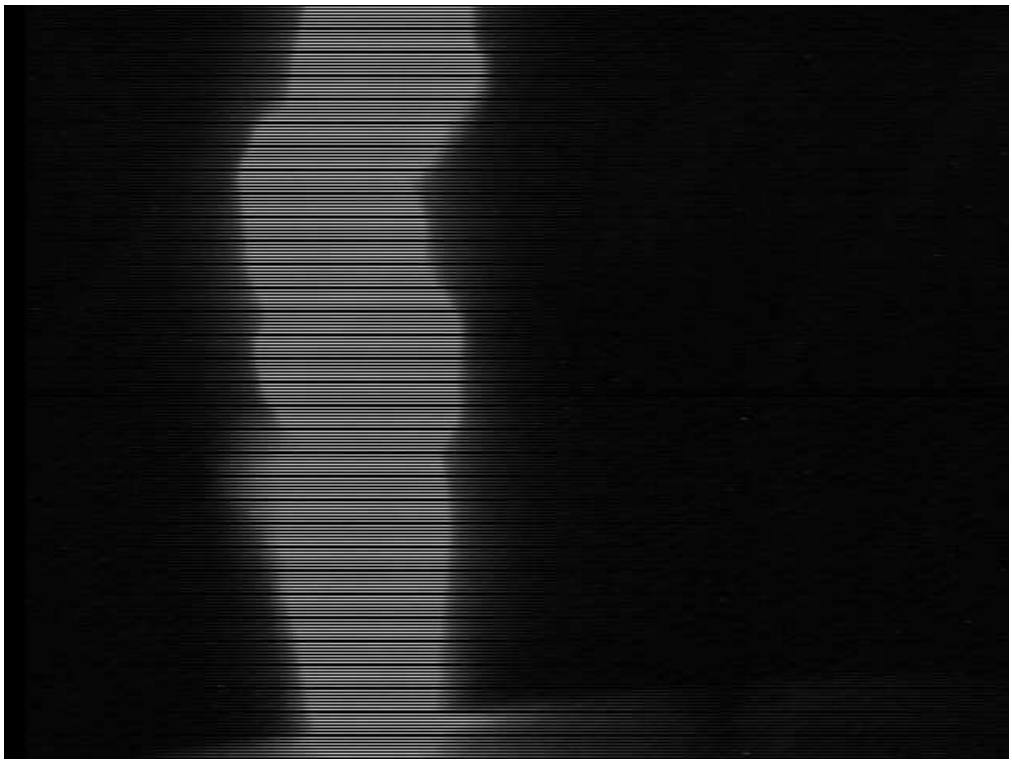


Figure B.60: Feature 59 L=12 mm $\phi = 19.4°$

References

[1] P. D. Maker, R. W. Terhume, and C. Savage, "Optical third harmonic generation." Proceedings of the 3rd IEEE international conference on quantum electronics, Paris, 1964.

[2] W. K. Pendleton and A. H. Guenther, "Investigation of a laser-triggered spark gap," *Review of Scientific Instruments*, vol. 36, no. 11, pp. 1546–1550, November 1965.

[3] L. L. Steinmetz, "Laser-triggered spark gap," *Review of Scientific Instruments*, vol. 39, no. 6, pp. 904–909, June 1968.

[4] A. H. Guenther and J. R. Bettis, "Laser-triggered megavolt switching," *IEEE Journal of Quantum Electronics*, vol. 3, no. 11, pp. 581–588, November 1967.

[5] C. G. Morgan, "Laser-induced breakdown of gases," *Reports on Progress in Physics*, no. 38, pp. 621–665, November 1975.

[6] P. X. Phuoc and C. M. White, "Optical characterisation of the laser-induced spark in air," National Energy Technology Laboratory.

[7] T. X. Phuoc, "An experimental and numerical study of laser-induced spark in air," *Optic and Lasers in engineering*, vol. 43, pp. 113–129, 2005.

[8] Y. I. Malakohov and Y. A. Rezunkov, "Lightning attachment based on laser-generated plasma channels in the atmosphere." International Conference on Lightning Protection, September 2002.

[9] M. Megumu, A. Wada, and T. Shindo, "Characteristics of upward leaders triggered by co_2 laser." International Conference on Lightning Protection, September 2004.

[10] R. A. Dougal, P. F. Williams, and A. H. Guenther, "Breakdown process in laser-triggered switching." 4th IEEE International Pulsed Power Conference, 1983.

[11] F. F. Chen, *Introduction to plasma physics and controlled fusion, Vol 1: Plasma physics.* Kluwer Academic / Plenum Publishers, 1984.

[12] A. E. Siegman, *Lasers.* University Science Books, 1986.

[13] *Introduction to lasers*, Department of Physics - LRI (University of Stellenbosch), 2004.

[14] R. A. Serway and R. J. Beichner, *Physics for scientists and Engineers*, fifth edition ed. Saunders College Publishing, 2000.

[15] E. Hecht, *Optics.* Addison Weasly, 2002.

[16] C. V. Bindhu, S. Harilal, M. S. Tillack, F. Najmabadi, and A. C. Gaeris, "Energy absorption and propagation in laser-created sparks," *Applied spectroscopy*, vol. 58, no. 6, 2004.

[17] Y.-L. Chen, J. W. L. Lewis, and C. Parigger, "Spacial and temporal profiles of pulsed laser-induced air plasma emissions," *Journal of quantitative spectroscopy and radiative transfer*, vol. 67, pp. 91–103, 2000.

[18] M. Villagran-Muniz, H. Sobral, and R. Navarro-Gonzalez, "Shock and thermal wave study of laser-induced plasmas in air by the probe beam deflection technique," *Measurements and Science Technoloy*, vol. 14, pp. 613–618, 2003.

[19] K. Attenborough and Q. Qin, "Aspects of laser-generated acoustic shock waves in air."

[20] M. Mathuthu, R. M. Raseka, H. G. C. Human, N. West, and A. Forbes, "Radial variation of air plasma parameters," submitted to IEEE Transactions on Plasma Science.

[21] N. J. West, I. R. Jandrell, and A. Forbes, "Preliminary investigation into the simulation of a laser-induced plasma by means of a floating object in a spark gap." 29th International Symposium on High Voltage, 2007.

[22] F. A. M. Rizk, "Effect of conducting objects on critical switching impulse breakdown of long air gaps." Cigre, 1994.

[23] G. Baldo, "Floating potential bodies and their interaction with discharge development." 6th International Symposium on High Voltage, 1989.

[24] N. J. West and I. R. Jandrell, "A study of laser-generated plasmas and their application to high voltage engineering." IEEE PES PowerAfrica 2007, 2007.

[25] E. Kuffel, W. S. Zaengl, and J. Kuffel, *High voltage engineering: fundamentals.* Newness, 2000.

[26] S. Haydon, *An introduction to discharge and plasma physics.* Department of University extension, the University of New England, 1964.

[27] D. J. Tedford, *High Voltage Technology.* Oxford University Press, 1968.

[28] M. Khalifa, *High Voltage Engineering: Theory and practice.* Marcel Dekker Inc., 1990.

[29] D. Kind and H. Karner, *High Voltage insulation technology.* Friedrich Vieweg und Sohn, 1985.

[30] T. J. Gallagher and A. J. Pearmain, *High Voltage: Measurement and testing.* John Wiley and Sons, 1983.